The role of beta arrestin 1 in vascular tone regulation of pulmonary arteries

Dissertation

zur

Erlangung des Doktorgrades (Dr. rer. nat.)

der

Mathematisch-Naturwissenschaftlichen Fakultät

der

Rheinischen Friederich-Wilhelms-Universität Bonn

vorgelegt von

Leonard Lebender

aus

Bonn, Deutschland

Bonn 2021

Angefertigt mit der Genehmigung der Mathematisch-Naturwissenschaftlichen Fakultät der Rheinischen Friedrich-Wilhelms-Universität Bonn

1. Gutachter: Prof. Dr. Bernd K. Fleischmann
2. Gutachterin: Prof. Dr. Evi Kostenis
Tag der Promotion: 30.08.2021
Erscheinungsjahr: 2021

Acknowledgements

Mein erster Dank gilt Herrn Prof. Fleischmann für seine Unterstützung als Doktorvater und als erster Gutachter dieser Arbeit, sowie Frau Prof. Daniela Wenzel für die enge und hervorragende Betreuung und stetige Unterstützung dieses Projektes. Ich danke weiterhin Frau Prof. Evi Kostenis für Ihre Betreuung als Co-supervisor und die tolle Zusammenarbeit. Dank gilt auch der fachlichen und finanziellen Unterstützung durch die DFG und das Graduiertenkolleg 1873 unter der Leitung von Prof. Alexander Pfeifer, welches erst diese Arbeit ermöglicht hat. Besonderen Dank möchte ich auch Herrn Prof. Volkmar Gieselmann aussprechen, welcher mir stets bei vielen Fragen zur Seite stand. Durch die enge Zusammenarbeit mit der Biochemie wurde dieses Projekt erst zu dem, was es heute ist.

Den Mitpromovierenden des GRK1873 möchte ich für die tolle gemeinsame Zeit und die moralische Unterstützung danken, wodurch bei unzähligen Seminaren, Vorträgen und Ausflügen nach Feierabend viel Freude aufkam.

Meine Arbeit als Doktorand wurde von der gemeinsamen Zeit mit den lieben Kollegen, welche mich stets begleiteten, sehr bereichert. Ich hatte großes Glück, in ein so tolles Team aufgenommen zu werden und habe viele schöne gemeinsame Stunden verbracht- sei es bei Franks Dinnerpartys, Elas DJ-Sets, Yokes Grillpartys oder der gemeinsamen Weihnachtsfeier. Vielen Dank Euch allen für diese aufregende Zeit!

Besonders hervorheben möchte ich die Arbeitsgruppe Wenzel, namentlich Jennifer Dietrich, Alexander Seidinger, Annika Simon, Dr. Sarah Rieck, Dr. Ela Matthey und Prof. Daniela Wenzel. Ich danke für die unschätzbare Unterstützung und den Zusammenhalt während meiner Doktorandenzeit. Gemeinsame Ausflüge, Konferenzen, aber auch die studentische Lehre und der Laboralltag waren ein tolles Erlebnis mit Euch!

Zum Schluss möchte ich meinen Freunden, meiner Familie sowie der Familie Prünte für die stetige Motivation, das offene Ohr und die emotionale Unterstützung danken. Eurem Rückhalt verdanke ich die Vollendung dieser Arbeit, Ihr seid großartig!

Letzter und größter Dank geht an Laura, welche mich in allen Situationen stets begleitet und ermutigt hat diesen Weg zu gehen! Du hast die gemeinsame Doktorzeit zu etwas Besonderem werden lassen, Du bist wunderbar!

Table of contents

Abbreviations

°C	Degrees Celsius
µL	Microliter
µm	Micrometer
µM	Micromolar
AC	Adenylyl cyclase
ACh	Acetyl choline
ANOVA	Analysis of variance
AP	Alkaline phosphates
apo-sGC	heme-deficient sGC
APS	Ammonium persulfate
$AT1_A$	Angiotensin II receptor type 1A
beta arr1	Beta arrestin 1
beta arr2	Beta arrestin 2
bmp	Beats per minute
BSA	Bovine serum albumin
ca.	Circa
CaCl2	Calcium chloride
CaM	Calmodulin
cAMP	Cyclic adenosine monophosphate
cDNA	Complementary desoxyribunucleic acid
cGMP	Cyclic guanosine monophosphate
CMC	Carboxymethyl cellulose
CTEPH	Chronic thromboembolic pulmonary hypertension
Cyb5r3	Cytochrome b5 reductase 3
DAG	Diacylglycerol
dH_2O	Aqua destillata (distilled water)
DMEM	Dulbecco's Modified Eagle Medium
DMSO	Dimethyl sulfoxide
DNA	Desoxyribunucleic acid
DPBS	Dulbecco’s Phosphate Buffered Saline
EDTA	Ethylenediaminetetraacetic acid
ELISA	Enzyme linked immunosorbent assay
et al.	And others ("et alii")
EtOH	Ethanol
FACS	Fluorescense-activated cell sorting
FCS	Fetal calf serum
Fsk	Forskoline
g	Gravity
GAP	GTPase activating protein
GDP	Guanosine diphosphate
GEF	Guanine-nucleotide exchange factor
GFP	Green fluorescent protein
GIRK	G-protein coupled inwardly rectifying potassium channel
GPCR	G protein-coupled receptor
G protein	Guanine nucleotide binding protein
GRK	G protein-coupled receptor kinases
GTP	Guanosine triphosphate
h	Hour
H&E	Hematoxylin and eosin
H_2O_2	Hydrogen peroxide
HCl	Hydrochloric acid
HEK293	Human embryonic kidney 293 cells
Hx	Hypoxia
i.p.	Intraperitoneal
i.v.	Intravenous
IB	Immunoblot
IBMX	3-isobutyl-1-methyxanthine
$InsP_3R$	Inositol triphosphate receptor
IP	Prostacycline receptor
IP_3	Inositol trisphosphate
IRAG	$InsP_3R$- associated PKG substrate isoform A
JNK	c-Jun N-terminal kinase
KCl	Potassium chloride
kg	Kilogram
KO	Knockout
LB	Lysogeny broth
LV	Left ventricle
LVSP	Left ventricular systolic pressure
MAPK	Mitogen-activated protein kinase
MBP	Maltose Binding Protein
MCh	Methacholine
$MgCl_2$	Magnesium chloride
$MgSO_4$	Magnesium sulfate
min	Minute
MLC_{20}	Regulatory myosin light chain
MLCP	Myosin light chain phosphatase
mM	Millimolar
mmHg	Millimeter mercury
mN	Millinewton
mPASMC	Murine pulmonary artery smooth muscle cell
mRNA	Messenger RNA
msec	Milisecond

Na_2HPO4	Sodium hydrogen phosphate
NaCl	Sodium chloride
$NaHCO_3$	Sodium bicarbonate
$NaIO_3$	Sodium iodate
NaOH	Sodium hydroxide
nM	Nanomolar
Nx	Normoxia
O_2	Oxygen
p	Passage
PA	Pulmonary artery
PAGE	Polyacrylamide gel electrophoresis
PAH	Pulmonary arterial hypertension
PAPm	Resting mean pulmonary arterial pressure
PBS	Phosphate-buffered saline
PCR	Polymerase chain reaction
PDE	Phosphodiesterase
PDE4D	Phosphodiesterase 4D
PDGF	Platelet derived growth factor
Pen-Strep	Penicillin-Streptomycin
PFA	Paraformaldehyde
PH	Pulmonary hypertension
PIP_2	Phospohatidylinositol-4,5-bisphosphate
PKA	Protein kinase A
PKC	Protein kinase C
PKG	Protein kinase G
PLB	Phospholamban
PLC	Phospholipase C
PLCβ	Phospholipase Cβ
pNpp	P-nitrophenyl phosphate
PSS	Physiological salt solution
PSS low Ca_{2+}	Physiological salt solution low Calcium
PTFE	Polytetrafluorethylen
PVDF-FL	Polyvinylidene fluoride low fluorescence
PVR	Pulmonary vascular resistance
qPCR	Quantitative polymerase chain reaction
RhoA	Ras homolog family member A
RIPA	Radioimmunoprecipitation assay buffer
ROCK	Rho-kinase
Roflu	Roflumilast
rpm	Rounds per minute
RT	Room temperature
RT qPCR	Real-time quantitative polymerase chain reaction
RV	Right ventricle
RVSP	Right ventricular systolic pressure
s.c.	Subcutan
s.e.m.	Standard error of the mean
S.O.C.	Super optimal broth with catabolite repression
SDS	Sodium dodecyl sulfate
sec	Second
SERCA	Sarco(endo)plasmic reticulum Ca^{2+}-ATPase
sGC alpha1	Soluble guanylyl cyclase subunit alpha1
sGC alpha1 beta 1	Soluble guanylyl cyclase alpha1 beta1
sGC alpha2	Soluble guanylyl cyclase subunit alpha2
sGC beta1	Soluble guanylyl cyclase subunit beta1
SNP	Sodium nitroprusside
SPF	Specific-pathogen-free
TBS	Tris-buffered saline
TBST	Tris-buffered saline + 0.1% tween-20
TEMED	N,N,N',N'-Tetramethyl ethylenediamine
Tris	Tris(hydroxymethyl)aminomethane
U	International units
V	Volt
VEGFR3	vascular endothelial growth factor receptor 3
VSMC	Vascular smooth muscle cell
WB	Western blot
Δbeta Arr1/2	Beta arrestin 1 and beta arrestin 2 double knockout

1 Introduction

1.1 Physiology of the vascular system

The vascular system consists of extensive networks with proper blood flow serving to maintain cellular homeostasis in the body .[1] Larger vessels mainly enable blood transport whereas smaller capillaries facilitate substance and nutrient exchange.[2] The vascular system of the body consists of a systemic circuit that enables blood supply to all tissues, and a pulmonary circuit that enables blood gas exchange in the lung.[3]

1.1.1 The systemic circuit

The heart pumps blood from the left ventricle through arteries, capillaries and veins in a circuit back to the right atrium.[2] Blood vessels highly differ in their structure depending on their function in the blood circuit. Large arteries are characterized by a high mean blood pressure (100 mmHg) and are subclassified as elastic and muscular types. Elastic arteries are responsible for the transport of large blood volumes and their high elasticity further enables continuous blood transport by dampening the large oscillations during systole and diastole. Muscular arteries are mainly responsible for rapid blood distribution. Compliance describes the adaptation of the vessel volume in response to blood pressure changes.[1] Thus, elastic arteries have a greater compliance compared to muscular arteries. Arteries split into smaller arterioles which again branch into capillaries. The blood pressure is highest in arteries and declines after the small resistance arteries. This is necessary for protection of the thin-walled capillaries, which connect the arterial with the venous system and enable solute and water exchange.[1,2] Capillaries and veins are both characterized by a low mean blood pressure (25 to 2 mm Hg). Leaving the capillaries, the blood returns to the heart through the venous system. Veins act as a reservoir for blood and prevent extensive pooling of blood in the extremities, some contain uni-directional valves.[2]

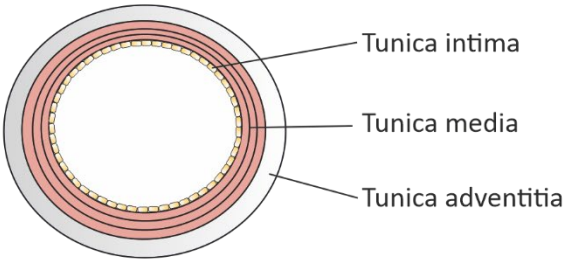

Figure 1: Cross section of an artery.
Arteries are typically divided in three different layers named tunica intima, tunica media and tunica adventitia. Each layer consists of different cell types and a complex interplay of intercellular signaling enables proper functionality regarding tone regulation, cellular homeostasis and substance exchange.

The structure of larger arteries is composed of three layers (Figure 1): The tunica intima mainly consists of endothelial cells, stratum subendotheliale and membrana elastica. Its main purposes are providing a primary diffusion barrier, regulation of blood coagulation, secretion of vasoreactive substances and participation in angiogenesis.[1,4] The tunica media mainly consists of smooth muscle cells and extracellular matrix and is essentially responsible for regulation of the vessel diameter by contraction or relaxation of muscle fibres. The Tunica adventitia contains connective tissue and fibroblasts and has supporting and supply function.[1,4] Capillaries are characterized by a lack of smooth muscle cells, consisting only of a single layer of endothelial cells and a basement membrane. The large total surface area and the rather weak barrier function enable the characteristic exchange of water and substances by diffusion.[1] Veins are structured, similar to arteries, in three different layers, but contain less smooth muscle and connective tissue. Thus, the vascular wall of veins is thinner than arterial walls resulting in a lower median blood pressure in the venous system.[1]

1.1.2 The pulmonary circuit

Deoxygenated blood is pumped from the right ventricle through pulmonary arteries (PAs) in a circuit to the left atrium. On its way, blood moves from large PAs to pulmonary capillaries, where an efficient gas exchange takes place in the alveoli. Reoxygenated blood is transported to the left atrium through pulmonary veins and is then distributed from the left ventricle to the systemic blood circuit.[2] The rather thin-walled and elastic pulmonary vessels are characterized by a high compliance and low resistance.[5] Due to the low resistance of pulmonary vessels, the mean blood pressure in PAs is much lower (15 mm Hg) than in their systemic counterpart.[2] The blood supply for organs like liver or brain is regulated by myogenic autoregulation, this mechanism enables a constant blood supply independent of blood pressure changes. This is different in the pulmonary system: blood pressure is kept relatively constant, but to meet an increased demand of oxygenated blood, vessels react passively to given pressure by

distention. An increase in cardiac output results in increased vessel diameter, while the pressure remains constant.[6] The main purpose of the pulmonary circuit is the exchange of oxygen and carbon dioxide; to optimize this process, perfusion and ventilation of the lungs have to be adjusted. While the ventilation of individual lung areas and thus the oxygen supply varies, the pulmonary circuit displays the unique phenomenon of hypoxic vasoconstriction (also known as Euler-Liljestrand mechanism): This mechanism ensures optimal oxygenation of the blood by adaption of perfusion. Vessels in areas with low partial pressure of oxygen (pO_2) constrict to redirect the blood to lung areas with higher oxygen supply, which improves gas exchange.

While systemic arteries and PAs share the basic three-layered wall structure, PAs have lower and more constant mean blood pressure, higher compliance and lower resistance than systemic arteries. In total, PAs are highly fragile yet very elastic vessels with previously introduced unique properties to enable optimal blood supply for the oxygenation process.

1.1.3 Molecular mechanisms of vascular tone regulation

Control of vascular tone is a complex process modulated by various endogenous compounds. Vascular tone is highly dynamic and adapts to the current physiological state. A complex interplay between constriction and relaxation of different vessels enables precise adaptation to altered demand of blood supply upon various physiological circumstances.[1]

Modulation of the blood circuit in general is achieved by local, hormonal or neuronal signals. Local signals such as release of nitric oxide (NO) and adenosine or changes in pO_2 are responsible for metabolic adaptation to local physiological changes. Hormones affect vessel tone either directly by receptor activation on the SMC surface such as adrenaline binding to beta2- or alpha1-receptors or indirectly by hormone-dependent release of local vasoactive substances such as endothelial endothelin-1-release caused by increased concentrations of antidiuretic hormone.[2,7] Neuronal control is mainly provided by sympathetic innervation and neuronal feedback mechanisms.[2]

1.1.3.1 Cross-bridge mechanism of smooth muscle cell contraction and relaxation

Tone regulation of vessels is mainly driven by contraction or dilatation of smooth muscle cell layers in the tunica media. The mechanism of cross-bridge cycling describes the attachment of myosin filament heads (also called cross-bridges) to actin filaments and the sliding of the actin filaments result in the development of force.[8,9] Cross-bridge cycling enables adjustment of the vessel diameter.[10] Muscle contraction is initiated by rising Ca^{2+} concentrations from intracellular stores or via channel transport from the extracellular space. Ca^{2+} ions interact with calmodulin and this complex activates myosin light chain kinase (MLCK). MLCK phosphorylates the regulatory light chain of myosin (MLC_{20}) and thus

enables the myosin-actin interaction causing muscle contraction.[2,10] Relaxation of the smooth muscle is driven by a decrease of the intracellular Ca^{2+} concentration and an increase of myosin light chain phosphatase (MLCP) activity. MLCP dephosphorylates the MLC_{20} and thereby prevents further myosin-actin interaction. Prolongation of contraction is further supported by inhibition of MLCP via Rho kinase activity.[10]

Intracellular Ca^{2+} concentrations are directly and indirectly regulated by either activation or inhibition of different receptors on the cell surfaces of vascular smooth muscle and endothelial cells.

1.2 G protein-coupled receptors (GPCRs) and their role in vascular smooth muscle cell (VSMC) tone regulation

Vascular tone is determined by a balance between vasoconstriction and vasorelaxation, which is mediated via various vasoactive substances. Most of them act through GPCRs activating different downstream signaling pathways. Therefore, GPCRs and their modulation play a crucial role in tone regulation of VSMCs.

1.2.1 GPCR signal transduction

GPCRs are the largest, diverse class of transmembrane receptors and play an essential role in physiology. As more than 25% of the FDA approved drugs target GPCRs, they are crucial molecules for today's treatment of diseases.[11]

GPCRs consist of seven conserved transmembrane protein helices located within the cellular membrane. Upon ligand binding at the extracellular site of the receptor, a signal is transduced to the intracellular site via conformational change of the receptor. Further signal transduction of the activated GPCR is mediated by intracellular dissociation of heterotrimeric guanine-nucleotide binding proteins (G proteins). [12,13]

Heterotrimeric G proteins consist of different subunits: The Gα subunit contains a high affinity binding site for guanosine nucleotides and binds guanosine diphosphate (GDP) in its inactive form. The Gβγ subunit, consisting of Gβ and Gγ, forms a tight complex and is regarded to be one unit. All three subunits are bound together and form the inactive G protein.[14] G proteins are divided in four major subclasses ($G\alpha_s$, $G\alpha_{i/o}$, $G\alpha_{q/11}$ and $G\alpha_{12/13}$) on base of sequence similiarity and downstream targets.[12,13,15,16]

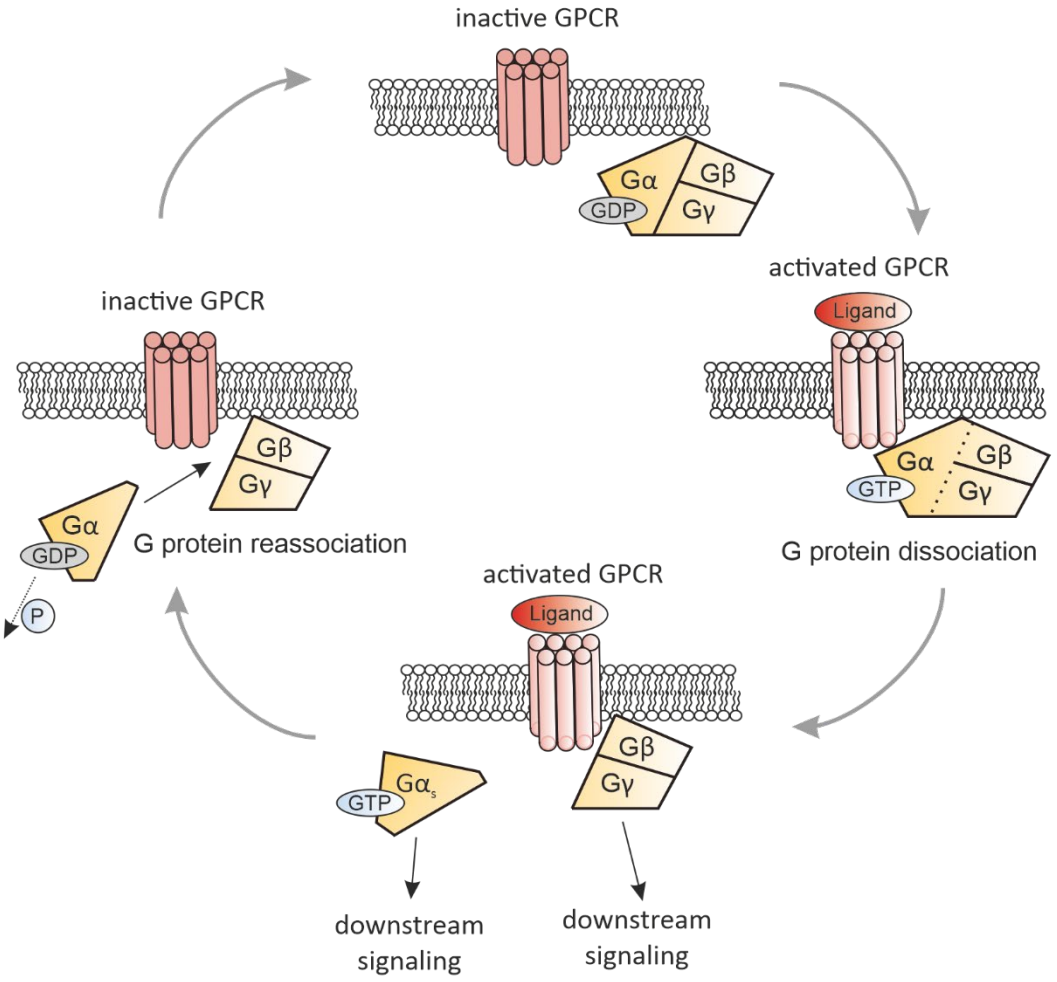

Figure 2: Process of GPCR activation.
GPCRs are located within the cellular membrane. In their inactive state, GPCRs are separated from their signaling effectors, the G proteins. Activation of the GPCR causes a conformational change of the receptor, resulting in binding of the G protein and exchange of GDP for GTP at the Gα-subunit. The GTP-bound and activated Gα-subunit dissociates from the G protein complex and both subunits, Gα and Gβγ, cause GPCR-initiated downstream signaling. Time-dependent cleavage of GTP to GDP and phosphate at the Gα-subunit terminates the signaling process and both G protein subunits reassemble.

Activation of the GPCR by a ligand enables binding of trimeric G proteins to the receptor.[17] A conformational change of the GPCR results also in rearrangement of transmembrane helices on the cytoplasmic site of the receptor. Especially the outward shift of transmembrane helix 6, along with other helix rearrangements, result in the exposure of an intracellular binding pocket that attracts G proteins, G protein coupled receptor kinases (GRKs) and beta arrestins.[16] While G proteins are the prime signaling effectors of activated GPCRs, GRKs and beta arrestins regulate GPCR activity.

The activated GPCR functions as a guanine-nucleotide exchange factor (GEF), causing an exchange of the bound GDP at the Gα subunit for guanosine triphosphate (GTP).[18] Next, the G protein complex dissociates and both resulting subunits, the GTP-binding Gα- and the Gβγ-subunit, induce further downstream signaling by activating or blocking various proteins. Both activated G protein subunits (Gα and Gβγ) have distinct signaling functions: Gα-subunits regulate andenylyl cyclases (AC),

phospholipase Cβ (PLCβ), cGMP phosphodiesterases or RhoGEFs. The Gβγ-subunit recruits GRKs, modulates G protein-coupled inwardly rectifying potassium (GIRK) channels and voltage-dependent Ca^{2+} channels, regulates ACs, phospholipases, phosphoinositide 3 kinase and mitogen-activated protein kinases (MAPK), to name a few. [16] The G protein-unbound and still active receptor can bind and activate another G protein, providing an amplification of the signal.[19]

These signaling processes of the G protein subunits are terminated by a time-dependent exchange of GTP to GDP at the Gα subunit. The GTP-bound Gα-subunit has a GTPase activity and is further catalyzed by GTPase activating proteins (GAP proteins), resulting in hydrolysis of the bound GTP and thus terminating the signaling process. Upon cleavage of the bound GTP, the inactive complex of G proteins associates (Figure 2). [12–15]

A signal turn-off of activated GPCRs is achieved by rapid phosphorylation of intracellular seryl-threonyl sites of active GPCRs by GRKs and subsequent beta arrestin binding.[19,20]

1.2.2 Regulators of GPCR activity: GRKs and beta arrestins

GRKs belong to a family of seven homologs and while GRK isoform 1 and 7 phosphorylate visual opsins, GRK isoform 2-6 target GPCRs and other cell-surface receptors. Arrestins belong to a family of four homologous arrestin proteins. The two visual arrestins (arrestin 1 and 4) target primarily photoreceptors whereas the two non-visual arrestins (arrestin 2 and 3; synonyms beta Arr1 and 2) interact primarily with GPCRs. GRKs and beta arrestins serve as universal GPCR regulators.

Arrestins were first discovered in the 1980s by Kühn et al. as proteins that are actively involved in the turn-off of light-activated rhodopsin in the retina[21]. Pioneer work on the beta2-adrenergic receptor discovered arrestin function aside from inactivation of retinal rhodopsin and allowed for the classification of visual arrestins and non-visual (beta) arrestins, which is still valid today. Cell culture experiments in the early 1990s by the nobel laureates B. K. Kobilka and R. J. Lefkowitz among others led to the discovery of today's best-known beta arrestin functions: GPCR desensitization and internalization.[22,23] The discovery of beta arrestin function is closely connected with the history of GRKs. It was nearly simultaneously discovered that beta arrestins and GRKs are modulators of activated GPCRs and are required for GPCR uncoupling activity.[24,25] Around 1999, first papers were published suggesting a role for beta arrestins as scaffolding molecules, modulating different downstream signaling pathways.[26]

1.2.2.1 Beta arrestin and GRK-facilitated GPCR desensitization

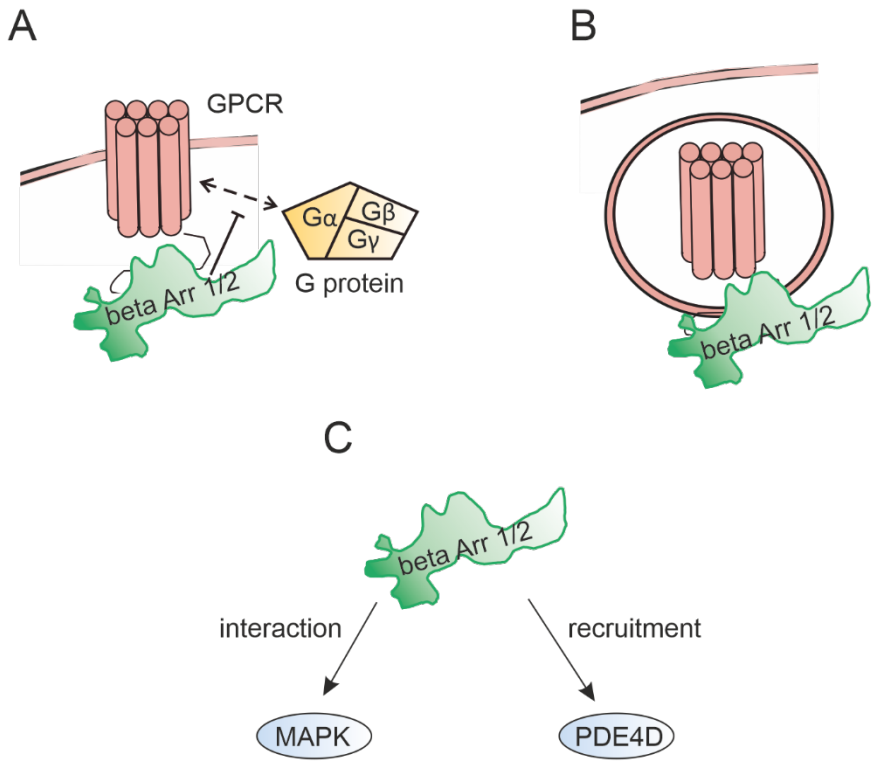

Figure 3: Versatile functions of beta arrestins.
Beta arrestins facilitate receptor desensitization and internalization and act as scaffolds for downstream signaling pathways. (**A**) Receptor desensitization is driven by beta arrestin-binding to the activated and phosphorylated GPCR. The bound beta arrestin blocks the G protein binding site and prevents further downstream signaling. (**B**) GPCR internalization is facilitated by beta arrestin-binding and thus transport of the receptor from the cell surface to the cytoplasm in clathrin-coated vesicles. (**C**) Recent literature suggests scaffolding functions of beta arrestins by i.e. interaction with mitogen-activated protein kinases (MAPPK) or recruitment of phosphodiesterase 4D (PDE4D).

GPCRs undergo a conformational change upon agonist-binding resulting in the dissociation of the G protein into subunits leading to various downstream signaling cascades. Activated GPCRs are under control of GRKs that are recruited by Gβγ subunits to the active receptor and phosphorylate multiple sites in the C-terminus and intracellular loops of the GPCR. This is followed by beta arrestin recruitment and binding to the GPCR, blocking further G protein binding by steric obstruction of the binding site. This process is known as receptor desensitization, as further G protein-mediated downstream signaling is inhibited by beta arrestin binding to the receptor (Figure 3A).[20,27] While different phosphorylation patterns are suggested to affect fine-tuning of beta arrestin binding, a recent study with rhodopsin suggests two key phosphorylation sites (pT340 and pS343) at the C-terminus necessary for beta arrestin binding.[28] Typical beta arrestin recruitment is a rather fast-paced mechanism and occurs within minutes.[29,30]

1.2.2.2 Beta arrestin-facilitated GPCR internalization

Besides receptor desensitization, beta arrestin binding also facilitates endocytosis of activated GPCRs. Indeed, beta arrestins are essential for receptor internalization upon agonist-induced receptor activation.[31] Beta arrestin binding to the GPCR enables beta arrestin interaction with adaptor protein 2 (AP2) which promotes endocytosis of the receptor-complex (Figure 3B). AP2 is a clathrin-adaptor that facilitates formation of clathrin-coated pits at the cell membrane, causing invagination of the activated GPCR. This is followed either by receptor recycling and new recruitment to the cell membrane or receptor degradation. Two patterns of receptor recruitment are described: Class A receptors (i.e. beta2-adrenergic receptors) are known for their low-affinity beta arrestin binding resulting in rather rapid recycling of the receptor upon internalization. Class B receptors (i.e. Angiotensin II receptor type 1A ($AT1_A$) are characterized by a much stronger beta arrestin binding and thus much slower receptor recycling.[20,27]

1.2.2.3 Beta arrestins and their new role as scaffolding proteins

In the past decade, a new role for beta arrestins as scaffolding proteins has been discovered. Besides their classical function as facilitators of receptor desensitization and internalization, they affect multiple signaling pathways upon binding to the GPCR. One of the first and most relevant discoveries of beta arrestin-mediated scaffolding function was the activation of MAPKs (Figure 3C). MAPKs describe a family of serine/ threonine kinases including ERK1/2, p38 kinases and c-Jun N-terminal kinases (JNK). These downstream effectors of MAPK are relevant for a huge variety of different cellular functions and signaling pathways.[27,32,33] For example, Defea et al. have shown that beta arrestins recruit the tyrosine kinase c-Src and that this recruitment is indeed necessary for the apoptosis-preventing effects of substance P.[34] Next, Lutrell et al. described the formation of a complex consisting of beta arrestin 2, ERK1/2, Raf-1 and MEK-1 upon activation of the $AT1_A$ receptor.[35] These pioneer discoveries gave rise to a completely new field of research about the effects of beta arrestins beyond desensitization and internalization. These findings indicate that beta arrestins can function as scaffold proteins for multiple signaling pathways by forming protein complexes and recruiting signaling molecules.[27]

1.2.3 GPCR downstream signaling: G protein subtypes and their role in tone regulation of vessels

While GRKs and beta arrestins represent the main regulators of GPCR function, signal transduction from receptor activation to actual cellular responses is mainly driven by G protein activation. The inactive G protein is a heterotrimeric complex consisting of a Gα and a Gβγ subunit. When both subunits are bound, the Gβγ subunit acts as a negative regulator for the Gα subunit. Upon G protein activation, both subunits dissociate and activate a wide array of signaling pathways. Gα subunit

downstream targets include ACs, PLCβ and RhoA which modulate vascular tone in various ways. Signaling of the Gβγ subunit appears similarly complex as Gα subunit signaling, but only little is known about its actual impact on tone regulation. The ability to recruit GRKs upon activation of the GPCR, thus participating in the modulation of the GPCR turn-off, appears to be a crucial mechanism of the Gβγ subunit.[36] Most GPCRs couple to different G proteins, which makes the understanding of signal transduction and downstream signaling targets very complex.[37] According to the topic of my thesis, the following chapters will introduce most relevant Gα subunit signaling pathways in vascular tone regulation.

1.2.3.1.1 Activation of $G\alpha_{q/11}$ and $G\alpha_{12/13}$ promotes contraction in VSMCs

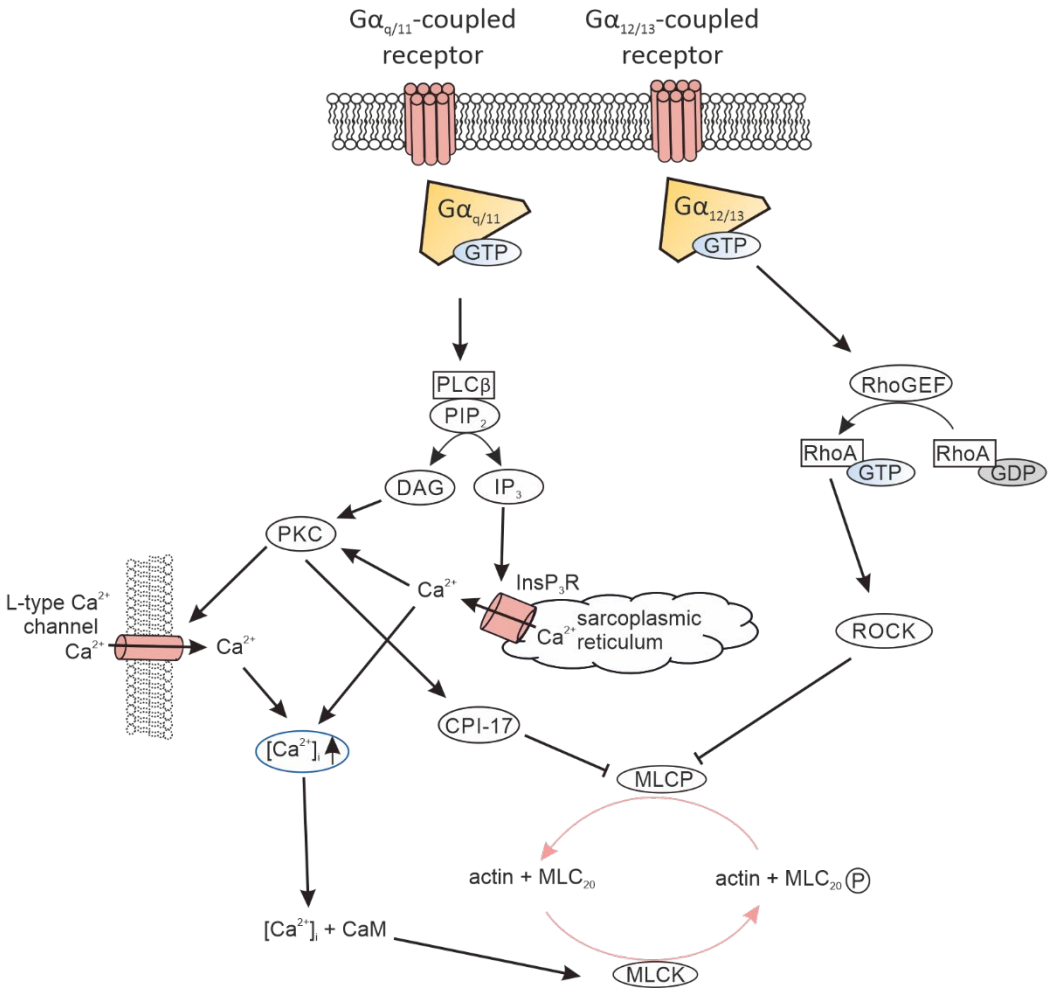

Figure 4: $G\alpha_{q/11}$ and $G\alpha_{12/13}$ downstream signaling in VSMC
Activation of $G\alpha_{q/11}$ and $G\alpha_{12/13}$-coupled receptors causes contraction of VSMCs. $G\alpha_{q/11}$ activates phospholipase C (PLC), an ezyme class responsible for the cleaveage of phospohatidylinositol-4,5-bisphosphate (PIP_2) in diacylglycerol (DAG) and inositol triphosphate (IP_3). IP_3 bindes to inositol triphospohate receptors ($InsP_3R$), releasing Ca^{2+} from the sarcoplasmic reticulum to the cytosol. Increased cytosolic Ca^{2+} levels and DAG activate proteinkinase C (PKC), an enzyme that opens L-type Ca^{2+} channels and enables a Ca^{2+} influx. Further, PKC phosphorylates protein phosphatase 1 regulatory subunit 14A (CPI-17) and subsequently inhibits MLCP. Increased intracellular Ca^{2+} interacts with calmodulin (CaM) and promotes MLCK activity. In total, activation of MLCK and inhibition of MLCP result in increased phosphorylation of MLC_{20} and thus increased contraction of VSMCs. Activation of $G\alpha_{12/13}$ promotes activation of the GTP-binding protein RhoA via the guanine exchange factor RhoGEF: activated RhoA stimulates the Rho kinase (ROCK) that inhibits MLCP and thus promotes VSMC contraction.

Activation of $G\alpha_{q/11}$ stimulates the enzyme phospholipase Cβ (PLCβ) which subsequently breaks phosphatidylinositol-4,5-bisphosphate (PIP_2) down into the second messenger molecules diacylglycerol (DAG) and inositol triphosphate (IP_3) (Figure 4). Cytosolic IP_3 causes Ca^{2+}-release by activation of Inositol triphosphate receptors ($InsP_3R$) on the surface of the sarcoplasmic reticulum. DAG, together with Ca^{2+}, recruits and activates protein kinase C (PKC).[10,38] Activated PKC phosphorylates different effectors i.e. protein phosphatase 1 regulatory subunit 14A (CPI-17) or L-type Ca^{2+} channels. Phosphorylated CPI-17 inhibits MLCP, while phosphorylation of L-type Ca^{2+} channels result in further increase of intracellular Ca^{2+} levels. Increased intracellular levels of Ca^{2+}, as well as reduced MLCP activity, promote the previously described (chapter 1.1.3.1) cross-bridge mechanism and result in contraction of VSMCs.[10,38] Well-known $G\alpha_{q/11}$-coupled receptors in VSMCs causing vasoconstriction are the muscarinic acetylcholine (M_1 and M_3) receptors, the adrenaline and noradrenaline (α_1) receptor, the angiotensin II (AT_1) and endothelin-1 ($ET_{A,\ B}$) receptor or the prostaglandin E_2 (EP_1) receptor.

Activated $G\alpha_{12/13}$ subunits signal via the guanine-exchange factor RhoGEF and are known to activate the small GTP-binding protein Ras homolog family member A (RhoA). RhoA activates the Rho kinase (ROCK) and ROCK phosphorylates the regulatory myosin-binding subunit of MLCP. Phosphorylation and thus inactivation of MLCP increases cross-bridge activity and leads to a Ca^{2+}-independent contraction. [10,38,39] While activation of $G_{q/11}$ results in a transient but strong contraction, activation of $G_{12/13}$ is responsible for a sustained and tonic contraction. Both signaling pathways appear to be closely connected and classical endogenously released vasoconstrictors such as endothelin-1 or angiotensin 2 are described to signal via $G\alpha_{q/11}$ and $G\alpha_{12/13}$ simultaneously, suggesting a synergistic effect of $G\alpha_{q/11}$ and $G\alpha_{12/13}$ for Ca^{2+}-dependent and Ca^{2+}-independent vasoconstriction.[10,38–40]

1.2.3.1.2 Activation of $G\alpha_s$ and inhibition of $G\alpha_{i/o}$ promotes relaxation in VSMCs

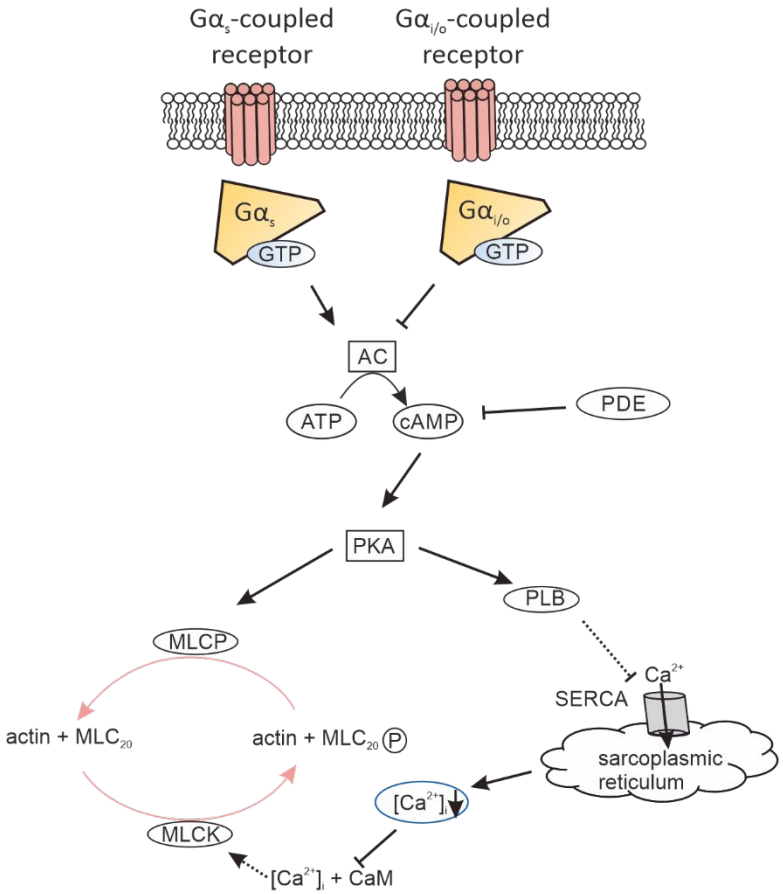

Figure 5 $G\alpha_s$ and $G\alpha_{i/o}$ downstream signaling in VSMC
Activation of $G\alpha_s$-coupled receptors promotes VSMC relaxation, while activation of $G\alpha_{i/o}$ inhibits VSMC relaxation. While $G\alpha_s$ activates the adenylyl cyclase (AC) and increases cAMP levels, activation of $G\alpha_{i/o}$ inhibits AC and decreases cAMP levels. CAMP activates proteinkinase A (PKA) but it is degraded by phosphodiesterases (PDE). PKA phosphorylates phospholamban (PLB) and activates MLCP. Unphosphorylated PLB inhibits sarcoplasmic reticulum Ca^{2+}-ATPase (SERCA) activity while phosphorylation of PLB enhances SERCA activity and results in a Ca^{2+} uptake from the cytosol to the sarcoplasmatic reticulum. Decreased intracellular Ca^{2+} results in lowered Ca^{2+}- CaM interaction and decreased MLCK activity. In total, an increased MLCP and a decreased MLCK activity upon $G\alpha_s$-activation results in decreased phosphorylation of MLC_{20} and thus promotes relaxation of VSMCs.

Upon activation, $G\alpha_s$ subunits activate ACs, a class of membrane-bound enzymes that catalyze the transformation of adenosine triphosphate (ATP) to the second messenger molecule cyclic adenosine monophosphate (cAMP) (Figure 5). In contrast, activated $G\alpha_{i/o}$ subunits inhibit AC and thus lower cAMP levels.[13] CAMP is able to directly activate protein kinase A (PKA).[38] PKA promotes relaxation of VSMCs in at least two ways: it activates MLCP leading to dephosphorylation of MLC_{20} and a lowered myosin-actin interaction. Furthermore, it phosphorylates phospholamban (PLB), an important controller of the intracellular calcium balance. Unphosphorylated PLB inhibits sarcoplasmic reticulum Ca^{2+}-ATPase (SERCA) activity. SERCA is responsible for Ca^{2+} reuptake in the sarcoplasmic reticulum. A phosphorylation of PLB by PKA leads to increased SERCA activity and to decreased cytosolic Ca^{2+} levels.[41,42] Both mechanisms, MLCP activation and Ca^{2+} reuptake result in vasorelaxation. Well-known

examples for $G\alpha_s$-coupled receptors are the beta1- and beta2-adrenergic (β_1 and β_2) receptors, while the alpha2-adrenergic (α_2) receptor is $G\alpha_{i/o}$-coupled.

Cellular cAMP levels are controlled by $G\alpha_s$ and $G\alpha_{i/o}$ -coupled receptors modulating AC activity. However, also phosphodiesterases (PDEs) control cyclic nucleotide levels directly by degradation of the phosphodiester bond of cyclic nucleotides such as cAMP or cGMP resulting in AMP or GMP molecules (overview in Figure 6).[38] 11 families of PDEs are currently described in literature. These molecules enable a precise regulation of local cyclic nucleotide levels depending on their expression and distribution throughout the body. PDE isozymes commonly exist as dimers and various isoforms are further subdivided into different PDE families.[43,44]

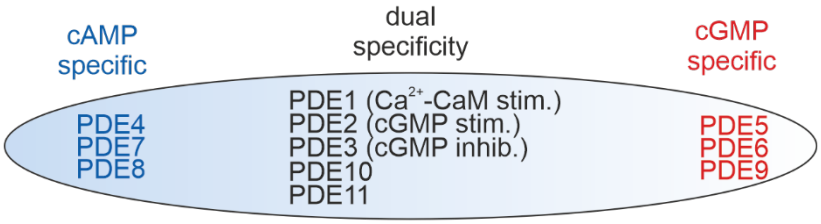

Figure 6: Classification of the PDE family.
PDEs may be classified with respect to their cyclic nucleotide target: PDE4, 5 and 8 are described as cAMP-specific. PDE5, 6 and 9 are known as cGMP-specific. Dual specificity is given for PDE1, 2, 3, 10 and 11. Further differences exist in regard to enzyme stimulation: PDE1 is known to be stimulated by Ca^{2+}-CaM, while PDE2 can be stimulated by cGMP and PDE3 is inhibited by cGMP.

While some PDE families are cAMP or cGMP-specific, most are dualspecific and able to degrade both cyclic nucleotides at different hydrolysis rates (overview in Figure 6). Besides targeting cAMP or cGMP to a different extent, differences also exist in the stimulation mechanism: While PDE1 is stimulated by the Ca^{2+}-CaM complex, PDE2 is stimulated by allosteric cGMP binding and the cAMP degrading capacity of PDE3 is dampened by cGMP binding. These examples emphasize that PDEs -besides direct cyclic nucleotide degradation- further participate in the cAMP/cGMP crosstalk and thereby allow an interplay of different signaling pathways.[43]

1.2.4 The canonical NO-cGMP-PKG signaling pathway in VSMCs

While cAMP and subsequent downstream signaling is directly modulated by $G\alpha_s$ and $G\alpha_{i/o}$ activation, the NO-cGMP-PKG signaling pathway is only indirectly modulated by GPCR activity. The NO-cGMP-PKG signaling pathway plays a critical role in VSMC tone regulation as NO is one of the strongest endogenous vasorelaxants. This signaling axis connects endothelial and vascular smooth muscle cells.[45]

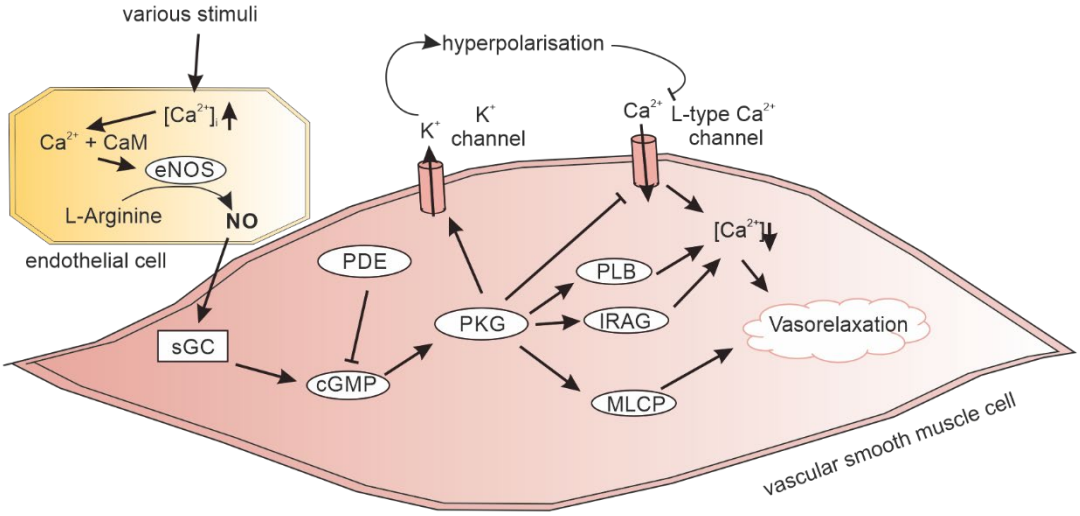

Figure 7 Signaling pathway of NO-mediated VSMC relaxation
Endothelial NO production evokes relaxation of VSMCs. Various stimuli such as activation of Gq-coupled receptors or shear stress increase intraendothelial Ca^{2+} levels. Ca^{2+} binds to CaM and activates the endothelial NO synthase (eNOS). NO is generated by eNOS and difuses into the VSMC where it activates the soluble guanylyl cyclase (sGC). The sGC enzyme generates cGMP that can be degraded by PDE. PKG is activated by increased cGMP levels and affects multiple signaling pathways resulting in vasorelaxation. It opens K^+ channels, causing a K^+ efflux-mediated hyperpolarization of the VSMC. The hyperpolarization reduces L-Type Ca^{2+} channel-mediated Ca^{2+} influx. Additionally, it further phosphorylates and thus inhibits L-type Ca^{2+} channels directly, resulting in decreased Ca^{2+} influx. It phosphorylates PLB and $InsP_3R$- associated PKG substrate isoform A (IRAG). Phosphorylation of PLB enables SERCA activity and results in Ca^{2+} uptake from the cytosol to the sarcoplasmatic reticulum. Phosphorylated IRAG prohibits Ca^{2+} release from the sarcoplasmic reticulum via $InsP_3R$. Decreased intracellular Ca^{2+} results in lowered Ca^{2+}- CaM interaction and decreased MLCK activity. Increased MLCP and decreased MLCP activity result in relaxation of the VSMC.

1.2.4.1 Activity of eNOS controls NO production in the vascular endothelial cell

NO is a small gaseous molecule with a very short half-life that is generated by either neuronal, inducible or endothelial nitric oxide synthase (nNOS; iNOS; eNOS). ENOS is responsible for the NO production in the vascular system. The eNOS enzyme is modulated by intraendothelial Ca^{2+}, Ca^{2+}-CaM binds to a corresponding domain of the eNOS enzyme leading to NO generation. In endothelial cells intracellular Ca^{2+} is regulated by various different stimuli. For example, humoral agonists such as acetylcholine cause a Ca^{2+} release via activation of the $G\alpha_q$-coupled endothelial M3 receptors while physical stimuli such as shear stress increase Ca^{2+} levels by a mechanism not yet understood completely.[46] Upon formation in the endothelial cell, NO diffuses into the smooth muscle cell and activates the sGC enzyme selectively.

1.2.4.2 The sGC as a unique and important regulator of VSMC relaxation

cGMP is generated in VSMCs by two different forms of guanylyl cyclases, the soluble guanylyl cyclase (sGC) and the particulate guanylyl cyclase (pGC). The pGC is a membrane-bound receptor and different

isoforms exist in the human body. Known agonists are natriuretic peptides which can be further subcategorized into atrial natriuretic peptide (ANP), brain natriuretic peptide (BNP) and natriuretic peptide type C (CNP).[47]

The sGC is a cGMP-generating enzyme located in the cytoplasm of the cell. It is a heterodimeric protein consisting of an α- and a β- subunit. Acting as intracellular NO receptor, activation of the enzyme by its endogenous ligand NO causes a conformational change leading to the formation of cGMP.[48]

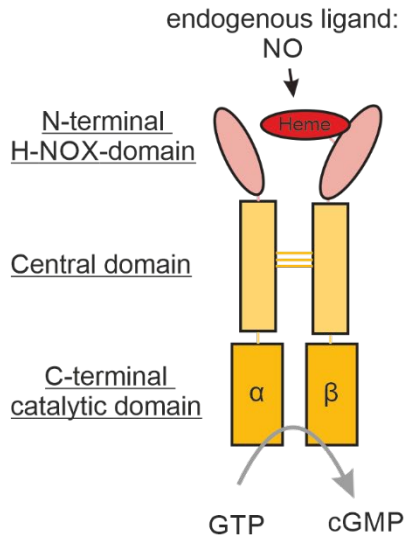

Figure 8: Structure of the soluble guanylyl cyclase (sGC).
The sGC heterodimer consists of an α- and a β-subunit. Each subunit contains a C-terminally located catalytic domain, a central domain responsible for dimerization and a N-terminally located heme-nitric oxide binding domain (H-NOX). The β-subunit contains an N-terminally located heme group, which enables binding of the endogenous ligand NO. NO binding causes a conformational change of the enzyme, leading to increased catalytic activity at the c-terminus.

Two different α subunits are described. α_1 is found to be highly expressed in all sGC-expressing cell types, while α_2 is primarily expressed in the brain. Even though there is genetic evidence that a β_2 subunit exists, the β_1 subunit is the only physiologically relevant binding partner for the α subunits in the human body. Homodimers are existent, however, only heterodimers are catalytically active.[49] The heterodimer can be structurally divided into three parts: The catalytic C-terminus responsible for cGMP generation, the central part mainly involved in dimerization and the N-terminus as the NO-binding site.

The β subunit contains a heme-binding domain located at its N-terminal site that enables NO binding. The prosthetic heme group is mandatory for sGC activation by endogenous NO and removal of the heme group abolishes any NO-mediated activity.[49,50] The prosthetic heme group at the β subunit contains a five-coordinated ferrous (Fe^{2+}) heme with a histidine (His-105) as its axial ligand and coordinating residue. Binding of NO occurs at the sixth position of the complex and results in an intermediate NO- Fe^{2+}-His complex. Next, a conversion to a five-coordinated nitrosyl heme complex is

described and the histidine bond is broken, resulting in the conformational change of the enzyme and the increased catalytic activity.[49,51] The histidine (His-105) as the axial ligand as well as the iron ion in its ferrous state is necessary for proper sGC function: mutations in the histidine site or oxidation to the ferric form (Fe^{3+}) lead to an insensitivity of the sGC enzyme for its endogenous ligand NO.[52,53]

Besides the endogenous ligand NO that can be also produced by synthetic NO donors, pharmacological sGC activators and stimulators exist that reportedly activate sGC by different mechanisms.[49]

1.2.4.3 Role of cGMP in vascular tone regulation

The cyclic nucleotide cGMP is degraded by PDEs. Thus, PDEs remain a crucial controller of cGMP-mediated vasorelaxation and cGMP-specific PDEs (i.e. PDE5) are established targets of modern pharmacotherapy.[54] Effects of cGMP on vascular tone are primarily mediated by activation of protein kinase G (PKG), while also cGMP-gated ion channels and allosteric PDE modulation should be mentioned. By binding to allosteric sites of the PKG enzyme, cGMP increases PKG phosphotransferase activity and affects various downstream targets. There exist two families of PKG, but only PKG1 is involved in NO-mediated cGMP signaling. There are two isoforms of PKG1 (PKG1α and PKG1β), both isoforms exist as homodimers. They are activated by allosteric binding of cGMP in the PKG regulatory domain, resulting in increased phosphotransferase activity.[55] Most relevant interactions for the relaxation of VSMCs will be introduced:

PKG is a modulator of PLB and MLCP, resulting in increased sarcoplasmic Ca^{2+} reuptake and decreased actin-myosin interaction. Furthermore, PKG opens Ca^{2+} -sensitive K^+ channels and the gradient-dependend K^+ efflux causes hyperpolarization of the VSMC. This hyperpolarization decreases Ca^{2+} influx via L-Type Ca^{2+} channels and in addition PKG directly inhibits these Ca^{2+} channels by phosphorylation. Finally, PKG phosphorylates the $InsP_3R$ -associated PKG substrate isoform A (IRAG) at the sarcoplasmic reticulum, resulting in decreased Ca^{2+} release.[56] In total, PKG lowers intracellular Ca^{2+} and increases MLCP activity, resulting in relaxation of the VSMC (Figure 7).

Intracellular crosstalk is given by interaction with PKA, RhoA, sGC and PDE5 activity.[55] The interaction of PKG with PKA and RhoA represents a cross-talk between the cGMP signaling pathway and GPCR signaling. Inhibition of sGC activity and increased PDE5 activity represent a negative feedback mechanism for the sGC-cGMP-PKG signaling axis.[55]

The paracrine effect of endothelial NO and the strong sGC expression in VSMCs reveal the NO-sGC-PKG signaling pathway as a relevant signaling axis for vasorelaxation. In contrast to the GPCR-mediated cAMP signaling pathway in VSMCs, generation of cGMP by NO is indirectly GPCR-dependent: while

generation of NO by the eNOS enzyme in the endothelium is partially driven by GPCR (i. e. M_3 receptors) activation, the NO signaling cascade does not rely on GPCR activation in the VSMC.

Disturbances in the NO-sGC-PKG signaling pathway are relevant in various cardiovascular diseases. Therefore the sGC enzyme is a promising target for specific pharmacotherapy.[45] An indication for sCG modulators is pulmonary arterial hypertension (PAH), where NO-mediated vasorelaxation represents current state-of-the-art therapy. The current role of beta arrestins in PAH is unknown.

1.3 Pulmonary arterial hypertension (PAH): a paradigm of dysregulated (pulmonary) vascular physiology

1.3.1 PAH and its clinical appearance

PAH is a severe disease with an incidence ranging from 2.0 to 7.6 cases per million adults and year. It is characterized by a dynamic obstruction due to vasoconstriction of PAs and by structural obstruction due to adverse vascular remodeling.[57,58] PAH is classified as a sub form of pulmonary hypertension (PH). PH is defined as a hemodynamic state characterized by an increased (≥ 25 mm Hg) resting mean pulmonary arterial pressure (PAPm).

The different PH subforms substantially differ in terms of incidence, relevance and treatment.[59] The WHO classifies PH into 5 groups depending either on its origin or associated malfunctions.

Table 1: WHO-classification of PH

WHO-classification of PH				
WHO group 1 pulmonary arterial hypertension (PAH)	WHO group 2 PH due to left heart disease	WHO group 3 PH due to lung disease	WHO group 4 Chronic thromboembolic PH (CTEPH)	WHO group 5 PH of uncertain multifactorial mechanism

*content of Table 1 has been modified from Hoeper, M. et al. 2017 - Pulmonary Hypertension. [59,60]

Cardinal symptoms of PH include increased exercise dyspnea, fatigue, edema and exercise-induced syncope.[59] PH is often caused by comorbidities such as left heart or lung disease.

1.3.2 PAH as a unique panvasculopathy in the PH setting

PAH is primarily caused by vasculopathies affecting the distal PAs.[61] It is characterized by pathophysiological alterations of all layers of the vascular wall.[61] Especially dysfunctional endothelial cells, smooth muscle cells, fibroblasts and immune cells contribute to disease progression.[57] An abnormal muscularization of distal, normally non-muscularized PAs, is an early sign for PAH development. In later stages, hyperplasia of the intima is described and this is linked to insufficient NO

generation as well as formation of abnormal channels in the vessel lumen.[62] A fully- developed PAH shows a strong phenotype of proliferation of endothelial cell in the intima, of smooth muscle cells in the media and of fibroblasts in the adventitia. This potentially leads to a complex interplay of endothelial dysfunction, vascular obstruction and fibrosis-induced vascular stiffening.[57]

1.3.3 Treatment of PH

PH is characterized by a plethora of different clinical symptoms and therapy greatly differs between different groups of PH. For the treatment of PAH six classes of drug (Table 2) are currently approved.[63] Treatment of PH group 2 and 3 targets primarily underlying diseases, namely left heart and lung disease, while drugs approved for PAH (PH group 1) treatment seem to be ineffective for these types of PH.[59] Treatment of choice for chronic thromboembolic pulmonary hypertension (CTEPH) is surgical pulmonary endarterectomy.

Table 2: Drug classes for PAH treatment

Drug classes for treatment of PAH					
Calcium channel blockers	Endothelin receptor antagonists	Phosphodiesterase type 5(PDE5) inhibitors	Guanylate cyclase stimulators	Prostacyclin analogues	IP receptor agonists

*content of Table 2 has been modified from Galiè, N. et al. 2015:
ESC/ERS Guidelines for the diagnosis and treatment of pulmonary hypertension.[63]

To date PAH remains incurable. The PAH treatment aims at symptom control and prevention of disease progression.[59] The selection of specific drug classes (Table 2) for mono or combi treatment is highly dependent on the severity of the PAH as well as the individuals response to the treatment.[59]

Besides the severity of diagnosed PAH also the clinical phenotype determines PAH treatment. Moreover also the course of the disease (typical or nontypical) as well as the bioavailability of oral drugs compared to intravenously applied drugs determine the choice of medication.[59]

1.3.4 Molecular mechanisms of drugs used in PAH treatment

1.3.4.1 Calcium channel blockers

Increasing Ca^{2+} concentrations in VSMCs lead to cross-bridge formation between myosin and actin and thus result in vasoconstriction.[42] Inhibition of L-type Ca^{2+}-channels by calcium channel blockers in the cell membrane results in lower intracellular Ca^{2+} concentrations and reduces vasoconstriction.[64]

1.3.4.2 Endothelin receptor antagonists

The polypeptide endothelin-1 is a very strong endogenous vasoconstrictor and secreted mainly from endothelial cells.[65] Endothelin-1 binds to different GPCRs, however vascular vasoconstriction is mainly driven by activation of $G_{q/11}$-coupled ET_A receptors. Activation of this receptor in VSMC results in

vasoconstriction by increasing Ca^{2+} concentrations released from the sarcoplasmic reticulum and by L-type Ca^{2+} -channel dependent influx.[66] Inhibition of the ET_A receptor via endothelin receptor antagonists reduces vasoconstriction of VSMCs.

1.3.4.3 sGC stimulators and PDE inhibitors

Previously introduced endothelin receptor antagonists and Ca^{2+} channel blockers reduce persisting vasoconstriction. An alternative therapeutic strategy is to enhance signaling pathways that mediate vasorelaxation, i.e. by the endothelium-dependent vasorelaxants NO and prostacyclin. As previously explained, endothelium-derived NO activates the sGC and increasing cGMP levels result in vasorelaxation. This sGC-mediated vasorelaxation can be pharmacologically induced by sGC activators.[54] Furthermore, cGMP degradation can be reduced by inhibition of PDE5.[67] Both drug classes - sGC activators and PDE5 inhibitors - are used for the treatment of PAH with the aim of increased vasorelaxation.

1.3.4.4 Prostacyclin analogues and IP receptor agonists

Prostacyclin is another important endogenous vasorelaxant secreted by the endothelium. Released prostacyclin activates G_s-coupled prostacyclin receptors (IP) on the surface of smooth muscle cells resulting in increasing cAMP levels causing vasorelaxation via activation of PKA.[68] Endogenous prostacyclin has only a short half-life. Therefore stable prostacyclin analogues and selective IP-receptor-agonists have been developed for and are currently used in the treatment of PAH.[63]

Remarkably, most of today`s approved drugs for PAH treatment either target GPCRs (endothelin receptor antagonists, prostacyclin analogues, IP agonists) directly or affect second messenger modulation (calcium channel blockers, PDE inhibitors, sGC stimulators). Furthermore, the development of PAH appears to be closely related to a disbalance of GPCR expression.[69]

Clinical trials classify PAH treatment with currently available drugs only as modest in regard to improvement of functional readouts (i.e. 6-minute walking test) and hemodynamics.[57,70] This underlines the urgent need for a better pathophysiological understanding of the disease and subsequent development of new pharmacological tools decreasing mortality.

1.4 Potential role of beta arrestins for vascular and lung physiology

Beta arrestins are well-known regulators of GPCR signaling and thus affect many physiological and pathophysiological processes that involve GPCR activation. The beta arrestin-mediated desensitization and internalization of GPCRs has been investigated and generation of genetically modified mice lacking beta Arr1 or 2 has allowed for intensive beta arrestin research in animal models. In contrast, the idea

of beta arrestins acting as scaffolding molecules is rather new and knowledge in this research field is still expanding.[71]

1.4.1 The role of beta arrestins in the functionality of airways smooth muscle cells

Relaxation of airway smooth muscle cells (ASMC) is essential for the management of bronchospasm in obstructive lung diseases. Desensitization and thus loss of response of beta2-adrenergic receptor signaling due to excessive inhalation of beta2-agonists in the treatment of asthma is one of the best-known examples of receptor downregulation in modern pharmacology. Deshpande et al. have addressed this desensitization phenomenon in an extensive study. They were able to show that the ablation of the beta Arr2 gene increases beta2-agonist-mediated ASM relaxation in murine tracheal rings. Moreover they demonstrated that the classical desensitization of beta adrenergic receptors by beta arrestins is of functional relevance for murine bronchorelaxation *in vivo*.[72] In a follow-up study, Pera et al. took a closer look at the different beta arrestin subtypes and their role for GPCR function in ASMC. They underline previous findings by proving that selective beta Arr2 knockdown or knockout (KO) augments beta2-adrenergic receptor signaling and function. Further, they highlight that selective beta Arr1 knockdown or KO does not affect beta2-adrenergic receptor signaling but selectively inhibited M3 muscarinic receptor signaling.[73] Expanding the view of beta arrestin function for asthma development beyond bronchorelaxation, Walker et al. claim that beta Arr2 is required for the development of allergic asthma. They were able to show that allergen-sensitized mice with genetic beta Arr2 deletion do not accumulate T lymphocytes in their airways and are protected from asthma-associated inflammation. This early regulation of the inflammatory cascade by beta Arr2 underlines the influence of beta arrestins on the development of allergic asthma and its potential as a future drug target.[74]

All these findings elucidate the manifold roles of beta arrestins in asthma and ASMC function. While beta Arr2 is considered to play a crucial role for bronchorelaxation and the response for asthmatic bronchodilative therapy, not much is known yet about the role of beta Arr1 in this setting.

1.4.2 Beta arrestins in the context of PAH

Little is known about the role of beta Arr1 in PAH. Only very recently, Ma et al. published a study on the role of beta Arr1 in the crosstalk between GPCRs and the vascular endothelial growth factor receptor 3 (VEGFR3) in pulmonary vascular endothelial cells. Previously, impaired VEGFR3 signaling has been linked to PH, because endothelium-specific knockout of *Vegfr3* was shown to exacerbate hypoxia-induced PH in mice.[75] Upon hypobaric hypoxia, mice lacking beta Arr1 developed a more severe PH compared to wildtype and beta Arr2-/- mice, suggesting a protective role of beta Arr1 for

PH development. Ma et al. further suggest an interaction of both beta Arr1 and VEGFR3 as a rational cause for the development of PH.[76] They claim that a direct interaction between beta Arr1 and VEGFR3 promotes VEGFR3 signaling and decreases VEGFR3 internalization. When beta Arr1 is lacking in pulmonary arterial endothelial cells, VEGFR3 signaling is reduced. This observation serves Ma et al. as central explanation for the pathogenesis of PH.[76]

This publication by Ma et al. is the first and only evidence so far for a distinctive role of beta Arr1 in the development of PH. While intensively focusing on the VEGFR signaling in the endothelium, it describes a strong phenotype of PH in beta arr1-/- mice. This underlines the role of beta arrestins as adaptor proteins by proving direct interaction with non-GPCR targets such as the VEGFR3.

2 Aim of the thesis

Since the discovery of beta arrestins as drivers of GPCR downregulation, numerous studies have been performed to evaluate the impact of these adaptor proteins. GPCRs are well-known for their role in the regulation of vascular tone and SMC differentiation. Altered expression levels and functions of GPCRs are also associated with the progression of PH.[38,69] In this context, beta arrestins are likely to play an important regulatory role for the development of PH and represent promising therapeutic targets.

While the role of beta Arr2 has been evaluated for ASMCs and the disease of allergic asthma, not much is known about beta arrestins with regard to VSMCs and PH. In 2019, Ma et al. suggested the lack of beta Arr1 expression as an important factor for the development of PH investigating signaling cascades in endothelial cells.[76] However, hardly anything is known yet about the role of beta Arr1 for tone regulation of SMCs.

This work attempts to fill this gap and analyzes the role of beta Arr 1 for tone regulation of PAs. Beta Arr1 or 2 knockout mice and HEK293 cells lacking either one or both beta arrestin subtypes were used *ex vivo*, *in vivo and in vitro* to precisely characterize the impact of beta Arr 1 on SMC-mediated vasorelaxation of PAs.

Ex vivo force measurements were performed in isolated PAs to analyze the physiological relevance of beta Arr1 for pulmonary vascular tone regulation. NO SMC signaling cascades in PA vasorelaxation were pharmacologically targeted to unravel relevant beta Arr1 interaction.

In vitro experiments in HEK293 cells were performed to evaluate the role of beta arrestins for cyclic nucleotide production. Molecular biology techniques were utilized to analyze beta Arr1-mediated effects on mRNA and protein expression levels. Immunoprecipitation experiments analyzed potential direct binding partners of beta Arr1.

Finally, *in vivo* experiments under normoxia and with hypoxia-induced PH in beta Arr1-/- mice aimed to analyze the relevance of beta Arr1 for a complex biological *in vivo* system under physiological and pathophysiological conditions. Pressure catheter measurements, analysis of right heart hypertrophy and histological analysis of lung slices assessed the role of beta Arr1 for PH.

3 Material and Methods

3.1 Chemicals and Materials

3.1.1 Chemicals used in the present work

Table 3: Chemicals

Substance	Order number	Company
1-Bromo-3-chloropropane	B9673	Sigma Aldrich (Taufkirchen, Germany)
2-Mercaptoethanol	31350010	Thermo Fisher Scientific (Waltham, USA)
2-Propanol	A0900	AppliChem (Darmstadt, Germany)
8-pCPT-cGMP	C5438	Sigma Aldrich (Taufkirchen, Germany)
Acetone	CP40.3	Carl Roth (Karlsruhe, Germany)
Acetonitrile	271004	Sigma Aldrich (Taufkirchen, Germany)
Acetylcholine (ACh)	A6625	Sigma Aldrich (Taufkirchen, Germany)
Acetyl-ß-methylcholine chlorid (Methacholine; MCh)	A2251	Sigma Aldrich (Taufkirchen, Germany)
Acrylamide 4K solution (40 %), Mix 37,5:1	A1577	AppliChem (Darmstadt, Germany)
Agarose Low Melt	6351.5	Carl Roth (Karlsruhe, Germany)
Ammonium persulfate (APS)	215589	Sigma Aldrich (Taufkirchen, Germany)
Ampuwa®	B315475	Fresenius Kabi Germany (Bad Homburg, Germany)
Aqua Poly/Mount	18606	Polysciences Europe (Hirschberg an der Bergstrasse, Germany)
BAY41-2272	4430	Tocris (Bristol, United Kingdom)
BAY58-2667	6052	Tocris (Bristol, United Kingdom)
Benzyl alcohol	366	Carl Roth (Karlsruhe, Germany)
Binding Control Agarose Beads	Bab-20	Chromotek (Planegg-Martinsried)
Bis-Benzimide H 33342 trihydrochloride (Hoechst)	B2261	Sigma Aldrich (Taufkirchen, Germany)
Bovine Serum Albumin	A2153	Sigma Aldrich (Taufkirchen, Germany)
Calcium chloride ($CaCl_2$)	C4901	Sigma Aldrich (Taufkirchen, Germany)
Chloral hydrate	47335-U	Sigma Aldrich (Taufkirchen, Germany)
Citric acid	100244	Merck über VWR (Darmstadt, Germany)
cOmplete™ Protease Inhibitor Cocktail Tabletten	11873580001	Roche Germany Holding (Grenzach-Wyhlen, Germany)
D-Glukose	G7021	Sigma Aldrich (Taufkirchen, Germany)
Dimethyl sulfoxide (DMSO)	D4540	Sigma Aldrich (Taufkirchen, Germany)
Disodium hydrogen phosphate (Na_2HPO4)	S7907	Sigma Aldrich (Taufkirchen, Germany)
Dulbecco`s Phosphate-buffered saline (DPBS) no calcium, no magnesium	14190-094	Life Technologies (Darmstadt, Germany)
Entellan®	107961	Sigma Aldrich (Taufkirchen, Germany)
Eosin Y solution 0.5 % in water	X883.2	Carl Roth (Karlsruhe, Germany)
Ethanol (EtOH) 70 % (v/v)	27669	Fischar (Saarbrücken, Germany)
Ethanol absolute for molecular biology	A8075	AppliChem (Darmstadt, Germany)
Ethidium bromide solution	46067	Sigma Aldrich (Taufkirchen, Germany)
Ethylenediaminetetraacetic acid disodium salt dihydrate (EDTA)	E4884	Sigma Aldrich (Taufkirchen, Germany)
Forskolin (Fsk)	F6886	Sigma Aldrich (Taufkirchen, Germany)
FuGENE® HD	E2311	Promega (Mannheim, Germany)

Substance	Order number	Company
G418 disulfate salt	A1720	Sigma Aldrich (Taufkirchen, Germany)
Gelatin from porcine skin	G1890	Sigma Aldrich (Taufkirchen, Germany)
GeneRuler™ DNA-ladder	SM0333	Thermo Fisher Scientific (Waltham, USA)
GFP-Trap® Agarose	Gta	Chromotek (Planegg-Martinsried)
Glycerol	49767	Sigma Aldrich (Taufkirchen, Germany)
Glycine	G8898	Sigma Aldrich (Taufkirchen, Germany)
Hämalaun Sauer nach Mayer	T865.1	Carl Roth (Karlsruhe, Germany)
Hematoxylin	104302	Merck via VWR (Darmstadt, Germany)
Heparin-Natrium 5000 U/ml	2047217	B. Braun (Melsungen, Germany)
Heparin-Natrium-25000-ratiopharm®	3029843	ratiopharm (Ulm, Germany)
HEPES	H3375	Sigma Aldrich (Taufkirchen, Germany)
IBMX	I5879	Sigma Aldrich (Taufkirchen, Germany)
Invitrogen™ TE-Puffer	12090015	Thermo Fisher Scientific (Waltham, USA)
Isoflurane (Forene®)		Abbott (Wiesbaden, Germany)
Isotonic saline 0,9%	4976844	Fresenius Kabi Germany (Bad Homburg, Germany)
Kanamycin sulfate from Streptomyces kanamyceticus	K1377	Sigma Aldrich (Taufkirchen, Germany)
Ketamine	799-760	Covetrus (Hamburg, Deutschland)
Lipofectamine ™ 3000 Transfection reagent	L3000015	Thermo Fisher Scientific (Waltham, USA)
Magnesium chloride ($MgCl_2$)	M8266	Sigma Aldrich (Taufkirchen, Germany)
Magnesium sulfate ($MgSO_4$)	M8150	Sigma Aldrich (Taufkirchen, Germany)
Methyl cellulose	M0512	Sigma Aldrich (Taufkirchen, Germany)
Myc-Trap® Agarose	yta-20	Chromotek (Planegg-Martinsried)
N,N,N',N'-Tetramethylethylenediamine (TEMED)	T7024	Sigma Aldrich (Taufkirchen, Germany)
Normal Donkey Serum	017-000-121	Jackson ImmunoResearch (Suffolk, England)
Phenylephrine hydrochloride	P6126	Sigma Aldrich (Taufkirchen, Germany)
Pierce™ Protein A Agarose	20334	Thermo Fisher Scientific (Waltham, USA)
Polyethylenimine, branched	408727	Sigma Aldrich (Taufkirchen, Germany)
Polyvinyl alcohol mounting medium with DABCO®, antifading (Fluka)	10981	Sigma Aldrich (Taufkirchen, Germany)
Potassium alum	102042	Merck via VWR (Darmstadt, Germany)
Potassium chloride (KCl)	P9333	Sigma Aldrich (Taufkirchen, Germany)
Precision Plus Protein™ Dual Color Standards	161-0374	BioRad Laboratories (Feldkirchen, Germany)
PTFE Paste	C50875	ÄRONIX Spezialschmierstoffe (Walldorf, Germany)
Restore™ Western Blot Stripping Buffer	46430	Thermo Fisher Scientific (Waltham, USA)
Richard-Allan Scientific™ Paraffin Typ 1, 3, 6, 9	8335	Thermo Fisher Scientific (Waltham, USA)
RNAlater stabilization solution	AM7024	Thermo Fisher Scientific (Waltham, USA)
RNAse Zap	R2020	Sigma Aldrich (Taufkirchen, Germany)
Rolfumilast (Roflu)	SML1099	Sigma Aldrich (Taufkirchen, Germany)
ROTI®Histofix 4 %	P087.1	Carl Roth (Karlsruhe, Germany)
Schiff's reagent	X900.2	Carl Roth (Karlsruhe, Germany)
Sildenafil citrate salt	PZ0006	Sigma Aldrich (Taufkirchen, Germany)
Skim Milk Powder	70166	Sigma Aldrich (Taufkirchen, Germany)
Sodium bicarbonate ($NaHCO_3$)	S6297	Sigma Aldrich (Taufkirchen, Germany)
Sodium Chloride (NaCl)	S5586	Sigma Aldrich (Taufkirchen, Germany)
Sodium dodecyl sulfate (SDS)	L4390	Sigma Aldrich (Taufkirchen, Germany)
Sodium hydrogen phosphate (Na_2HPO4)	S7907	Sigma Aldrich (Taufkirchen, Germany)
Sodium hydroxide (NaOH)	S8045	Sigma Aldrich (Taufkirchen, Germany)

Substance	Order number	Company
Sodium iodate ($NaIO_3$)	106525	Merck über VWR (Darmstadt, Germany)
Sodium nitroferricyanide (III) dihydrate (SNP)	228710	Sigma Aldrich (Taufkirchen, Germany)
TissueTek® O.C.T. ™ Compound	4583	Sakura Finetek Germany (Staufen, Germany)
Triton X-100	T8787	Sigma Aldrich (Taufkirchen, Germany)
Trizma® Base (TRIS base)	93352	Sigma Aldrich (Taufkirchen, Germany)
TRIzol®	15596-018	Life Technologies (Darmstadt, Germany)
Tween 20	P9416	Sigma Aldrich (Taufkirchen, Germany)
Tween 80	P4780	Sigma Aldrich (Taufkirchen, Germany)
UltraPure DNAse/RNAse freies Wasser	12060346	Thermo Fisher Scientific (Waltham, USA)
Xylazine		Alvetra (Neumünster, Deutschland)
Xylene	2517692714	AppliChem (Darmstadt, Germany)

3.1.2 Consumables

Table 4: Consumables

Consumables	Company
Austerlitz Insect pins	Entomoravia (Slavkov u Brna, Czech Republic)
Axygen® 0.5 mL thin wall PCR tubes	Corning (Kaiserslautern, Germany)
BD Micro-Fine™ insulin syringe	BD (Heidelberg, Germany)
BD Microlance 3™ Needles (27Gx1/2)	BD (Heidelberg, Germany)
BD Microlance 3™ Needles Nr.1 (20Gx11/2)	BD (Heidelberg, Germany)
BD Microlance 3™ Needles Nr.17 (24Gx1)	BD (Heidelberg, Germany)
Cell culture flask Falcon® (25 & 75 cm2)	VWR (Langenfeld, Germany)
Cell culture plate Falcon® (35 mm, 24 well, 6 well)	Corning (Kaiserslautern, Germany)
Cellstar® Cell culture dish 60/15mm	Greiner bio-one (Frickenhausen, Germany)
Combitips advanced® 0,5ml, 5ml	Eppendorf (Hamburg, Germany)
Conductive Filter tips, (50 & 200 µl)	Qiagen (Hilden, Germany)
Corning® Thermowell™ GOLD 0.2 mL Polypropylene PCR Tubes with Flat Cap	Corning (Kaiserslautern, Germany)
Cover slips (24x50mm, 12 mm, 30 mm)	VWR International (Darmstadt, Germany)
Cryotubes 1,8 ml	Thermo Fisher Scientific (Waltham, USA)
Falcons (15 & 50 ml)	VWR (Langenfeld, Germany)
Hard-Shell® 96-Well PCR Plates	Bio-Rad Laboratories (Feldkirchen, Germany)
Immersol™ 518F	Carl Zeiss (Oberkochen, Germany)
Insuline syringe Omnican® U-40	B. Braun (Melsungen, Germany)
Leukosilk®	BSN medical (Hamburg, Germany)
Microscope slides	VWR (Langenfeld, Germany)
Microseal 'B' PCR Plate Sealing Film, adhesive, optical	Bio-Rad Laboratories (Feldkirchen, Germany)
Mikrotom blade C35	Pfm medical (Köln, Germany)
Omnican® 40, U-40-Insulin, 0,30 x 12 mm G 30	B. Braun Melsungen AG (Melsungen, Germany)
Parafilm M	Bemis Company Inc. (Oshkosh, USA)
Pasteur pipettes (1 & 3 ml)	VWR (Darmstadt, Germany)
Pipette tips	Sarstedt (Nümbrecht, Germany)
Pipette tips with filter	Nerbe plus (Winsen, Germany)
PTFE paste	Äronix (Walldorf, Germany)

Consumables	Company
razor blades	Wilkinson (Solingen, Germany)
Reaction tubes (0,2 & 0,5 ml)	VWR (Darmstadt, Germany)
Reaction tubes (2 & 1,5 ml)	Sarstedt (Nümbrecht, Germany)
Reaction tubes 1,5 ml Safe-lock	Eppendorf (Hamburg, Germany)
Rotor-Disc 100	Qiagen (Hilden, Germany)
Rotor-Disc Heat Sealing Film	Qiagen (Hilden, Germany)
Serological pippets (5 & 10 & 25ml)	Greiner bio-one (Frickenhausen, Germany)
Silk treat	Gütermann (Gutach-Breisgau, Germany)
Stainless Steel Beads, 7 mm	Qiagen (Hilden, Germany)
Syringe (2 & 5 ml)	BD (Heidelberg, Germany)
Tissue-Tek® Mega-Cassette™	Sakura Finetek (Staufen, Germany)
VDF-FL Membrane, Low Fluorescence	Biozym Scientific (Hessisch Oldendorf, Germany)
Venofix®, 21 G	B. Braun (Melsungen, Germany)

3.1.3 Laboratory instruments and equipment

Table 5: Instruments and equipment

Instrument/Equipment	Company
Anesthetic vaporizer 19.3 (Isoflurane)	Dräger (Lübeck, Germany)
Aria Pressure-Volume Conductance System	Millar (Houston, USA)
Camera AxioCamMrc5	Carl Zeiss (Oberkochen, Germany)
Catheter 1.4F	Millar (Houston, USA)
Centrifuge VWR Mini Star	VWR (Darmstadt, Germany)
CFX96 Touch™ Real-Time PCR Detection	Bio-Rad Laboratories (Feldkirchen, Germany)
ChemiDoc™ MP Imaging System	Bio-Rad Laboratories (Feldkirchen, Germany)
CO2-Inkubator Hera Cell 240i	Thermo Scientific (Waltham, USA)
DUMONT - forceps	Plano (Wetzlar, Germany)
Duomax rocker 1030	Heidolph (Schwabach, Germany)
Fine scale XS205	Mettler Toledo (Gießen, Germany)
Fluorescence camera Axiocam 512 mono	Carl Zeiss AG (Oberkochen, Germany)
Freezer (-20°C, -80°C)	Thermo Scientific (Waltham, USA)
Fridge (4°C)	Liebherr (Biberach an der Riss, Germany)
Gel chamber for electrophoresis (Mini-PROTEAN Tetra System)	Bio-Rad Laboratories (Feldkirchen, Germany)
Gel documentation system Intas GelStick	Intas (Göttingen, Germany)
Halogen cold light source KL 1500 LCD	Schott (Mainz, Germany)
Hardened fine scissors	Plano (Wetzlar, Germany)
Heating stirrer	VWR (Langenfeld, Germany)
Heating/Cooling Dry Block CH-100	Peqlab (Erlangen, Germany)
Herasafe KS	Thermo Fisher Scientific (Waltham, USA)
Horizental shaker	Gesellschaft für Labortechnik (Burgwedel, Germany)
Hypoxia chambers	BioSpherix (Redfield, USA)
Incubator Heracell 240	Thermo Fisher Scientific (Waltham, USA)
Incubator Heratherm	Thermo Scientific (Waltham, USA)
Lab centrifuge Rotanta 460R	Hettich (Tuttlingen, Germany)
Leica HI1220 Flattening table for clinical histopathology	Leica (Wetzlar, Germany)

Instrument/Equipment	Company
Leica SM2000 R Sliding microtome	Leica (Wetzlar, Germany)
M3 Stereolupe	Wild Heerbrugg (Heerbrugg, Suisse)
Microcentrifuge 5415 R	Eppendorf (Hamburg, Germany)
Microm EC 350-1	Thermo Fisher Scientific (Waltham, USA)
Microm STP-120	Thermo Fisher Scientific (Waltham, USA)
Microscope Axiostar plus	Carl Zeiss (Oberkochen, Germany)
Microscope Axiovert 200M	Carl Zeiss (Oberkochen, Germany)
Microscope Axiovert 40C	Carl Zeiss (Oberkochen, Germany)
Microscope Leica M651 MSD	Leica (Wetzlar, Germany)
Microscope Observer Z1 with Apotome	Carl Zeiss (Oberkochen, Germany)
MiniVent Ventilator Model 845	Hugo Sachs Elektronik (March-Hugstetten, Germany)
Multi Bio RS-24	biosan (Riga, Latvia)
Multi Myograph System 620M	Danish MyoTechnology (Aarhus, Dänemark)
Multipipette E3	Eppendorf (Hamburg, Germany)
N2 container	Tec-lab (Taunusstein, Germany)
Neubauer chamber	VWR (Darmstadt, Germany)
Osmometer, Vapro 552	Wescor (Langenfeld, Germany)
OxyCycler A84	BioSpherix (Redfield, USA)
PCR Thermocycler Professional Trio	Biometra (Göttingen, Germany)
PH-Meter 765	Knick (Berlin, Germany)
Pipetboy2	Integra Biosciences (Biebertal, Germany)
Pipettes	Eppendorf (Hamburg, Germany)
Pipettes	Gilson (Limburg, Germany)
Pipetting robot Corbett Cas-1200	Corbett Life Science, jetzt Qiagen (Hilden, Germany)
Power supply for electrophoresis PowerPac™ HC	Bio-Rad Laboratories (Feldkirchen, Germany)
Powerlab 4/25 oder 16/30	ADInstruments (Spechbach, Germany)
Pressure catheter Millar 1F (1/3mm) SPR-1000	Millar (Houston, USA)
Realtime PCR Corbett Rotor-Gene 6000	Qiagen (Hilden, Germany)
Rotor Disc® Heat Sealer	Qiagen (Hilden, Germany)
Sonopuls Mini20	Bandelin (Berlin, Germany)
Spark® multimode microplate reader	Tecan (Männedorf, Schweiz)
Spectral photometer Nanodrop ND-1000	Peqlab (Erlangen, Germany)
Stereomicroscope Axio Zoom V16	Carl Zeiss (Oberkochen, Germany)
Sterile benches Hera Safe & Hera Safe KS	Thermo Scientific (Waltham, USA)
Tempered centrifuge 5415 R	Eppendorf (Hamburg, Germany)
Thermo mixer HLC (MKR13, MKR23)	Ditabis (Pforzheim, Germany)
Tissue Float Bath 1052	GFL (Burgwedel (Germany)
TissueLyser LT	Qiagen (Hilden, Germany)
Ultrasonic bath	VWR (Darmstadt, Germany)
Vacuum pump with filter	Vacuubrand (Wertheim, Germany)
Vaporiser VetMed Vapor (Isoflurane)	Dräger (Lübeck, Germany)
Vortex mixer	VWR (Darmstadt, Germany)
Western Blot equipment	Bio-Rad Laboratories (Feldkirchen, Germany)
Western Blot Trans-Blot Turbo	Bio-Rad Laboratories (Feldkirchen, Germany)
Wide Mini-Sub Cell GT Cell	Bio-Rad Laboratories (Feldkirchen, Germany)

3.1.4 Prepared buffer and solutions

TAE buffer

component	final concentration
TRIS Acetate	40 mM
Acetic acid	20 mM
EDTA	1 mM
in dH_2O	

Physiological salt solution (PSS)

component	final concentration
NaCl	118 mM
Na_2HPO_4	1.2 mM
KCl	5 mM
$MgCl_2$	1.2 mM
$CaCl_2$	1.6 mM
HEPES	24 mM
Glucose	10 mM
in dH_2O	
adjust pH to 7.4	

Physiological salt solution low Calcium (PSS low Ca^{2+})

component	final concentration
NaCl	118 mM
Na_2HPO_4	1.2 mM
KCl	5 mM
$MgCl_2$	1.2 mM
$CaCl_2$	0.16 mM
HEPES	24 mM
Glucose	10 mM
in dH_2O	
adjust pH to 7.4	

LB medium

component	final concentration
Trypton	1%
yeast extract	0.50%
NaCl	1%
in dH_2O	
autoclave prior to use	

TRIS HCl 1.5 M pH 8.8

component	final concentration
TRIS base	1,5 M
in dH_2O	
adjust pH to 8.8 with HCl	

TRIS HCl 1 M pH 6.8

component	final concentration
TRIS base	1 M
in dH_2O	
adjust pH to 6.8 with HCl	

5X loading buffer

component	final concentration
TRIS HCl 1 M pH 6.8	312,5 mM
Glycerol	50 % (V/V)
2-Mercaptoethanol	7.5 % (V/V)
SDS	10 % (m/V)
Bromphenol blue	0.1 % (m/V)
in dH_2O	

Tank blot buffer

component	final concentration
TRIS base	25 mM
Glycin	192 mM
Methanol	20% (V/V)
in dH_2O	

1X running buffer

component	final concentration
TRIS base	25 mM
Glycin	192 mM
SDS	1% (m/V)
in dH_2O	

10X TBS

component	final concentration
TRIS base	500 mM
NaCl	1.5 M
in dH2O	
adjust pH to 7.5 with HCl	

1X TBS

component	final concentration
10x TBS	10%
in dH2O	

1X TBST

component	final concentration
Tween-20	0.1 % (V/V)
in 1X TBS	

20% SDS

component	final concentration
SDS	20% (m/V)
in dH_2O	

10% APS

component	final concentration
APS	10% (m/V)
in dH_2O	

RIPA buffer

component	final concentration
NaCl	150 mM
IGEPAL®	1 % (V/V)
Sodium Deoxycholate	0.1 % (V/V)
SDS	0.1 % (V/V)
EDTA	2 mM
TRIS base	25 mM
in dH_2O	
protease inhibitors freshly added	

5% BSA

component	final concentration
BSA	5 % (m/V)
in 1X TBST	
freshly prepared prior usage	

5% skim milk

component	final concentration
skim milk powder	5 % (m/V)
in 1X TBST	
freshly prepared prior usage	

Immunoprecipitation buffer

component	final concentration
Triton-X	0.5 % (V/V)
In TBS	

3.1.5 Solutions for histology

Hoechst

component	final concentration
Hoechst 33342; 1 mg/ml	0.1 % (m/V)
in DPBS	

Eosin staining solution

component	final concentration
Eosin G-Solution, 0,5%, aqueous	0.5 % (V/V)
filtrated prior use	

Hematoxylin staining solution

component	final concentration
Hematoxylin	0.1 % (m/V)
$NaIO_3$	0.02 % (m/V)
Potassium alum	5 % (m/V)
Chloralhydrat	5 % (m/V)
Citric acid	0.1 % (m/V)
in dH_2O	
filtrated prior use	
Mayer's hemalum solution	1% (V/V)

3.1.6 Assay kits

Table 6: assay kits used in this work

Equipment	article number	Company
cGMP complete ELISA kit	ADI-901-164	Enzo life sciences (Lörrach, Germany)
EndoFree® Plasmid Maxi Kit	12362	Qiagen (Hilden, Germany)
Pierce™ BCA Protein Assay Kit	23225	Thermo Fisher Scientific (Waltham, USA)
Pierce™ ECL Western Blotting	32106	Thermo Fisher Scientific (Waltham, USA)
QIAprep® Spin Miniprep Kit	27104	Qiagen (Hilden, Germany)
SuperScript VILO	1174-050	Invitrogen (Darmstadt, Germany)
Taq DNA Polymerase, recombinant	10342020	Thermo Fisher Scientific (Waltham, USA)

3.1.7 Software

Table 7: software used in this work

Software	Company
AxioVison 4,8	Carl Zeiss (Oberkochen, Germany)
Bio-Rad ImageTM Software version 5.2.1	BioRad (München, Germany)
Biorad software q-RT-PCR	BioRad (München, Germany)
Clone Manager 9	Sci-ed Software (Westminster, USA)
Coral Draw 2020	Corel Corporation (München, Germany)
GraphPad Prism 5	GraphPad Software (La Jolla, USA)
Labchart 7	ADInstruments (Spechbach, Germany)
Microsoft Office 2019	Microsoft (Unterschleißheim, Germany)
SigmaPlot 14.0	Systat Software (Erkrath, Germany)
ZEN blue	Carl Zeiss (Oberkochen, Germany)

3.1.8 Gases

All used gases were obtained by Linde Gas Therapeutics (Oberschleißheim, Germany).

Gases used in this dissertation: oxygen (O_2), nitrogen (N_2), calibration gas for hypoxia chambers (1% CO_2 + 99 % O_2).

3.1.9 Cell culture media

Table 8: Media, buffer, supplements and growth factors

Name	Product number	Company
0.05% Trypsin-EDTA	25300054	Life Technologies (Darmstadt, Germany)
231® Medium	M231500	Thermo Fisher Scientific (Waltham, USA)
DMEM	41965-039	Thermo Fisher Scientific (Waltham, USA)
DPBS	14190-94	Thermo Fisher Scientific (Waltham, USA)
FCS	FBS-11A	Capricorn scientific (Ebsdorfergrund, Germany)
Opti-MEM	31985-070	Thermo Fisher Scientific (Waltham, USA)
Pen-Strep (Penicillin/Streptomycin)	15140-122	Life Technologies (Darmstadt, Germany)
SGMS	S00725	Thermo Fisher Scientific (Waltham, USA)
S.O.C.	15544034	Thermo Fisher Scientific (Waltham, USA)

Table 9: HEK293 cells medium

Ingredient	amount
DMEM	500 ml
FCS	50 ml
Pen-Strep (Penicillin/Streptomycin)	5 ml
*G418 Sulfate (stock: 300ug/ ml)	*833.33 µl

*added if HEK293 cells have been transfected with a plasmid containing neomycin resistance

Table 10: mPASMC medium

Ingredient	amount
231® Medium	500 ml
SGMS	25 ml
Pen-Strep (Penicillin/Streptomycin)	5 ml

3.1.10 Antibodies

Table 11: primary antibodies

Target protein	Antibody	Species	Company	Cat. No.	Dilution factor
beta Arr1	beta-Arrestin 1 (D803J) Rabbit mAb	rabbit	Cell Signalling	12697	1:1000
beta Arr2	beta-Arrestin 2 (C16D9) Rabbit mAb	rabbit	Cell Signalling	3857	1:1000
c-myc	Anti-Myc (Ab-1) Mouse mAb (9E10)	mouse	Sigma-Aldrich	OP10	1:1000
c-myc	Anti-Myc tag goat polyclonal Ab	goat	Abcam	9132	1:1000
GFP	Living Colors® A.v. Monoclonal Antibody (JL-8)	mouse	Clontech	632381	1:1000
pMBP	IgG control: anti-pMBP (#24)	rabbit	Given and generated by Institute of Biochemistry and Molecular Biology, Bonn	-	For IP usage only
sGC beta1	Anti-Guanylyl Cyclase beta1 (ER-19) rabbit polyclonal Ab	rabbit	Sigma-Aldrich	G4405	1:1000
Cyb5r3	CYB5R3 Polyclonal antibody	rabbit	proteintech	10894-1-AP	1:1000

Table 12: secondary antibodies

Antibody	Company	Car. No.	Dilution	Used for detection of
Alexa Fluor® 647 AffiniPure Goat Anti-Mouse IgG, Fcγ subclass 2a specific	Jackson ImmunoResearch	115-605-206	1:3000	c-myc, GFP
Mouse Anti-rabbit IgG (Conformation specific) (L27A9) mAb (HRP Conjugate)	Cell Signalling	5127	1:2000	beta Arr1, sGC beta1 (IP)
Peroxidase AffiniPure Goat Anti-Mouse IgG (H+L)	Jackson ImmunoResearch	115-035-146	1:10000	c-myc, GFP
Peroxidase AffiniPure Goat Anti-Rabbit IgG (H+L)	Jackson ImmunoResearch	111-035-144	1:10000	beta Arr1, beta Arr2, sGC beta1 (WB)
Peroxidase AffiniPure rabbit Anti-Goat IgG (H+L)	Jackson ImmunoResearch	305-035-003	1:10000	c-myc
Alexa Fluor® 647 AffiniPure Donkey Anti-Goat IgG, Fcγ subclass 2a specific	Jackson ImmunoResearch	705-605-147	1:3000	c-myc

3.1.11 Plasmids

GFP-beta Arr1 in pcDNA3.1+

Expression vector for the human GFP-beta Arr1 fusion protein (N-terminal fusion); gift from Prof. Evi Kostenis (Institute of Pharmaceutical Biology, Nussallee 6, 53115 Bonn).

GFP-beta Arr2 in pcDNA3.1+

Expression vector for the human GFP-beta Arr2 fusion protein (N-terminal fusion); gift from Prof. Evi Kostenis (Institute of Pharmaceutical Biology, Nussallee 6, 53115 Bonn).

GUCY1A1 Human Tagged ORF Clone in pCMV6-Entry

Expression vector for the human sGCa1 subunit (myc-DDK tagged at the C-terminus); obtained from Origene (gene number: NM_000856; cat. number: RC206063).

GUCY1B1 Human Tagged ORF Clone in pCMV6-Entry

Expression vector for the human sGCb1 subunit (myc-DDK tagged at the C-terminus); obtained from Origene (gene number: NM_000857; cat. number: RC208205).

CYB5R3 Human Tagged ORF Clone in pCMV6-Entry

Expression vector for the Human cytochrome b5 reductase 3 (CYB5R3) (myc-DDK-tagged at the C-terminus), transcript variant 1; obtained from Origene (gene number (NM_000398; cat. number: RC201592)

Laptm4a Mouse Tagged ORF Clone in pCMV6-Entry

Expression vector for the murine Laptm4a protein (myc-DDK tagged at the C-terminus); gift from Prof. Volkmar Gieselmann (Institute of Biochemistry and Molecular Biology, Nussallee 11, 53115 Bonn).

3.1.12 Experimental animals

All animal experiments were performed with in-house bred beta Arr1-/- and beta Arr2-/- mice and C57BL/6J wildtype mice obtained from Charles River (Sulzfeld, Germany) or Janvier (Le Genest St Isle, France). Animals at 8-18 weeks of age and both genders were used.

Beta Arr1-/- mice (B6.129X1(Cg)-Arrb1^{tm1Jse}/J) were obtained from Jackson Laboratories (Bar Habor, Maine, USA) [https://www.jax.org/strain/011131]. Originally, beta Arr1-/- mice were generated and described by Robert Lefkowitz from Duke University Medical Center.[77] Breeding of homozygous animals was performed in-house. C57BL/6J wildtype animals were used as controls recommended by the breeder.

Beta Arr2-/- (B6.129X1(Cg)-Arrb2tm1Rjl/J) mice were a kind gift from Prof. Jonel Trebicka (Laboratory for Liver Fibrosis and Portal Hypertension, University of Bonn). Originally, the animals were obtained from Jackson Laboratories (Bar Habor, Maine, USA) [https://www.jax.org/strain/023852]. Mice were generated and characterized by Robert Lefkowitz from Duke University Medical Center.[78] Breeding of homozygous animals was performed in-house. C57BL/6J wildtype animals were used as controls recommended by the breeder.

Correct genotype and knockout for beta Arr1 or beta Arr2 was confirmed by protein analysis in organs known for high expression of the respective proteins.

Mice were housed in a specific-pathogen-free (SPF) animal facility. Animals were exposed to 12 hours of light (6:00 AM – 6:00 PM) and darkness (6:00 PM - 6:00 AM. Mice had *ad libitum* access to food and water and were housed at a room temperature of 24 ± 1°C.

3.1.13 Qualitative PCR primer

The following PCR primers were used for qualitative PCR experiments n in murine tissue:

Table 13: Qualitative PCR primers

Primer	Sequence	length of PCR product
mur beta Arr1 for	AGCGTTAATGTCCACGTCAC	306 bp
mur beta Arr1 rev	ACGATGATGCCCAGGATTTC	
mur beta Arr2 for	ACTCTGTGCGGCTTATCATC	313 bp
mur beta Arr2 rev	GACACCTGGTCATCTTGTTC	

3.1.14 Applied Biosystems™ TaqMan® Assays

The following Applied Biosystems™ TaqMan® Assays were used for analysis of sGC gene expression in murine tissue:

Table 14: Applied Biosystems™ TaqMan® Assays

Gen symbol	Gen name	Applied Biosystems™ TaqMan® Assay	Article number
18S	18s rRNA	Eukaryotic 18S rRNA Endogenous Control	4318839
Gucy1a3	guanylate cyclase 1, soluble, alpha 3	Mm01220285_m1	4448892
Gucy1a2	guanylate cyclase 1, soluble, alpha 2	Mm01253540_m1	4448892
Gucy1b3	guanylate cyclase 1, soluble, beta 3	Mm00516926_m1	4448892

3.2 Cell culture

Two different cell lines were used in this work to characterize the role of beta Arr1 for the regulation of vascular tone. MPASMCs were isolated from wildtype and beta Arr1-/- mice. HEK293 cells were used as an alternative *in vitro* system for translation to the human system. HEK293 parental and Δbeta Arr1/2 cells were generously supplied by Prof. Evi Kostenis (Institute of Pharmaceutical Biology, Nussallee 6, 53115 Bonn) and Prof. Asuka Inoue (Graduate School of Pharmaceutical Science, Tohoku University, Sendai, 980-8578, Japan).[79] In HEK293 Δbeta Arr1/2 cells reexpression of GFP-beta Arr1 and 2 was performed in cooperation with Eva Pfeil from AG Kostenis (Institute of Pharmaceutical Biology, Nussallee 6, 53115 Bonn).

General handling of cell culture is described in chapter 3.2.1 while generation and specific handling of selected cell lines is described in detail in chapters 3.2.2 and 3.2.3.

3.2.1 General handling of cell culture

3.2.1.1 Cultivation of cell lines

Cultivation of cells was exerted under sterile conditions in an incubator at 37°C, 5% CO_2 and 100% humidity. Cultivation of mPASMCs was performed in Smooth Muscle Cell Medium (Gibco™ 231 supplemented with Gibco™ SMGS and 1% Penicillin/Streptomycin (Pen-Strep)). Cultivation of HEK293 cells was performed in Dulbecco's Modified Eagle Medium (DMEM) supplemented with 10% fetal calf serum (FCS) and 1% Pen-Strep.

3.2.1.2 Passaging of cell lines

Passaging of cells was performed when cells had reached 90% confluency. For this purpose, cell medium was aspirated and cells were washed by addition of PBS. PBS was removed and trypsin was added. Cells were incubated with trypsin for 3 min in the incubator. Upon detachment of the cells, trypsin reaction was terminated by addition of cell medium including serum. The cell solution was then centrifuged for 5 min at room temperature and 1000 rpm. The supernatant was aspirated and the cell pellet was reconstituted by addition of 1 ml medium. The cell number was determined in 10 µl of cell suspension using a Neubauer chamber. Passaging of the cells was completed by seeding the cells onto new culture flasks. Table 15 briefly summarizes passaging and cultivation procedures of the different cell lines used in this work.

Table 15: General cell culture handling

	General information		Passage		seeding density [cell number]	
Container	area	Medium volume	trypsin volume	PBS wash volume	mPASMC	HEK293
6-well plate	9,5 cm^2	2 ml	0,5 ml	2 ml	2x 10^5	3x 10^5
60 mm dish	21,5 cm^2	4 ml	0,8 ml	3 ml	2,5 x10^5	4x 10^5
25 cm^2 flask	25 cm^2	5 ml	1 ml	4 ml	3x 10^5	5x 10^5
100 mm dish	58 cm^2	10 ml	2 ml	8 ml	4x 10^5	8x 10^5
75 cm^2 flask	75 cm^2	15 ml	3 ml	10 ml	5x 10^5	1x 10^6

3.2.1.3 Cryopreservation and revival of cell lines

To cryopreserve cells in liquid nitrogen, cells were detached and washed as described before (chapter 3.2.1.2). Upon cell counting, cells were transferred to cryogenic vials (2x 10^6 HEK293 cells or 5x 10^5 mPASMCs). Freezing solution was added to the cell suspension in the cryogenic vial at a 1:1 ratio. It contained 80% FCS and 20% DMSO (Dimethyl sulfoxide) to prevent formation of ice crystals in the sample during the freezing process. The cryogenic vials were then stored for 2 days at -80°C in a

Nalgene® Mr Frosty freezing container and then transferred to the liquid nitrogen long-term storage container.

Revitalization of frozen cells was performed by transferring the vials to a water bath and rapid reconstitution in 15 ml of pre-warmed medium on a 75cm^2 cell culture flask. After 24h, medium was changed to ensure all freezing medium was removed.

3.2.2 Generation of murine pulmonary artery smooth muscle cell lines

Wildtype and beta Arr1-/- mice at 8-16 weeks of age were sacrificed by cervical dislocation and PAs were isolated and dissected according to chapter 3.7.1. Upon successful isolation, PAs were kept in ice-cold PSS buffer. Then, they were opened by a longitudinal cut and fixed on the preparation plate by the aid of Austerlitz insect pins. The endothelium of the vessel was removed with a scalpel and then PAs were cut into 2mm sections. These sections were transferred to a 6-well-plate and placed inside-down into small droplets of Gibco™ 231 Medium. The 6-well plate was left open under the bench to enable evaporation of liquid resulting in attachment of the tissue pieces on the bottom of the well. Next, all successfully attached tissue sections were provided with 2 ml of cell culture medium and stored in the incubator. Sprouting of mPASMCs were detected after 14-21 days of incubation (Figure 9) while fresh cell culture medium was added daily. Then, the tissue was removed. As soon as the cells reached 80% confluency they were transferred to a 6 cm cell culture dish. The cells were further expanded to a 25 cm^2 and 75 cm^2 flask. Then, cells were cryopreserved in liquid nitrogen.

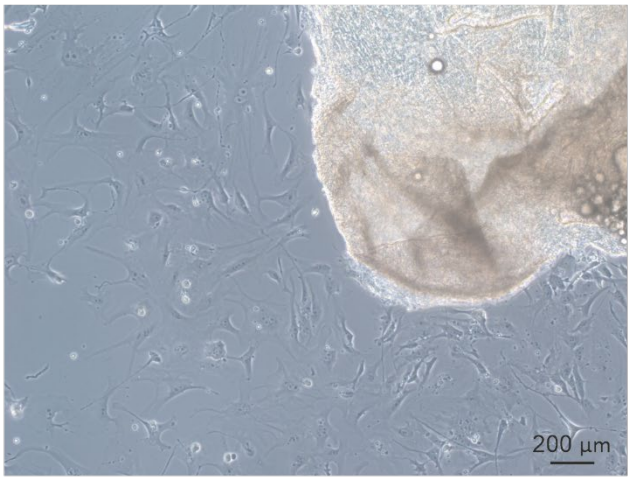

Figure 9: Isolation of smooth muscle cells from murine PAs.
10x magnification of PASMCs sprouting from a tissue piece of PA.

3.2.3 Stable transfection of HEK293 cells with GFP-beta Arr1 and GFP-beta Arr2 constructs

To distinguish between effects mediated by beta Arr1 or beta Arr2, HEK293 Δbeta Arr1/2 cells were stably transfected with either a GFP-beta Arr1 or a GFP-beta Arr2 construct. Briefly, human constructs

for GFP-beta Arr1 and GFP-beta Arr2 were amplified in competent XL-1 blue bacteria cells. The amplified pcDNA3.1(+) vectors (Invitrogen™), containing either the beta Arr1 or 2 constructs with a linked N-terminal GFP, were linearized by PVU1 enzyme. HEK293 Δbeta Arr1/2 cells were then transfected with the help of FuGENE® HD (Promega). For this purpose, 8 µg of the corresponding plasmid was mixed with 21 µl FuGENE® HD-solution and dissolved in 1 ml of PBS. This transfection mixture was transferred to a 100 mm cell culture dish containing 80% confluent HEK293 Δbeta Arr1/2 cells. To select for HEK293 Δbeta Arr1/2 cells that incorporated the constructs into their genome successfully, transfected cells were cultured in cell medium containing 500 µg/ml G418 (Invitrogen). The transfected constructs contain a neomycin resistance cassette that protects cells from the effect of G418. G418 inhibits polypeptide synthesis in eukaryotic cells and thus prevents cell growth of non-transfected cells.[80]

After four weeks of cultivation under G418 selection fluorescence-activated cell sorting (FACS) was performed to purify GFP-positive cells. GFP-positive cells were kept in culture and expanded further; alternatively, they were cryopreserved (chapter 3.2.1.3) for long-term storage in liquid nitrogen.

3.2.4 Transient transfection of HEK293 cells with sGC beta1/ sGC alpha1/ Cyb5r3/ control constructs

Table 16: transient transfection protocol

Day 1	Day 2	Day 3	Day 4
Cell Seeding: 2x 10^6 cells per 100 mm cell culture dish	Transfection	no action	harvest of transfected cells; protein isolation

2x 10^6 HEK293 cells were seeded on a 100 mm cell culture dish on day 1. Next day, cells were transfected with a total amount of 8 µg plasmid (chapter 3.1.11). If two plasmids were transfected in parallel, 4 µg of each plasmid was used. The ideal amount of plasmid for transfection in HEK293 cells was extensively tested by AG Kostenis and has been adopted for this work. To enable proper transfection, Lipofectamine™ 3000 Transfection Reagent (Thermo Fisher Scientific) was used. According to the manufacturer`s protocol two pre-mixes were prepared, pre-mix 1 contained 250 µL Opti-MEM and 30 µL Lipofectamine™ 3000 Reagent and pre-mix 2 containing 250 µL Opti-MEM, 8 ug plasmid and 40 µL P3000™ Enhancer Reagent. Both pre-mixes were added and the mixture was incubated for 15 min at room temperature. After incubation, the mix was pipetted to the HEK293 cells. After 48 h of incubation time, transfected cells were harvested for protein analysis as described later (chapter 3.5.1).

3.3 Standard methods of molecular biology

3.3.1 Heat-shock transformation

For heat-shock transformation, One Shot™ Match1-T1R™ Chemically Competent E. coli (Invitrogen™) were thawed on ice and 1 µL plasmid was added and incubated for 30 min on ice. Next, a heat-shock was performed at 42°C for 30 sec in a pre-warmed thermomixer (Eppendorf). The suspension was cooled for 2 min on ice, then 250 µL S.O.C. medium was added and the mixture was kept for 1h at 37°C while shaking at 300 rpm. Kanamycin-containing agar plates were prepared and 50 to 150 µL of transformed bacterial suspension was spread on these agar plates and incubated overnight at 37°C. On the following day, grown colonies from the agar-plates were picked, transferred to vials containing 5 ml LB medium and incubated at 37°C overnight.

3.3.2 Isolation of plasmid DNA

Upon successful transformation of E. coli cells DNA was isolated via anion exchange chromatography. For small amounts of bacteria the kit QIAprep® Spin Miniprep Kit (Qiagen) and for large amounts of bacteria EndoFree® Plasmid Maxi Kit (Qiagen) were used according to the manufacturer`s protocol. Isolated DNA was washed with 70% ethanol, resuspended in endotoxin-free water (Ampuwa®) and stored at -20°C for further usage. DNA concentration was determined by a Nanodrop (Peqlab).

3.3.3 Glycerol stock generation of bacteria

To enable quick amplification of plasmid DNA, successfully transformed E. coli bacteria were stored in glycerol stocks at –80°C.

To generate glycerol stocks, 800 µL of bacterial suspension were mixed with 200 µL of glycerol and stored at -80° C. Small amounts of this mixture were added to LB medium to enable reconstitution of the bacteria.

3.4 RNA expression analysis

3.4.1 RNA isolation

RNA isolation was performed from cells or isolated murine tissue. Cells were grown on a 6-well plate to 90% confluency (chapter 3.2.1) and washed by PBS. PBS was discarded and cells were lysed by

addition of 300 µL TRIzol® reagent per well. Using the bottom of a 1 ml pipette tip cells were scraped from the 6-well plate and transferred to a 1.5 ml reaction tube.

Tissue samples were isolated on ice in RNAlater™ Solution and transferred to 2 ml micro tubes. 300-1000 µL TRIzol®-reagent as well as 2.5 mm stainless steel beads (Qiagen, Germany) were added to each micro tube and the samples were lysed for 8 min with a Tissuelyzer LT (Qiagen). Afterwards, the micro tubes were centrifuged (11,800 rpm, 10 min, 4°C) and the supernatant was transferred to a fresh 1.5 ml reaction tube.

Cell or tissue samples were then incubated for 5 min at room temperature and 300 µL 1-Bromo-3-chloropropane per ml TRIzol®-reagent was added. Samples were vortexed for 30 sec and incubated for 3 min at room temperature. For separation of protein, RNA and DNA the samples were centrifuged (11,800 rpm, 15 min, 4°C). Proteins dissolved in the phenolic phase at the bottom of the micro tube while DNA appeared mainly in the interphase and RNA concentrated predominantly in the hydrophilic upper phase of the tube. The clear upper phase was transferred to a fresh 1.5 ml tube and 500 µL 2-propanol / ml TRIzol®-reagent was added. Samples were vortexed for 30 sec and incubated for 10 min at room temperature. Afterwards, samples were centrifuged again (11,800 rpm, 10 min, 4°C) and the supernatant was discarded. The RNA -pellet was washed 3 times with 500 µL 70% ethanol and after each washing step samples were centrifuged (13,000 rpm, 5 min, 4°C) to form the RNA -pellet. The RNA -pellet was air-dried at room temperature and dissolved in 20 µL RNAse free water (Ampuwa®). RNA concentration and purity were measured by a Nanodrop (Peqlab).

3.4.2 Reverse transcription cDNA synthesis

For transcription of isolated RNA into cDNA the SuperScript Vilo cDNA Synthesis kit was used according to the manufacturer's manual.

Table 17: Recipe for cDNA reaction mix

Substance	Amount
RNA	1000 ng
5X VILO™ Reaction Mix	4 µL
10X SuperScript® Enzyme Mix	2 µL
Ampuwa®	ad 20.0 µL

All components were pipetted according to Table 17, vortexed and centrifuged briefly. For transcription of mRNA the following program (Table 18) was used in the thermocycler. Samples were either used directly, stored overnight at 4°C or frozen at -20°C for long-term storage.

Table 18: Thermocycling program for mRNA transcription

Step #	Temp °C	Time [min]
1	25	5
2	42	60
3	85	5
4	4	∞

3.4.3 Qualitative PCR

For qualitative PCR the following primers (Table 19) were used. All components were mixed according to Table 19 and for PCR the program according to Table 20 was used.

Table 19: PCR ingredients

Substance	Amount
cDNA	100 ng
10X buffer	2 ul
2.5 mM dNTPs	1.6 ul
50 mM $MgCl_2$	0.6 ul
Taq-Polymerase	0.4 ul
10 uM primer forward	2 ul
10 uM primer backward	2 ul
Nuclease free water	ad 20 ul

Table 20: PCR thermocycler programm

Step #	Temp °C	Time [sec]	notes
1	95	300	
2	95	45	step 2-4: 30 cycles
3	Annealing temp	45	
4	42	45	
5	42	180	
6	4	∞	

3.4.4 Gel electrophoresis

Agarose gel electrophoresis was performed to visualize the PCR results. To generate a 1.5% agarose gel, 0.75 g agarose was dissolved in 50 ml TAE-buffer by cautious heating. When all solid agarose was dissolved, 2 drops of 1% ethidium bromide-solution were added and mixed. The mixture was transferred to a gel chamber and suitable combs were added. Upon complete polymerisation, gels were transferred to a running chamber and the chamber was filled with TAE-buffer. 20 ul of each sample was mixed with 4 ul of 6X loading buffer and loaded onto the gel. GeneRuler™ DNA Ladder Mixes were used to determine the size of the PCR prodcut. Electrophoresis was performed at 90 V for approximately 60 mins.

3.4.5 RT qPCR

Samples were pipetted according to Table 21 by use of the pipetting robot Cas 1200 (Corbett) in 96-well plates and processed by the Bio-Rad CFX96 Real- Time System according to the protocol in in

Table 22. The second derivative maximum method was used to quantify gene expression and ribosomal 18s RNA was used as internal control.

Table 21: RT qPCR Applied Biosystems™ TaqMan® Assay recipe

Substance	Amount
TaqMan™ Master-Mix (2X)	10 µL
specific Applied Biosystems™ TaqMan® Assay (20X)	1 µL
cDNA	2 µL
Ampuwa®	ad 20 µL

Table 22: RT qPCR Applied Biosystems™ TaqMan® Assay program

Step #	Temp °C	Time [sec]	notes
1	95	600	
2	95	15	step 2-4: 38 cycles
3	60	30	
4	72	30	

3.5 Protein analysis

3.5.1 Protein isolation

For protein isolation of cells, cells were first enzymatically detached from the cell culture dish. Therefore, cells were washed with PBS followed by 3 min incubation at 37°C with trypsin. Trypsin reaction was stopped by adding a 3-fold amount of full medium to the cells. This solution was transferred to a 15 ml Falcon® tube. After 5 min of centrifugation at 1,000 rpm cells formed a pellet at the bottom of the Falcon® tube. Medium was discarded and the pellet was further washed in 3x volume of PBS followed by centrifugation for 5 min at 1,000 rpm. PBS was discarded and the cell-pellet was lysed in an adequate amount of ice-cold RIPA buffer. The mixture was kept for approximately 10 min on ice and was then sonicated for 1 min by Sonopuls mini20 (Bandelin). The resulting solution was incubated for 20 min on ice followed by centrifugation for 15 min at 13,000 rpm at 4°C. The supernatant was separated and stored at -80°C.

Protein isolation of tissue (PAs, lungs) was performed after isolation of organs as described in chapter 3.7.1. Upon fixation of the heart lung package on the preparation slide with Austerlitz insect pins the pulmonary vascular system had to be flushed once by PBS via infusion into the right ventricle using a 5 ml syringe and an attached 24G cannula. Next, lungs were dissected and transferred to a 2 ml tube

and stored in ice-cold RIPA buffer. PAs were dissected in total after flushing and stored in a 2 ml microtube in ice-cold RIPA buffer. The following steps were identical for lung and PA protein isolation: Two 5 mm stainless-steel beads (Qiagen, Germany) were added to each tube and the samples were lysed for 8 min with a Tissuelyzer LT (Qiagen). Afterwards, the stainless-steel beads were carefully removed and the mixture was sonicated for 1 min by Sonopuls mini20 (Bandelin). The resulting solution was incubated for 20 min on ice followed by centrifugation for 15 min at 13,000 rpm at 4°C. The supernatant was stored at -80°C.

3.5.2 Measurement of protein concentration

Protein concentration was measured by use of the Pierce™ BCA Protein Assay kit (Thermo Fisher) according to the user's manual. 10 µL of samples were pipetted in a 96-well plate and 200 µL BCA™ Working Reagent was added. The 96-well plate was gently shaken for 30 sec and incubated at 37°C for 30 min. The plate was cooled down to room temperature and absorbance was photometrically measured at 562 nm by a Spark® plate reader (Tecan). A standard curve was generated by measurement of different known BSA concentrations. Sample protein concentrations were calculated based on the standard curve. Samples were adjusted to similar protein concentrations and either used directly or stored at -80°C.

3.5.3 Sodium dodecyl sulfate polyacrylamide gel electrophoresis (SDS PAGE)

Protein samples were thawed on ice or directly used upon protein concentration measurement (see above). Protein samples were further diluted by addition of RIPA buffer to equal concentrations. Corresponding volumes of 5x SDS loading buffer were added to obtain protein samples with 1x SDS loading buffer. These mixtures were incubated at 95°C for 7 minutes and were afterwards kept at room temperature prior to loading of the SDS gel.

Table 23: recipe for separating and stacking gels

separating gel (12%)		separating gel (8%)		stacking gel (4%)	
component	volume/gel	component	volume/gel	component	volume/gel
TRIS HCl 1.5 M pH 8.8	1 ml	TRIS HCl 1.5 M pH 8.8	1 ml	TRIS HCl 1 M pH 6.8	0.5 ml
20% SDS	160 µL	20% SDS	160 µL	20% SDS	80 µL
Acrylamid 40%	1.21 µL	Acrylamid 40%	800 µL	Acrylamid 40%	200 µL
dH_2O	1.63 ml	dH_2O	2.04 ml	dH_2O	1.22 ml
TEMED	2.5 µL	TEMED	2.5 µL	TEMED	2.5 µL
APS 10%	40 µL	APS 10%	40 µL	APS 10%	20 µL

SDS gels (4% stacking/ 8% separation gel or 12% separation gel) were prepared according to Table 23. For proteins sizes of 50 kDa or larger, 4% stacking and 8% separation gels were prepared. For proteins

smaller than 50 kDa, 4% stacking and 12% separation gels were prepared. Gels with a thickness of 1.0 mm were generated. Upon complete polymerisation of the separation gel, the stacking gel was transferred on top and 10-well 1 mm combs were used.

Electrophoreses was performed by Mini-PROTEAN Tetra Cell electrophoresis system with 1x SDS-Buffer for 30 min at 80V followed by 120V until the coloured marker had reached the bottom of the gel.

3.5.4 Western blotting

Western blotting was performed by the tank blot method. Gels were blotted on PVDF-FL (low fluorescence) membrane (Biozym) in tank blot buffer upon constant stirring at 4°C by usage of a Mini-PROTEAN Tetra Cell electrophoresis system running for 90 min at 110V. Afterwards, the membrane was washed once with TBST and blocked in 5% skim milk solution for 60 min during constant horizontal shaking at room temperature.

Primary antibody incubation was performed in a 50 ml tube containing 5 ml of 5% BSA solution. The membranes were incubated overnight at 4°C under constant rotation of the falcons.

After overnight primary antibody incubation membranes were washed 3 times with TBST for 15 min in total. Secondary antibody incubation was performed in 5% skim milk solution. Secondary antibodies were added according to Table 12 and membranes were incubated for 30 min under constant horizontal shaking at room temperature. After secondary antibody incubation, membranes were washed again 3 times with TBST for 15 min in total and developed by incubation with Pierce™ ECL Western Blotting substrate. Pictures at different exposure times were taken by ChemiDoc™ MP Imaging System (Bio-Rad) and processed by Bio-Rad Image™ Software version 5.2.1.

If multiple proteins had to be detected, blots were stripped after development by incubation with Restore™ Plus Western Blot Stripping buffer for 10 min at 37°C under constant horizontal shaking. Membranes were washed 3 times with TBS for 15 min in total. Afterwards, the membranes were blocked again in skim milk solution (5%) for 60 min under constant horizontal shacking at room temperature. This was followed by primary antibody incubation.

3.5.5 Immunoprecipitation experiments

Immunoprecipitation experiments were performed in close cooperation with Prof. Volkmar Gieselmann (Institute of Biochemistry and Molecular Biology, Nussallee 11, 53115 Bonn).

Immunoprecipitation of beta Arr1 and sGC alpha1 beta1 was performed by use of primary antibodies (beta Arr1 Ab and sGC beta1 Ab) and Protein A Agarose. Immunoprecipitation of beta Arr1 and Cyb5r3 was performed by usage of nanobody-coated myc- and GFP-Trap® Agarose (chromotek).

3.5.5.1 Protein isolation

Protein isolation and measurement of protein concentration was performed according to previous chapters (3.5.1 and 3.5.2). However, for immunoprecipitation a lysis buffer composed of TBS was used to enable cell lysis with concomitant preservation of protein interaction. transfected cells were lysed in TBS buffer and frozen at -80° C.

3.5.5.2 Immunoprecipitation of beta Arr1 and sGC alpha1 beta1 and control protein

Frozen samples were thawed on ice and Triton was applied with the respective antibodies according to the following table:

Table 24: standard sample preparation for antibody and Pierce™ Protein A Agarose pulldown

sample	#1: HEK GFP-beta Arr1 + sGC alpha1 beta1	#2: HEK GFP-beta Arr1 + sGC alpha1 beta1	#3: HEK293 Δbeta Arr1/2+ sGC alpha1 beta1
lysate [ug]	60	60	60
Triton 10% [µL]	5	5	5
unspecific (MBP) antibody [µL]	2		
target antibody (anti-beta Arr1 or anti-sGCb1) [µL]		4	4
TBS	ad 100 µL	ad 100 µL	ad 100 µL

Samples were incubated overnight at 4°C under constant turnover movement to enable sufficient binding of the antibody to the antigen. On the next day, 90 µL Pierce™ Protein A Agarose bead solution was washed 3 times by addition of 500 µL TBS + 0.3% Triton, short centrifugation (1 min, 100 g) and disposal of washing solution. 30 µL of the washed Pierce™ Protein A Agarose bead solution was added to each sample. Samples were incubated for 1 h at constant turnover movement at 4°C to enable binding of the Fc-part (heavy chain) of the target rabbit IgG antibody (beta Arr1 or sGCb1) to the Protein A. After incubation, the following complex was formed:

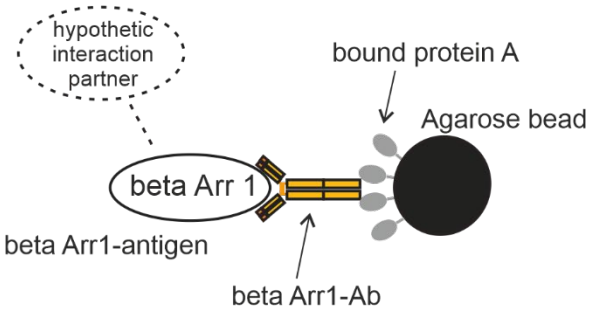

Figure 10: Scheme of protein binding for immunoprecipitation
Protein A Agarose binds the Fc-part of the beta Arr1-Ab. Beta Arr1-Ab is bound to beta Arr1-antigen from the sample, still connected to other potential interaction partners.

Next, samples were separated into a supernatant and a pellet fraction. The pellet fraction was washed 3 times with 500 µL TBS + 0.3% Triton to ensure complete depletion of non-bound proteins in the pellet fraction. The resulting supernatant and pellet fractions were either frozen and stored at -80°C or processed immediately.

3.5.5.3 Immunoprecipitation of beta Arr1 and Cyb5r3

Frozen samples were thawed on ice and samples were prepared according to the following table:

Table 25: sample preparation for GFP- and myc-Trap® Agarose pulldown

sample	HEK GFP-beta Arr1 + Cyb5r3	HEK GFP-beta Arr1 + Cyb5r3	HEK293 Δbeta Arr1/2+ Cyb5r3
lysate [ug]	60	60	60
Triton 10% [µL]	5	5	5
TBS	ad 100 µL	ad 100 µL	ad 100 µL
GFP- or myc-Trap® Agarose [µL]		40	40
Binding Control Agarose [µL]	20		

Lysate, Triton 10% solution and TBS were mixed according to Table 25. GFP- or myc-Trap® Agarose as well as Binding Control Agarose were washed 3 times by addition of 500 µL TBS + 0.3% Triton, short centrifugation (1 min, 100 g) and disposal of the washing solution. 20 or 40 µL of the corresponding washed Agarose bead solution was added to each sample. Samples were incubated overnight at constant turnover movement at 4°C to enable binding of the nanobody-coated Agarose beads to the target (GFP- or myc tag). Next, samples were separated into the supernatant and the pellet fraction. The pellet fraction was washed 3 times with 500 µL TBS + 0.3% Triton to ensure complete depletion of non-bound proteins in the pellet fraction. The resulting supernatant and pellet fractions were either frozen and stored at -80°C or processed immediately.

3.5.5.4 SDS PAGE

Pellet and supernatant fractions were prepared for SDS PAGE: 25 µL of the supernatant fraction as well as the complete pellet fraction were transferred to fresh 1.5 ml tubes. To enable SDS-separation, 5 µL of 5x SDS Sample buffer was added to the supernatant fraction samples and 30 µL of 2x SDS Sample buffer was added to the pellet fraction samples. Both mixtures were incubated at 95°C for 7 minutes and afterwards kept at room temperature prior to loading of the SDS gel. Heat and SDS-Sample buffer destroyed any potential antigen-antibody-binding and consequently the previously formed binding partners (Figure 10) were separated. Next, denatured proteins in the samples were separated by their size with the help of SDS-Page.

SDS gels were prepared as described previously (chapter 3.5.3) and two gels (4% stacking/ 8% separation gel for beta Arr1 + sGC alpha1 beta1 or 4% stacking/ 12% separation gel for beta Arr1 + Cyb5r3) were loaded with the prepared fraction samples and run as described earlier (chapter 3.5.3).

3.5.5.5 Western blotting

Protein transfer from gel to (low fluorescence) PVDF-membrane was performed according to chapter 3.5.4 and membranes were incubated with primary antibodies according to Table 11 similar as described above (chapter 3.5.4).

3.5.5.6 Development of membranes

IP experiments always require detection of multiple proteins. When primary antibodies targeting different proteins were derived from the same species (i.e. rabbit), blots were stripped in between the two developments. When antibodies for the pull-down (i.e. beta Arr1 pulldown: rabbit origin) and the detection of at least one of the two binding partners had similar species origin (i.e. sGC beta1: rabbit origin) a conformation specific secondary antibody (Table 12) was used to prevent detection of light- and heavy chain antibody fragments derived from the pull-down antibody and enabled precise detection solely of intact primary antibodies.

3.6 cGMP measurements: ELISA experiments

3.6.1 Cell treatment for cGMP measurements

CGMP measurements were performed in HEK293 cells. 1x 10^6 HEK293 cells were seeded on 0.1% gelatin-coated six-well plates. 24 h later serum-containing media was aspirated and cells were washed once by addition of PBS. Serum-free DMEM was added for the following cell treatment. 3-isobutyl-1-methyxanthine (IBMX) 10^{-5} M was added and cells were incubated for 30 min to prevent phosphodiesterase (PDE)-driven cGMP degradation. Next, either sodium nitroprusside (SNP dissolved in DMEM, 20 µL of 10^{-3} M) or a similar volume of serum-free DMEM was added to the corresponding

wells. Upon 30 min of incubation time media was removed and the incubation was terminated by addition of 400 µL 10^{-1} M HCl to each well. After ten minutes, cells were scraped with a cell scraper and cell lysate were transferred to a 1.5 ml reaction tube. Cell lysates were centrifuged for 10 min at 13,000 rpm at 4°C and the supernatant was taken. Supernatant was split into two samples, 150 µL for cGMP measurement and 150 µL for measurement of protein concentration. Samples were frozen at -80°C.

3.6.2 Protein measurement for cGMP ELISA

To normalize the amounts of cGMP to proteins protein concentrations of samples were measured. This was performed according to the protocol described in chapter 3.5.2.

3.6.3 cGMP measurement

Measurement of cGMP levels was performed according to the manufacturer`s protocol. Briefly, samples were thawed, acetylated by addition of an acetylation reagent and applied to anti-IgG antibody-pre-coated wells supplied by the manufacturer. Addition of alkaline phosphatase (AP)-conjugated cGMP and anti-cGMP-antibody (IgG) enabled competitive binding of conjugate or native cGMP to the added anti-cGMP-antibody. The binding complex of antigen (either conjugate or cGMP from sample) and anti-cGMP-antibody (IgG) was immobilized on the 96-well plate by binding of the anti-cGMP-antibody to the pre-coated anti-IgG-antibody. Following washing steps and incubation with p-nitrophenyl phosphate (pNpp) substrate provided a signal of bound AP-conjugate. The amount of the bound AP-conjugate behaves reciprocal to the amount of cGMP in the sample. Preparation of a standard curve enabled cGMP level measurements. Measurements of cGMP levels were normalized to protein.

3.7 Isometric force measurements

3.7.1 Preparation of PAs

Wildtype, beta Arr1-/- and beta Arr2-/- mice were sacrificed by cervical dislocation and fixed with five needles. The skin was cut from abdomen to throat. Then the chest was opened medially and tissue was removed from the trachea. Next the heart lung package was isolated and stored in ice-cold PSS low calcium buffer. Preparation of PAs was executed under a Wild M3 stereomicroscope at 6.4x magnification. At first, thymus and attached connective and fat tissue was removed and heart atria were dissected to facilitate PA preparation. Next, connective and fat tissue were removed from the

vessels and left and right PAs were separated. Left and right PAs were cut into 2 mm rings and stored in ice-cold PSS low calcium buffer prior to mounting in the wire myograph.

3.7.2 Wire myograph: mounting of vessel rings and force normalization

Four PA rings were measured simultaneously in the Multi Myograph 620M. Therefore, 2 mm long PA rings were mounted on the jaws of the wire myograph in ice-cold PSS low calcium buffer.

First, a wire of 40 mm diameter was cut into 2,2 cm long sections and mounted onto the upper left screw. The tissue ring was mounted on the wire and positioned between the jaws. Next, the loose end of the wire was fixed under the lower left screw. A second wire was passed through the lumen of the vessel ring and the ends were fixed under the right upper and lower screws. When all four PA rings were mounted properly the PSS low calcium buffer was changed to PSS normal calcium buffer and heated to 37°C while continuously gassed with oxygen.

In order to remove the endothelium in some rings, a twine was passed through the lumen of the pre-stretched vessel and used to scratch off the endothelium by 5 clockwise and 5 counter-clockwise rotations, scraping the inner vessel wall.

Tissue segments were pre-stretched to 5 mN force on the wire myograph to enable optimal force development.[81] This was followed by a an equilibration phase of 20 min.

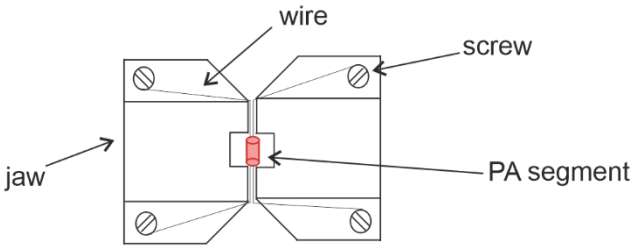

Figure 11: Wire myograph setup
Positioning and mounting of 2 mm long PA segments between the jaws of the wire myograph setup.

3.7.3 Wire myograph: Dose-response curves

After the equilibration phase vessel rings were maximally pre-constricted by application of phenylephrine 10^{-5} M (Phe). After reaching a plateau, vessels were washed every 3 min for 15 min by changing the PSS normal buffer. When baseline force (5 mN) was reached, Phe 10^{-7} M was applied for submaximal contraction. After the force reached a plateau again, dose-response curves were performed by application of the different compounds (Table 26) every 2 min and forces were recorded.

For measurements without endothelium, another submaximal Phe 10^{-7} M contraction was performed followed by application of methacholine (MCh) 10^{-4} M to test for remaining endothelial activity. If application of MCh 10^{-4} M caused less than 20% total relaxation, vessel rings were considered as sufficiently denuded.

Whenever receptor blockers or enzyme inhibitors were tested, compounds (Table 26) were applied 5 min prior to submaximal Phe 10^{-7} M contraction and the respective dose-response curve.

Table 26: Substances used in wire myograph experiments

Substance	dose-response concentration range	application prior dose-response curve
8-pCPT-cGMP	10^{-6} M - $3x10^{-3}$ M	
BAY41-2272	10^{-7} M - $3x10^{-3}$ M	
BAY58-2667	10^{-9} M - $3x10^{-5}$ M	
Forskolin (Fsk)	10^{-7} M - 10^{-4} M	-
Metacholine (MCh)	-	10^{-4} M
Phenylephrine (Phe)	-	10^{-5} M; 10^{-7} M
Roflumilast (Roflu)	-	10^{-5} M
Sildenafil	-	10^{-5} M
Sodium nitroprusside (SNP)	10^{-10} M - 10^{-5} M	-

3.8 Disease model of PH

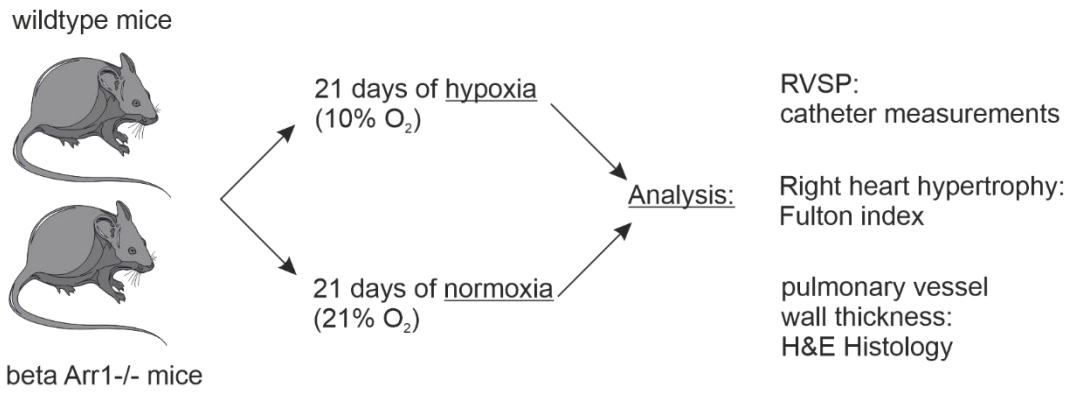

Figure 12: protocol for *in vivo* experiments
Wildtype and beta Arr1-/- mice were subjected to 3 weeks of chronic hypoxia (10% O_2) or kept under normoxic conditions (21% O_2). (RVSP: right ventricular systolic pressure) For illustration of this figure artwork of Servier Medical Art by Servier (licensed under a Creative Commons Attribution 3.0 Unported License) was used, https://smart.servier.com. (10.06.2020).

Wildtype and beta Arr1-/- mice were kept for 3 weeks in hypoxic chambers (BioSpherix). Animals had *ad libitum* access to food and water while oxygen content was measured continuously by the Oxycycler control unit. Stable oxygen levels were provided by infusion of nitrogen to the chamber. After 3 weeks, mice were analyzed. Therefore, three different parameters (right ventricular systolic pressure (RVSP),

pulmonary vessel wall thickness and right heart hypertrophy (Fulton index)) were measured in order to characterize the severity of PH in all experimental groups.

3.8.1 Right ventricular systolic pressure experiments

Analgesia was induced by an i.p. application of Ketamine (50mg/kg) and Xylazine (5mg/kg). For induction of anesthesia inhalation of 5% Isoflurane via a face mask was applied. For maintenance of narcosis 1-1.5 % Isoflurane was used. The skin above the throat was opened by a paramedian cut and salivary glands were separated and dislocated. Next, preparation of the jugular vein was performed. Upon removal of connective and fat tissue two ligations were positioned at the cranial and caudal part of the jugular vein. The cranial ligature was permanently occluded while the caudal ligature was reversibly closed. A small hole was cut into the jugular vein in between both ligatures and the caudal ligature was shortly opened to enable insertion of the catheter. The caudal ligature was tightened after catheter insertion to prevent blood loss during catheter measurements.

For right heart pressure catheter measurements, a 1F Millar pressure catheter in combination with the Aria system (Millar) was used. The catheter was passed via the jugular vein into the right ventricle. Upon a brief equilibration phase of few minutes pressure measurements were performed when a steady and stable signal was obtained. At the end of the measurement the mouse was sacrificed by cervical dislocation.

Evaluation of the recorded data was performed by the LabChart 7 software. The mean systolic pressure was recorded in millimetres of mercury (mmHg) and heart frequency was registered in beats per minute (bpm). Both parameters were analyzed during a period of 8 seconds.

3.8.2 Perfusion of heart lung package for histology

After completion of haemodynamic measurements (chapter 3.8.1) heart and lungs were further processed for histology and analysis of right heart hypertrophy (chapters 3.8.5; 3.8.6). The package of heart and lungs was removed from the chest and washed in ice-cold PBS. A cannula was inserted into the trachea and fixed by a ligature. Then, the cannula was mounted on a perfusion device and the pulmonary vessels were flushed via a butterfly needle positioned in the right ventricle. The pulmonary vessels were perfused for five minutes with ice-cold PBS at a pressure of 62.5 cm H_2O while the trachea and the connected lung segments were perfused at a pressure of 25 cm H_2O. For histology both, pulmonary vessels and lungs were fixed by perfusion with 4% Roti-Histofix.[82] Perfused lungs were separated and stored in 4% Roti-Histofix solution at 4°C overnight.

3.8.3 Paraffin embedding and slicing of lung lobes

Lung lobes were isolated and transferred to embedding cassettes, flushed with tab water for 1h and stored in 70% 2-Propanol at 4°C. Tissues were dehydrated with increasing concentrations of isopropanol, followed by xylene (Table 27).

Table 27: Dehydration program for paraffin embedding

Solution	isopropanol 70%	isopropanol 80%	isopropanol 90%	isopropanol 96%	isopropanol 100%	xylene	paraffin
duration [in h]	3	2x 1	2x 1	2	2x 2	2x 1	2x 1

After dehydration lung lobes were embedded in liquid paraffin at 60°C by use of Microm EC 350-1 and solidified on a cooling plate. The embedded tissues were cut into 5 µm thick sections and transferred to a water bath at 37°C. Then, sections were mounted on microscopic glass slides and dried at 37°C for 24h.

3.8.4 Lung sections: haematoxylin and eosin staining

Sections were stained by incubation in different staining solutions according to the following protocol (Table 28). Nuclei were stained in blue by haematoxylin and cytoplasm was stained in red by eosin.

Table 28: Hematoxylin and eosin staining protocol

Solution	time
xylene	3x 10 min
ethanol 100%	2x 5 min
ethanol 90%	5 min
ethanol 70%	5 min
distilled water	5 min
hematoxylin	4 min
warm water	3 min
eosin 0.5%	2 min
distilled water	5 dips
ethanol 70%	5 dips
ethanol 90%	5 dips
ethanol 100%	5 dips
xylene	3x 5 min
mounting in Entellan	

3.8.5 Evaluation of pulmonary arterial wall thickness

Pulmonary arterial wall thickness was evaluated in haematoxylin and eosin-stained lung sections (chapter 3.8.4). Only arteries adjacent to airways with a diameter between 30 and 70 µm were analyzed.

Sections were examined with an Axiostar plus microscope with 40x magnification and pictures were taken with an AxioCam Mrc5. Measurements were performed with of the Axio-Vision 4.8 Software. At least 10 arteries per mouse were analyzed and the relative arterial wall thickness was determined according to the following formula:

$$\frac{2x\ arterial\ wall\ thickness}{arterial\ outer\ diameter}\ x\ 100$$

3.8.6 Fulton index: evaluation of right heart hypertrophy

The Fulton index was calculated to quantify right heart hypertrophy. Upon perfusion of the heart lung package (chapter 3.8.2) hearts were isolated and blood vessels were removed. Then, left and right atria were removed and the remaining heart ventricles were separated in right and left ventricle including septum. Both parts of the heart were dried at 37°C overnight and dry weight was measured. Fulton index was determined according to following formula:

$$\frac{dry\ weight\ of\ right\ ventricle}{dry\ weight\ of\ left\ ventricle + septum}\ x\ 100$$

Increased levels of Fulton index indicated the development of right heart hypertrophy.

3.9 Statistics

All data presented in this thesis are shown as mean ± standard error of the mean (s.e.m.). Statistical analysis was performed with GraphPad Prism Software Version 5. For comparison of two groups two-tailed t-test was applied. For comparison of more than two groups one-way analysis of variance (ANOVA) was used followed by Tukey´s post-hoc test. Levels of significance are defined as following: * $p < 0.05$; ** $p < 0.01$; *** $p < 0.001$.

3.10 Cooperation partners

The following experiments were performed with or by the following cooperation partners. The use of following data from cooperation partners has been authorized by Prof. Daniela Wenzel and Prof. Bernd Fleischmann.

Table 29: cooperation partners

experiment/ task	performed by	location
Generation of HEK293 cells stable expressing GFP-beta Arr1 /2	Eva Pfeil, AG Prof. Evi Kostenis	Institute of Pharmaceutical Biology, Nussallee 6, 53115 Bonn
RVSP catheter measurements	Alexander Seidinger	Institute of Physiology 1, Venusberg-Campus 1, 53127 Bonn
Immunoblot protein analysis of GFP-beta Arr1 /2 expressing HEK293 cells	Dr. Sarah Rieck	Institute of Physiology 1, Venusberg-Campus 1, 53127 Bonn

4 Results

The objective of the thesis was to uncover the role of beta Arr1 in the tone regulation of PAs. Results of my work are structured in five chapters:

Chapter 4.1 analyzes beta Arr1 signaling in murine PAs. It contains beta Arrestin expression analysis and *ex vivo* wire myograph experiments in wildtype, beta Arr1-/- and partially beta Arr2-/- mice. First, beta Arr1 and 2 mRNA expression in various murine wildtype tissues and beta Arr1 and 2 protein expression in lung murine lysates was examined. Next, the relevance of beta Arr1 and 2 for nitric oxide (NO)-mediated vasorelaxation was tested by application of the NO-donor Sodium nitroprusside (SNP). The NO-sGC-PKG signaling pathway was further investigated by application of the PKG activator 8-pCPT-cGMP and the influence of the $G\alpha_s$-mediated signaling pathway was characterized by application of the adenylyl cyclase activator Forskolin (Fsk). PDE-dependent cGMP degradation was characterized in regard of PA vasorelaxation by incubation with the PDE5 inhibitor Sildenafil. Lastly, activation of the sGC was further examined by dose-response curves with sGC stimulator BAY41-2272 and sGC activator BAY 58-2667.

In chapter 4.2 experiments are displayed analyzing sGC expression and activity. Protein and mRNA expression of sGC in PAs from wildtype and beta Arr1-/- mice were characterized by immunoblotting and RT qPCR experiments. To analyze cGMP production, we took advantage of modified HEK293 cells and measured cGMP levels upon stimulation with SNP. Further, beta Arr1 and 2 expression was analyzed in HEK293 cells by immunoblotting.

In chapter 4.3, I characterized the direct protein interaction between beta Arr1 and sGC by Co-immunoprecipitation (Co-IP) experiments in lysates from HEK Δbeta Arr1/2 and GFP-beta Arr1 cells.

Chapter 4.4 contains the protein expression of Cyb5r3 in HEK293 cells and an analysis of a potential beta Arr1-Cyb5r3 protein interaction by IP experiments.

Finally, chapter 4.5 describes the role of beta Arr1 in the *in vivo* setting of PH. Wildtype and beta Arr1-/- mice were kept under chronic hypoxic (10% O_2) conditions to induce PH and right ventricular systolic pressure (RVSP), right heart hypertrophy and pulmonary vessel wall thickness were measured after 3 weeks.

4.1 Beta Arr1 signaling in the murine PA

4.1.1 Beta Arr1 and 2 is expressed in murine wildtype tissue

To investigate if beta Arr are expressed in murine wildtype lung, airways and vessels, I performed qualitative PCR with specific primers for beta Arr1, 2 and GAPDH as a control.

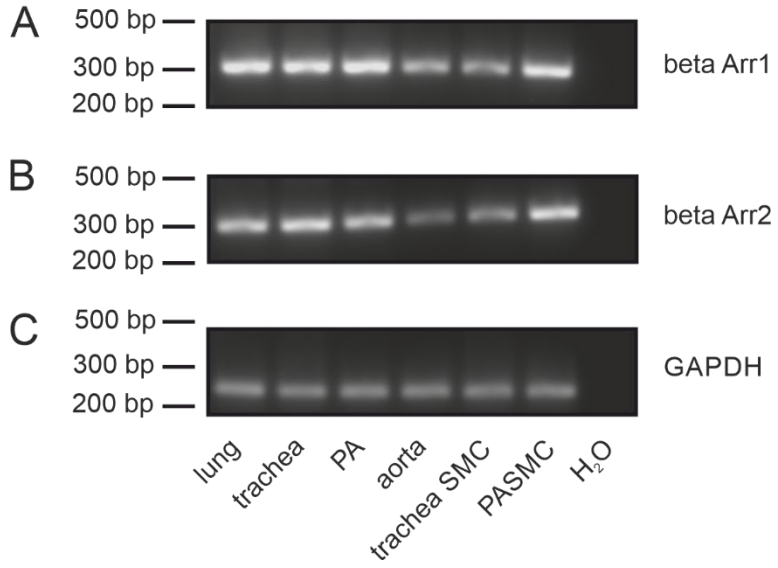

Figure 13: Beta Arr1 and 2 mRNA expression in different murine wildtype tissues using PCR.
PCR results of beta Arr1, beta Arr2 and GAPDH mRNA expression in lung, trachea, PA, aorta, trachea SMC and PASMC from wildtype mice. H_2O served as a loading control. (**A**) Beta Arr1 mRNA (fragment size:313 bp) was expressed in lung, trachea, PA, aorta, trachea, SMC and PASMC. (**B**) Beta Arr2 mRNA (fragment size: 306 bp) was expressed in lung, trachea, PA, aorta, trachea SMC and PASMC. (**C**) GAPDH mRNA (fragment size: 250 bp) as a housekeeper was expressed in all tissues and cells.

These PCR experiments revealed expression of beta Arr1, beta Arr2 and GAPDH mRNA in lung, trachea, PA, and aorta tissue as well as in SMCs from trachea or PA taken from wildtype mice (Figure 13). H_2O served as a loading control.

4.1.2 Immunoblots reveal absence of beta Arr1 and 2 protein in beta Arr1-/- and 2-/- mice

Homozygous beta Arr1-/- or beta Arr2-/- mice are known from literature to behave and breed normally and to show no phenotypic abnormalities. Conner et al. first described beta Arr1-/- mice in literature and demonstrated an altered cardiac response to beta adrenergic stimulation of these mice. Bohn et al. first characterized beta Arr2-/- mice and revealed a potentiated and elongated analgesic effect of morphine.[77,78]

The original investigators of this mouse line established Southern and Western blotting to verify the absence of beta Arr1.[77] In accordance, I performed beta arrestin Western blots (IBs) (Figure 14) in lung lysates to prove the specific knockout of beta Arr1 or 2 in the corresponding mouse line.

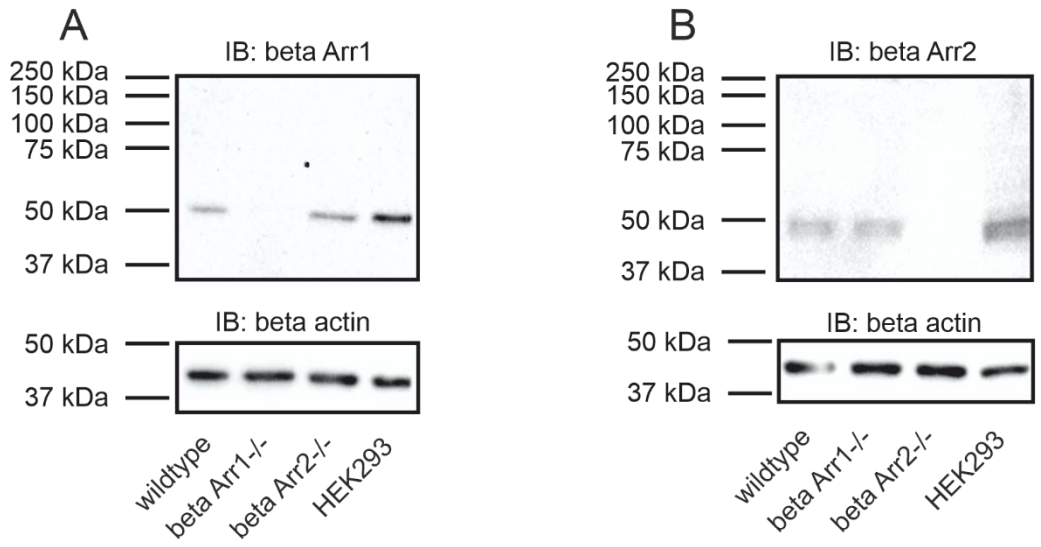

Figure 14: Beta Arr1 and 2 protein expression in lung lysates of wildtype, beta Arr1-/- and beta Arr2-/- mice using immunoblots (IB).
IBs of beta Arr1 (50 kDa) and beta Arr2 (50 kDa) in murine lung lysates obtained from wildtype, beta Arr1-/- and beta Arr2-/- mice. HEK293 lysates served as positive controls. (**A**) IBs of beta Arr1 and beta actin of murine lung lysate and HEK293 lysate revealed absence of beta Arr1 in beta Arr1-/- lung lysates. (**B**) IBs of beta Arr2 and beta actin of lung lysate and HEK293 lysate revealed absence of beta Arr2 in beta Arr2-/- lung lysates.

To prove the lack of beta Arr1 (Figure 14A) and beta Arr2 (Figure 14B) in the respective knockout mice, protein was isolated from lung tissues and HEK293 cells as positive control. IBs with beta Arr1 antibody revealed protein signals in lungs of wildtype and beta arr2-/- mice, as well as in HEK293 cells (Figure 14A). As expected, no beta Arr1 protein was detected in lung tissue of beta Arr1-/- mice (Figure 14A). No beta Arr2 protein was detected in lung tissue from beta Arr2-/- mice, whereas beta Arr2 was present in lung tissue from beta Arr1-/- mice, wildtype mice and HEK293 cells. Beta actin was expressed in all samples in both IBs and served as a housekeeping signal. These IB experiments proved the absence of either beta Arr1 or beta Arr2 in the respective knockout mice. Moreover, the presence of beta Arr1 and beta Arr2 protein signals in HEK293 cells revealed that both beta Arr antibodies are also reactive against the respective human beta Arr proteins.

Taken together, PCR experiments proved mRNA expression for beta Arr1 and 2 in murine wildtype lung, trachea, PA and aorta tissue and tracheal and PASMC while IBs for beta Arr1 and 2 revealed protein expression in murine wildtype lung tissue. Both findings were fundamental for all following experiments with beta Arr1 and 2 knockout animals and tissues.

4.1.3 SNP-mediated PA vasorelaxation is impaired in absence of beta Arr1

Nitric oxide (NO) is a strong endogenous vasorelaxant and crucial for vascular smooth muscle cell relaxation.[83] Release of NO, a gaseous molecule with a very short half-life, can be induced by application of NO donors like Sodium nitroprusside (SNP), an anorganic substance that directly generates NO by spontaneous enzymatic degradation.[84,85] SNP is a prominent drug used in the clinics for rapid reduction of blood pressure in case of hypertensive crisis or surgery and is commonly used in research because of its stable and consistent NO release.[84,86] To explore the effect of beta Arr1 or 2 deletion on NO-mediated vasorelaxation, I performed isometric force measurements in PAs using a wire myograph. In these experiments I determined the dose-dependent relaxation of wildtype, beta Arr1-/- and beta Arr2-/- PAs by application of SNP. PA rings were submaximally preconstricted with the alpha1 adrenoceptor agonist Phe (10-7 M). Then, dose-response curves with SNP (10^{-10} to 10^{-5} M) were performed and relaxation of vessels was measured. In the analysis the extent of relaxation is displayed as percentage relative to maximal precontraction.

I compared the half maximal effective concentration (pEC_{50}) of wildtype PAs to beta Arr1-/- and beta Arr2-/- PAs in order to analyze the influence of beta Arr1 or 2 deletion on the vasorelaxation of PAs.

These experiments were performed in PAs either with intact endothelium (Figure 15 A, B) or upon removal of the endothelial cell layer (Figure 15 C, D) to additionally characterize the vascular tone response in the absence of any endogenously generated NO. I scratched off the endothelial layer by passing a twine through the lumen of the pre-stretched vessel. Removal of the endothelial layer was validated by application of methacholine (MCh). MCh served as an agonist for muscarinergic ACh receptors and is characterized by a paradoxical effect on vascular cells: activation of M3 muscarinergic receptors on the endothelial surface results in a release of NO, causing a strong vasorelaxation of the PAs. In absence of the endothelial layer, the vasorelaxant and NO-generating effect of MCh is absent and activation of M_3 muscarinergic receptors on the surface of remaining smooth muscle cells causes vasoconstriction of the PAs instead.[87] MCh (10^{-4} M) was applied upon submaximal Phe 10^{-7} M preconstriction to test for remaining endothelial activity. Endothelial layer was considered as removed when application of MCh 10^{-4} M reduced constriction by less than 20% (<20% relaxation).

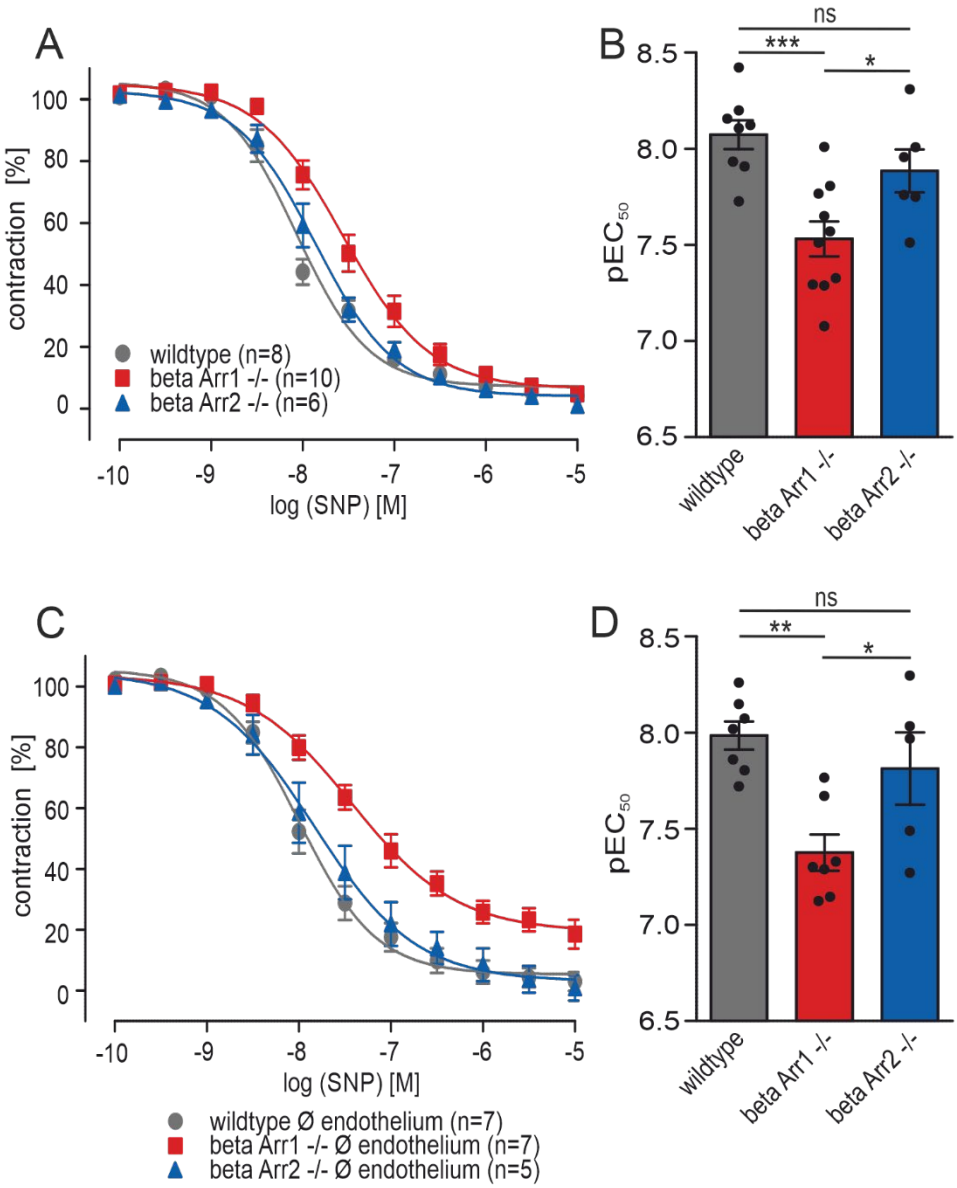

Figure 15: Vasorelaxation by application of the NO donor Sodium nitroprusside (SNP) in PAs of wildtype, beta Arr1-/- and beta Arr2-/- mice.
(**A**) Dose-response curves of wildtype (grey; n=8), beta Arr1-/- (red; n=10) and beta Arr2-/- (blue; n=6) mice in the presence of the NO donor SNP (10^{-10} – 10^{-5} M) revealed a right shift in beta Arr1-/- PAs. (**B**) Analysis of the pEC_{50} values obtained from the dose-response curves shown in A revealed an impaired SNP-mediated vasorelaxation in beta Arr1-/- PAs. (**C**) Dose-response curves of SNP (10^{-10} – 10^{-5} M) in PAs in absence of the endothelial cell layer from wildtype (grey; n=7), beta Arr1-/- (red; n=7) and beta Arr2-/- (blue; n=5) mice displayed a preserved right shift in beta Arr1-/-. (**D**) Analysis of the pEC_{50} values obtained from SNP dose-response curves after removal of the endothelial cell layer shown in C revealed an impaired vasorelaxant response in beta Arr1-/- in absence of the endothelial cell layer. One-way ANOVA, post-hoc test: Tukey. ***$p < 0.001$, **$p < 0.01$, *$p < 0.05$, ns $p > 0.05$. All data are shown as means ± s.e.m.

Wildtype (n=8) and beta Arr2-/- PAs (n=6) displayed comparable SNP dose-response curves, whereas dose-response curves of beta Arr1-/- PAs (n=10) were shifted to the right (Figure 15A). Comparison of EC_{50} values revealed similar values for wildtype and beta Arr2-/- PAs (pEC_{50} wildtype= 8.1 ± 0.1; pEC_{50} beta Arr2-/-= 7.9 ± 0.1), whereas the pEC_{50} value of beta arr1-/- (pEC_{50} beta Arr1-/-= 7.5 ± 0.1) was significantly decreased (Figure 15B). When the endothelial cell layer was removed, wildtype (n=7) and

beta Arr2-/- PAs (n=5) presented comparable SNP-dose-response curves and beta Arr1-/- PAs (n=7) were again shifted to the right (Figure 15C). Further analysis of pEC_{50} values revealed comparable results for wildtype and beta Arr2-/- (pEC_{50} wildtype= 8.0 ± 0.1; pEC_{50} beta Arr2-/-= 7.8 ± 0.2) while beta Arr1-/- pEC_{50} (pEC_{50} beta Arr1-/-= 7.4 ± 0.1) was significantly decreased (Figure 15D). Impaired vasorelaxation of beta Arr1-/- PAs upon SNP-stimulation is a novel finding and suggests an important role of beta Arr1 in vascular relaxation induced by the NO-sGC-PKG signaling pathway. Further, this effect does not require GPCR activation, because NO released by SNP directly activates intracellular sGC. Additionally, comparison of SNP dose-response curves revealed a comparable impairment of vasorelaxation in beta Arr1-/- PAs with intact and with removed endothelial cell layers in both experimental set-ups. This finding indicates that impaired SNP-mediated vasorelaxation in PAs is dependent on SMC beta Arr1.

4.1.4 Beta Arr1 does not affect Proteinkinase G (PKG)-mediated vasorelaxation in PAs

Our previous findings of impaired SNP-mediated vasorelaxation in beta Arr1-/- PAs (chapter 4.1.3) suggest a functional role of beta Arr1 in the NO-sGC-PKG pathway. To validate this hypothesis and to identify the molecule that is functionally impaired when beta Arr1 is lacking, I used the membrane permeable, chemically stable and non-hydrolysable cGMP analogue 8-pCPT-cGMP that directly activats PKG.

PKG activated by cGMP plays a central role for the NO-mediated vasorelaxation as it directly activates MLCP, leading to vasorelaxation.[40] Dose-response curves of 8-pCPT-cGMP (10^{-6} – $5x10^{-4}$ M) were performed in PAs from wildtype and beta Arr1-/- animals with the endothelium removed.

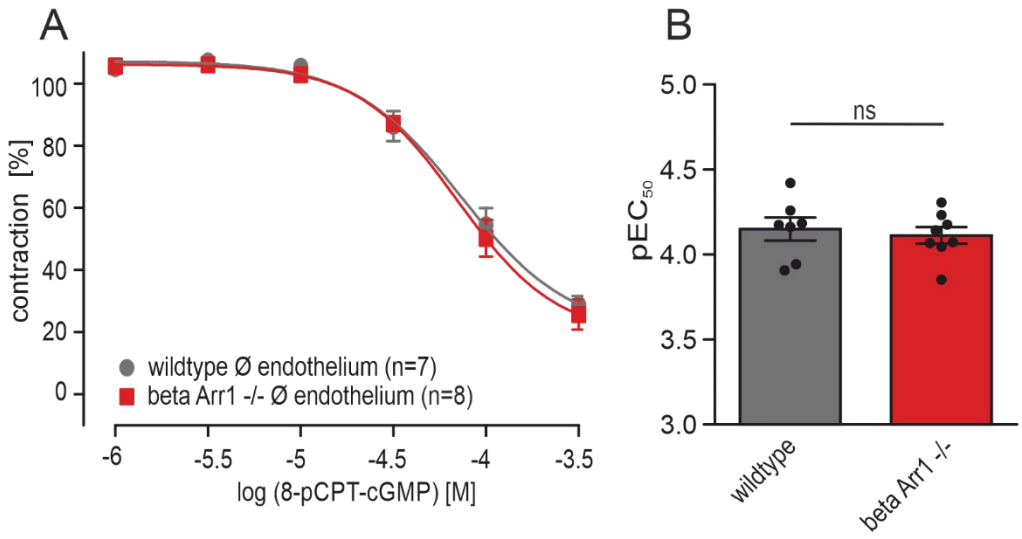

Figure 16: Vasorelaxation mediated by the PKG activator 8-pCPT-cGMP in wildtype and beta Arr1-/- PAs.
(**A**) Dose-response curves of 8-pCPT-cGMP (10^{-6} – $5x10^{-4}$ M) in PAs from wildtype (grey; n=7) and beta Arr1-/- (red; n=8) mice revealed similar responses. The endothelial cell layer was successfully removed prior to the measurements. (**B**) Analysis of pEC_{50} values obtained from 8-pCPT-cGMP dose-response curves shown in A revealed very similar values for wildtype and beta Arr1-/-. T-test, ns $p > 0.05$. All data are shown as means ± s.e.m.

Direct activation of PKG by 8-pCPT-cGMP revealed a similar degree of vasorelaxation for wildtype (n=7) and beta Arr1-/- PAs (n=8) (Figure 16A). Comparison of EC_{50} values showed similar values for wildtype (pEC_{50} wildtype= 4.2 ± 0.1) and beta Arr1-/- PAs (pEC_{50} beta Arr1-/-= 4.1 ± 0.1) (Figure 16B). Comparable vasorelaxation of PAs by 8-pCPT-cGMP in absence of beta Arr1 suggests that PKG activity is not directly affected by beta Arr1. The observed effect is endothelium-independent, as endothelial cell layers were removed prior to agonist application.

So far my experiments revealed that the vasorelaxant response of beta Arr1-/- PAs was impaired when stimulated with NO (chapter 4.1.3) while direct activation of PKG revealed equal vasorelaxant responses (chapter 4.1.4). This suggests that beta Arr1 is required for proper function of the NO-sGC-PKG signaling pathway in PAs. Furthermore, the signaling mechanism responsible for the impaired beta Arr1-/- PA vasorelaxant response is potentially located upstream of PKG but downstream of endothelial NO production.

4.1.5 Beta Arr1 does not affect PDE5 activity during SNP-mediated vasorelaxation

My earlier results suggested an impairment of the NO-sGC-PKG signaling pathway in beta Arr1-/- PAs. CGMP levels are also controlled by PDEs, a class of enzyms responsible for degradation of cyclic nucleotides. While 11 isoforms of PDEs exist, PDE5 is the predominant PDE isoform responsible for cGMP degradation in the lung. Sildenafil is a well-known PDE5 antagonist commonly used in the clinics

for the treatment of PAH. To test potential effects of beta Arr1 knockout on PDE-mediated cGMP degradation, the PDE5-specific inhibitor sildenafil was used. [88,89]

The influence of PDE5 on the vasorelaxation of beta Arr1-/- PAs was tested by incubation of the PAs with sildenafil (10^{-5} M) prior to dose-response curves with SNP. Furthermore, the PA's endothelium was removed to exclude endogenous NO production.

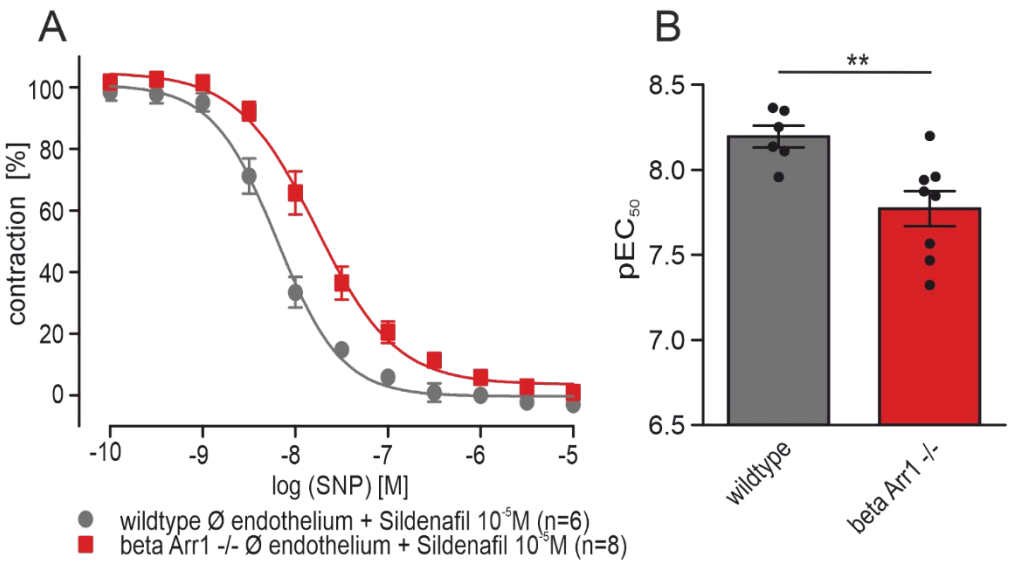

Figure 17: SNP-mediated vasorelaxation upon incubation with PDE5 inhibitor sildenafil in wildtype and beta Arr1-/- PAs. Dose-response curves of SNP (10^{-10} – 10^{-5} M) in PAs from wildtype (grey; n=6) and beta Arr1-/- (red; n=8) mice upon PDE5 inhibition by incubation with sildenafil (10^{-5} M) revealed a right shift in beta Arr1-/- PAs. The endothelial cell layer was successfully removed prior to measurements. (**B**) Analysis of pEC_{50} values obtained after sildenafil (10^{-5} M) incubation shown in A revealed a reduced pEC_{50} for beta Arr1-/-. T-test, **p < 0.01. All data are shown as means ± s.e.m.

In presence of sildenafil (10^{-5} M), dose-response curves of SNP were shifted to the right in beta Arr1-/- PAs (n=8) compared to wildtype PAs (n=6) (Figure 17A). When comparing pEC_{50} values, those for beta Arr1-/- (pEC_{50} beta Arr1-/-= 7.8 ± 0.1) were significantly decreased compared to wildtype (pEC_{50} wildtype= 8.2 ± 0.1) (Figure 17B). A similar right-shift was also observed when beta Arr1-/- PAs were treated with SNP without PDE5 inhibition in chapter 4.1.3. These results indicate that PDE5 is not involved in the right shift of SNP dose-response curves in betaArr1-/- Pas compared to wildtype PAs.

In summary, previous experiments revealed impaired NO vasorelaxation in beta Arr1-/- PAs and this was unrelated to PKG and PDE5 activity.

4.1.6 Vasorelaxation of PAs by adenylyl cyclase (AC) activation is unaffected by beta Arr1

Besides the NO-sGC-PKG signaling pathway, the activation of $G\alpha_s$-coupled GPCRs is a well-known mechanism for vasorelaxation. Upon activation of a $G\alpha_s$-coupled GPCR, the $G\alpha_s$-subunit directly activates membrane-bound adenylyl cyclases (ACs) and activated ACs generate the second messenger

cAMP, causing vasorelaxation in vascular smooth muscle cells.[90] Furthermore, crosstalk between the AC-cAMP and the sGC-cGMP signaling axis was revealed by i.e. cyclic-nucleotide dependent PDE modulation.[91] The diterpene forskolin (Fsk) is a well-known strong and direct activator of the AC isoforms 1-8.[92] To explore the potential role of beta Arr1 for this signaling pathway, I applied increasing doses of Fsk (10^{-7} to 10^{-4} M) in isometric force measurements, causing dose-dependent vasorelaxation of PAs upon submaximal preconstriction. To exclude any potential influence of endogenously generated NO the endothelial cell layer of the PAs was removed prior to the experiments as previously stated.

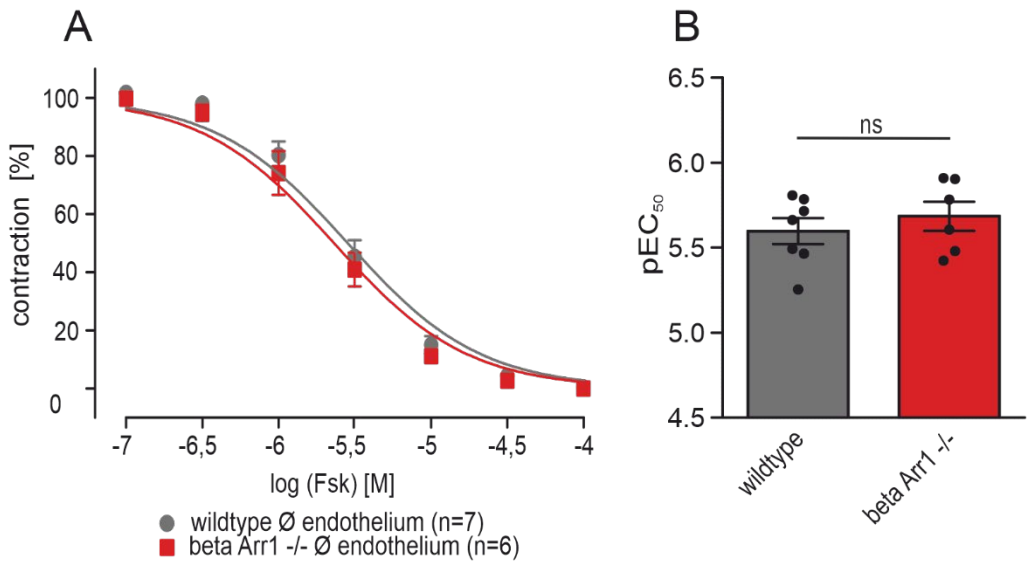

Figure 18 Vasorelaxation caused by the AC activator forskolin (Fsk) in wildtype and beta Arr1-/- PAs.
(**A**) Dose-response curves of Fsk (10^{-7} – 10^{-4} M) in PAs from wildtype (grey; n=7) and beta Arr1-/- (red; n=6) mice revealed equal responses to Fsk. Endothelium was successfully removed prior to the measurements. (**B**) Analysis of pEC_{50} values obtained from Fsk dose-response curves dispayed in A revealed similar values for wildtype and beta Arr1-/-. T-test, ns $p > 0.05$. All data are shown as means ± s.e.m.

When increasing concentrations of Fsk (10^{-7} – 10^{-4} M) were applied in the wire myograph similar vasorelaxant responses of wildtype (n=7) and beta Arr1-/- PAs (n=6) were found (Figure 18A). Comparison of EC_{50} values revealed similar values for wildtype and beta Arr1-/- PAs (pEC_{50} wildtype= 5.7 ± 0.1; pEC_{50} beta Arr1-/-= 5.6 ± 0.1) (Figure 18B). While AC plays a central role for $G\alpha_s$-mediated vasorelaxation, dose-response curves with Fsk indicate that the AC and the corresponding downstream signaling pathway are unaffected by beta Arr1 knockout.

4.1.7 Application of sGC modulators and sGC activators reveals different vasorelaxant responses in beta Arr1-/- PAs

Next, we investigated if sGC activity is impaired in betaArr1-/- PAs. The sGC enzyme can be activated by NO binding to the ferrous (Fe^{2+}) ion located in the center of the heme group of the sGC. A

subsequent conformational change of the enzyme leads to the generation of cGMP. Thereby, NO is either endogenously generated by endothelial eNOS in a physiological vascular setting or it can be also generated, as explained above, by taking advantage of NO donors (i.e. SNP). Alternatively, sGC stimulators can activate the enzyme by allosteric binding, they require the reduced and intact ferrous (Fe^{2+}) form of the iron ion in the heme moiety for activation of the enzyme.[93] SGC activators are able to bind to the unoccupied heme domain mimicking the NO-bound heme, resulting in activation of the sGC enzyme.[94] Activators are more effective when the iron ion in the heme moiety is oxidized and in a ferric state (Fe^{3+}) or even in absence of the heme group.[93]

Substances of both families -sGC stimulators and activators- were tested in the wire myograph setup on PAs to identify, if sGC function is compromized in beta Arr1-/- PAs. To do so dose-response curves with of BAY41-2272 (sGC stimulator; 10^{-7} – $5x10^{-4}$ M) and BAY58-2667 (sGC activator; 10^{-9} – 10^{-5} M) were performed upon removal of the endothelial cell layer in murine wildtype and beta Arr1-/- PAs.

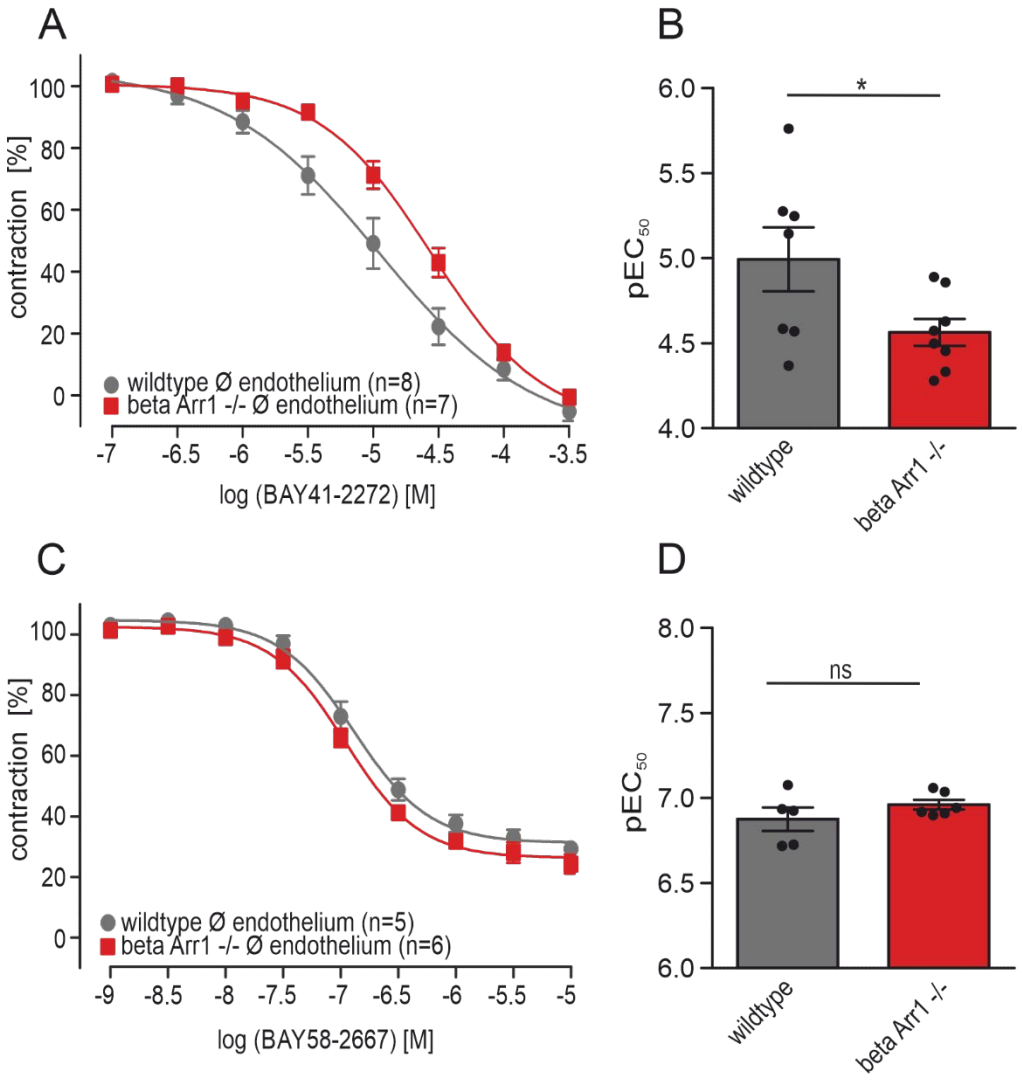

Figure 19: Vasorelaxation mediated by the sGC stimulator BAY41-2272 and the sGC activator BAY58-2667 in murine PAs of wildtype and beta Arr1-/-.
(**A**) Dose-response curves of the sGC stimulator BAY41-2272 (10^{-8} – $5x10^{-4}$ M) in PAs from wildtype (grey; n=8) and beta Arr1-/- (red; n=7) mice revealed a right shift in beta Arr1-/- PAs. (**B**) Analysis of pEC_{50} values obtained from BAY41-2272 dose-response curves shown in A reflect an impaired vasorelaxation of beta Arr1-/- upon sGC stimulator incubation. (**C**) Dose-response curves of the sGC activator BAY58-2667 (10^{-9} – 10^{-5} M) in PAs from wildtype (grey; n=5) and beta Arr1-/- (red; n=6) mice revealed similar responses in wildtype and beta Arr1-/- (**D**) Analysis of pEC_{50} obtained from BAY58-2667 dose-response curves shown in C reported similar vasorelaxation of wildtype and beta Arr1-/- PAs upon sGC activator incubation. The endothelial cell layer was successfully removed prior to measurement in all experiments. T-test, *$p < 0.05$; ns $p > 0.05$. All data are shown as means ± s.e.m.

Dose-response curves of BAY41-2272 (10^{-7} – $5x10^{-4}$ M) were shifted to the right in beta Arr1-/- PAs (n=7) compared to wildtype PAs (n=8) (Figure 19 A), while we found similar vasorelaxant responses of wildtype (n=5) and beta Arr1-/- PAs (n=6) when increasing concentrations of BAY58-2667 (10^{-9} – 10^{-5} M) were applied (Figure 19C). Comparison of pEC_{50} values for BAY41-2272 treatment revealed significantly attenuated pEC_{50} values of beta arr1-/- (pEC_{50} beta Arr1-/-= 4.6 ± 0.1) compared to wildtype (pEC_{50} wildtype= 5.0 ± 0.2) (Figure 19B), while the treatment with BAY58-2667 displayed comparable pEC_{50} values for wildtype (pEC_{50} wildtype= 6.9 ± 0.1) and beta Arr1-/- (pEC_{50} beta Arr1-/-= 7.0 ± 0.03) (Figure 19D). An impaired vasorelaxation of beta Arr1-/- PAs compared to wildtype upon

BAY41-2272 treatment corroborates earlier findings that NO-dependent sGC activity is diminished when beta Arr1 is absent. Activation of the sGC by the sGC stimulator BAY41-2272 is dependent on the intact form of the heme moiety while the sGC activator BAY58-2666 activates the sGC enzyme independent of the heme moiety. Impaired vasorelaxation in beta Arr1-/- PAs upon BAY41-2272-treatment and similar vasorelaxant responses upon BAY58-2666-treatment suggest an impairment of the heme moiety in absence of beta Arr1.

4.2 Investigation of cGMP production and sGC protein analysis in absence of beta Arr1

SGC mRNA and protein expression was tested in PAs from wildtype and beta Arr1-/- mice. CGMP production of transgenic HEK293 cells was measured to identify the effect of beta Arr1 for sGC activity. HEK293 cells lacking both beta Arr without and with overexpression of either GFP-beta Arr1 or 2 were generated and used as a model for cGMP measurement to allow translation from murine to human test systems. Furthermore, beta Arr expression in modified HEK293 cells was characterized on protein level.

4.2.1 Expression of sGC subunit mRNA is unaffected by the absence of beta Arr1 in murine PAs

To distinguish whether altered sGC expression levels affect cGMP production in PAs or whether sGC activity is impaired, first sGC mRNA expression was measured in PAs of wildtype and beta Arr1-/- animals. Therefore, TaqMan® Assays for sGC alpha1, alpha2 and beta1 subunits were used.

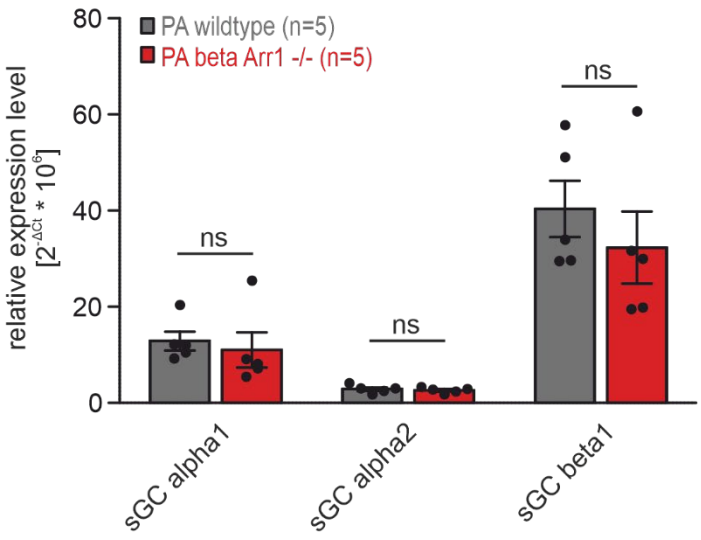

Figure 20: Relative sGC subunit mRNA expression in PAs of wildtype and beta Arr1-/- mice using RT qPCR.
Relative mRNA expression by RT qPCR of PAs of wildtype (grey; n=5) and beta Arr1-/- (red; n=5) mice. Expression data was normalized to 18s housekeeper expression. No significant difference in sGC subunit mRNA expression was found in wildtype and beta Arr1-/- PAs. T-test, ns $p > 0.05$. All data are indicated as means ± s.e.m.

Analysis of relative mRNA expression levels of sGC subunit alpha1, alpha2 or beta1 revealed similar mRNA expression levels in wildtype (n=5) and beta Arr1-/- (n=5) PAs for each sGC subunit tested (Figure 20). MRNA expression levels of sGC subunit alpha1, alpha2 or beta1 were not altered when beta Arr1 was absent compared to wildtype. This result excluded a reduction of sGC mRNA expression in absence of beta Arr1.

4.2.2 SGC beta1 protein levels are unaffected by the absence of beta Arr1 in murine PAs

RT qPCR experiments revealed a similar expression pattern for sGC subunits in wildtype and beta Arr1-/- PAs. Next, protein expression of sGC subunit beta1 was analyzed by IBs to compare wildtype and beta Arr1-/- PA sGC protein expression levels.

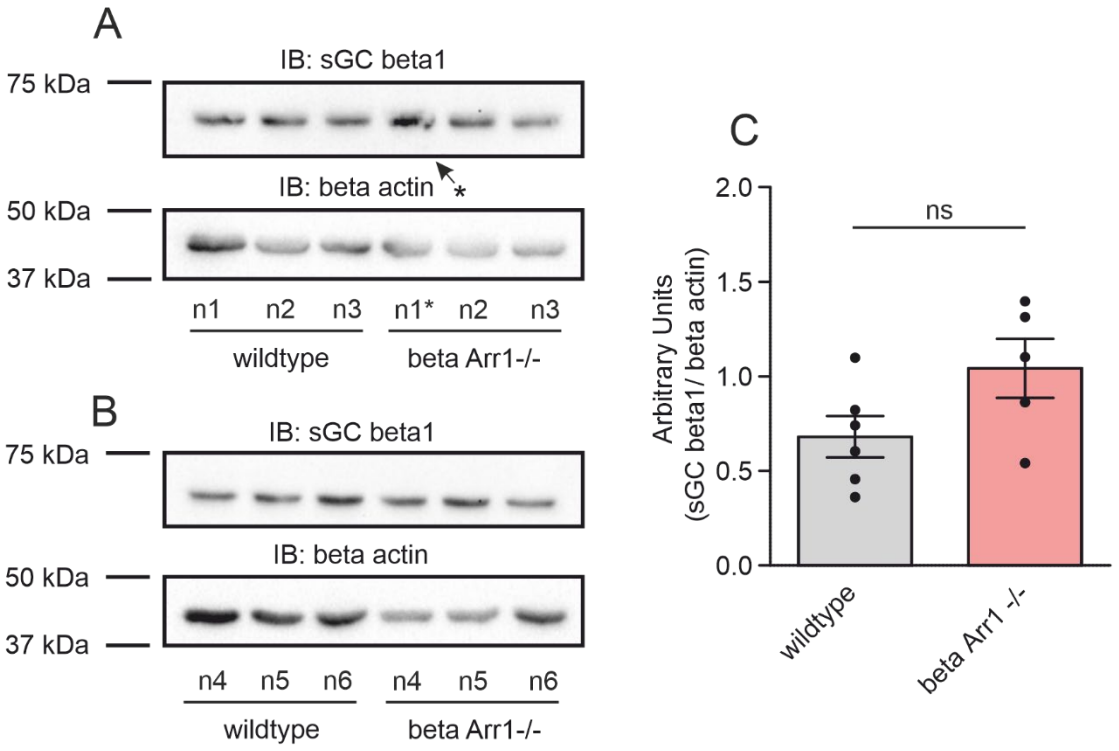

Figure 21: Quantification of sGC beta1 protein expression in wildtype and beta Arr1-/- PAs using IBs.
(**A**) IBs of sGC beta1 and beta actin in wildtype and beta Arr1-/- PAs (n1-3). (**B**) IBs of sGC beta1 and beta actin in wildtype and beta Arr1-/- PAs (n4-6). (**C**) Quantification of sGC beta1 protein expression normalized to beta actin expression in wildtype (n=6) and beta Arr1-/- PAs (n=5) shown in A and B. Quantification revealed similar sGC beta 1 expression in wildtype and beta Arr1-/- PAs. T-test, ns $p > 0.05$. All data are represented as means ± s.e.m.

IBs for the sGC beta 1 subunit and beta actin revealed expression of the respective proteins in wildtype (n1-3) and beta Arr1-/- PAs (n1-3) (Figure 21A). Beta Arr1 -/- (n1) was excluded for quantification due to a blochy signal (asterisk). In wildtype (n4-6) and beta Arr1-/- (n4-6) PAs, IBs again revealed protein expression for sGC beta1 and beta actin (Figure 21B). Expression of sGC beta1 protein was normalized to the housekeeper beta actin and quantified (Figure 21C). Wildtype and beta Arr1-/- PAs revealed similar sGC beta1 protein expression levels.

These results indicated that sGC beta1 expression remained unaltered when beta Arr1 is absent. Taken together, sGC protein levels appeared to be unchanged when beta Arr1 is absent while NO-dependent relaxation of beta Arr1/- PAs (chapter 4.1.3) was impaired.

4.2.3 Beta Arr1 and 2 proteins are expressed in GFP-beta Arr1 and 2-transfected HEK293 cells

To investigate the role of beta Arr1 for cGMP production we used HEK293 cells lacking beta Arr1 or beta Arr2. HEK293 parental (wildtype) and Δbeta Arr1/2 (lacking both beta arrestins) cells were kindly provided by Prof. Evi Kostenis from the Institute of Pharmaceutical Biology in Nußallee 6, 53115 Bonn. Re-expression of GFP-beta Arr1 or 2 in HEK293 Δbeta Arr1/2 cells was achieved by stable transfection

with GFP-beta Arr1 or a GFP-beta Arr2 construct according to chapter 3.2.3 in close cooperation with Eva Pfeil (Institute of Pharmaceutical Biology in Nußallee 6, 53115 Bonn). To ensure that a stable transfection with the GFP-beta Arr1 or 2 constructs was achieved, I performed IBs to analyze beta Arr1 and 2 protein expression in HEK293 parental, Δbeta Arr1/2, GFP-beta Arr1 and GFP-beta Arr2 cells.

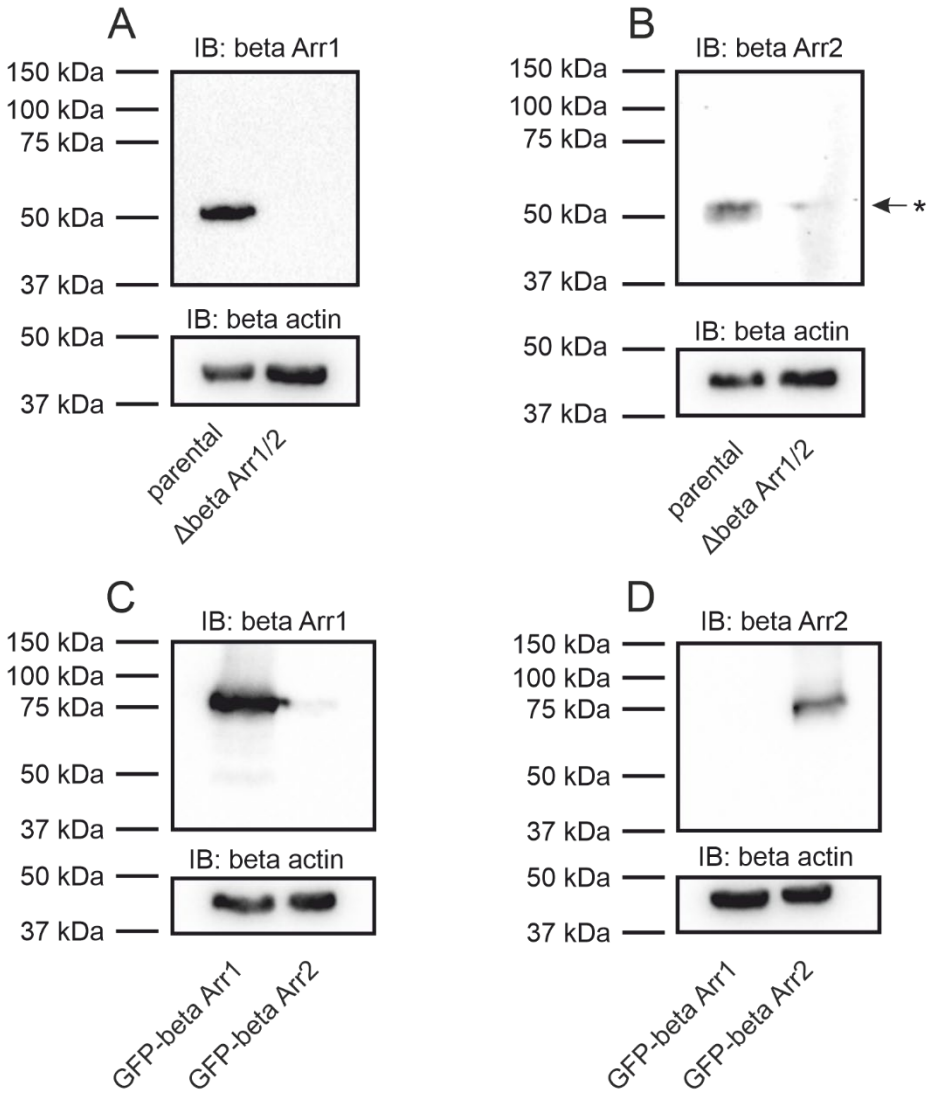

Figure 22: Beta Arr1 and 2 protein expression in HEK293 cells using IBs.
IBs of beta Arr1 (50 kDa), beta Arr2 (50 kDa), GFP-beta Arr1 (75 kDa) and GFP-beta Arr2 (75 kDa) of HEK293 parental and HEK293 Δbeta Arr1/2 cells as well as HEK293 Δbeta Arr1/2 cells expressing GFP-beta Arr1 or 2. (**A**) IBs of beta Arr1 and beta actin revealed beta Arr1 protein expression in HEK293 parental cells and absence of beta Arr1 in Δbeta Arr1/2 HEK293 cells. (**B**) IBs of beta Arr2 and beta actin revealed beta Arr2 protein expression in HEK293 parental cells and absence of beta Arr2 in Δbeta Arr1/2 HEK293 cells. A minor non-specific band for the beta Arr2 antibody in HEK293 Δbeta Arr1/2 cells was reported in literature previously (asterisk).[95] (**C**) IBs of beta Arr1 and beta actin revealed expression of GFP-beta Arr1 in HEK293 Δbeta Arr1/2 cells transfected with the GFP-beta Arr1 construct and no unspecific beta Arr1 expression in HEK293 Δbeta Arr1/2 cells transfected with the GFP-beta Arr2 construct. (**D**) IBs of beta Arr2 and beta actin revealed expression of GFP-beta Arr2 in HEK293 Δbeta Arr1/2 cells transfected with the GFP-beta Arr2 construct and no unspecific beta Arr2 expression in HEK293 Δbeta Arr1/2 cells transfected with the GFP-beta Arr1 construct. Beta actin was used as a loading control.

First, HEK293 parental cells were compared with double knockout Δbeta Arr1/2 HEK. The beta Arr1 IB revealed beta Arr1 protein expression in HEK293 parental cells, while absence of beta Arr1 was

detected in Δbeta Arr1/2 HEK (Figure 22A). The beta Arr2 IB presented beta Arr2 protein expression in HEK293 parental cells and no signal in Δbeta Arr1/2 HEK293 (Figure 22B). A minor non-specific band, which I observed for the beta Arr2 antibody in HEK293 Δbeta Arr1/2 cells, was reported in literature previously (asterisk). [95]

Then, re-expressing cells were analyzed. The beta Arr1 IB of Δbeta Arr1/2 HEK cells stably transfected with GFP-beta Arr1 or 2 revealed a strong signal for beta Arr1 in GFP-beta Arr1 expressing cells and no signal in GFP-beta Arr2 expressing cells (Figure 22C). The beta Arr2 IB of Δbeta Arr1/2 HEK cells stably transfected with GFP-beta Arr1 or 2 proved a strong beta Arr2 protein expression in GFP-beta Arr2 expressing cells and no signal in GFP-beta Arr1 expressing cells (Figure 22D). Beta actin was expressed to a similar extend in all samplesand served as a housekeeper. These data prove a complete knockout of beta Arr1 and 2 in Δbeta Arr1/2 cells HEK293 and specific (re-)expression of GFP-beta Arr1 or 2 in the corresponding HEK293 cell lines, respectively.

In conclusion, these results proved that the generation of transgenic Δbeta Arr1/2 HEK293 cells expressing GFP-beta Arr1 or 2 was successful.

4.2.4 CGMP production upon SNP-stimulation is reduced in HEK293 cells lacking beta Arr1

To determine NO-dependent cGMP production in the presence and absence of betaArr1 or betaArr2, GFP-beta Arr1 and 2 HEK293 cells were used for ELISA measurements. The choice of HEK293 cells expressing different arrestins had two advantages: High numbers of cells with the respective genotype can be produced and the results so far obtained in murine PAs can be transferred to the human system and generalized to other cell types than PASMCs.

CGMP concentration was measured under basal conditions and upon SNP stimulation (10^{-5} M) in different HEK293 cells: HEK293 parental, GFP-beta Arr1 (= beta Arr2-/-) and GFP-beta Arr2 (=beta Arr1-/-) HEK293 cells were incubated with IBMX (10^{-5} M) and stimulated with SNP (10^{-5} M) for 30 mins.

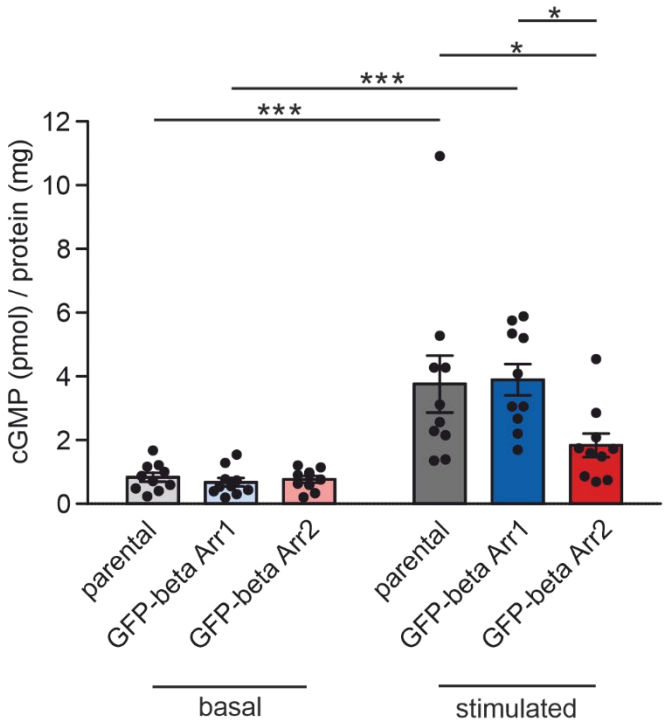

Figure 23: SNP-dependent cGMP production of HEK293 parental, GFP-beta Arr1 and GFP-beta Arr2 cells using ELISA. cGMP levels of different HEK293 cell passages (n=10) were measured under basal conditions and upon SNP stimulation (10^{-5} M; 30 mins) in presence of the pan-PDE inhibitor IBMX (10^{-5} M). HEK293 parental, beta Arr2-/- and beta Arr1-/- cells showed no significantly different cGMP levels under basal conditions. Upon SNP stimulation (10^{-5} M; 30 mins) HEK293 parental and beta Arr1 revealed a significant increases of cGMP levels while beta Arr2 showed no significant cGMP level increase. One-way ANOVA, post-hoc test: Tukey. ***p < 0.001, **p < 0.01, *p < 0.05. All data are indicated as means ± s.e.m.

ELISA measurements of cGMP concentrations in 10 independent passages (n=10) of HEK293 cells revealed similar cGMP levels under basal conditions in HEK293 parental (basal= 0.8 ± 0.1 pmol/mg), GFP-beta Arr1 HEK293 (basal= 0.7 ± 0.1 pmol/mg) and GFP-beta Arr2 HEK293 cells (basal= 0.8 ± 0.1 pmol/mg) (Figure 23). Upon SNP stimulation (10^{-5} M; 30 mins), GFP-beta Arr2 HEK293 cells revealed a lower increase in cGMP levels (SNP-stimulated= 1.8 ± 0.4 pmol/mg) compared to HEK293 parental (SNP-stimulated= 3.8 ± 0.9 pmol/mg) and GFP-beta Arr1 HEK293 cells (SNP-stimulated= 4.0 ± 0.5 pmol/mg) that revealed a similarly strong cGMP production (Figure 23). Comparable cGMP production under basal conditions and impaired cGMP production under SNP stimulation in absence of beta Arr1 revealed an impaired SNP stimulation of the sGC enzyme when beta Arr1 is missing in HEK293 cells.

In Summary, I discovered an impairment of cGMP production upon sGC activation in HEK293 cells lacking beta Arr1 (chapter 4.2.4). This suggested that the beta Arr1-dependent sGC impairment is a general mechanism independent of species or cell type.

4.3 Investigation of protein interaction of beta Arr1 and sGC beta1 in HEK293 cells

Previous results demonstrated an impaired NO-mediated vasorelaxation of PAs in *ex vivo* wire myograph experiments of beta Arr1-/- mice (chapter 4.1.3) and a decreased cGMP production upon SNP stimulation in HEK293 cells lacking beta Arr1. *Ex vivo* myograph experiments with sGC modulators and activators indicated decreased sGC activity when beta Arr1 is absent and further suggested an impairment of the heme site. These findings raised the question why sGC stimulation is decreased when beta Arr1 is missing and if there is an interaction between beta Arr1 and sGC. To address this, myc-tagged sGC alpha1 and beta1 were transiently expressed in Δbeta Arr1/2 HEK293 and GFP-beta Arr1 HEK293 cells and co-immunoprecipitation (Co-IP) experiments were performed. In Co-IP experiments a protein is pulled down by the use of antibody-coated agarose beads. Potential binding partners of the precipitated protein are then detected by an immunoblot targeting the potential binding partner.

Results presented in the following chapter always contain IBs of the Co-IP-supernatant as well as the pellet. In the supernatant all proteins of interest should be detectable apart from the precipitated protein. In the pellet, only the signal of the precipitated protein as well as direct binding partners should appear.

Lane 1 always represents an important control (mock) for the specificity of the immunoprecipitating antibody: lysate of HEK293 cells expressing GFP-beta Arr1 and sGC alpha1 beta1 was used, precipitation was performed with an IgG control antibody (mock) without the capacity to bind beta Arr1. The IgG control antibody is a rabbit antibody against the Maltose Binding Protein (MBP) from E. coli and has no binding capacities in human cells. No precipitation should occur in this sample and no signal should appear in the pellet IB.

Lane 2 represents our main target of interest: lysate of HEK293 cells expressing GFP-beta Arr1 and sGC alpha1 beta1 was precipitated with beta Arr1 antibody. We hypothesized a beta Arr1 signal in the pellet but not in the supernatant, as most proteins of interest should be precipitated.

Lane 3 represents a control for our hypothesis that beta Arr1 and sGC interacts: lysate of Δbeta Arr1/2 HEK293 cells expressing sGC alpha1 beta1 was precipitated with beta Arr1 antibody. We expect no pulldown, as no beta Arr1 was present in the sample. When GFP-beta Arr1 and sGC beta1 are coimmunoprecipitated in lane 2 but no comparable signals are detected in lane 1 and 3 we are able to conclude a specific interaction of both binding partners.

All following Co-IP experiments were performed in close collaboration with and under kind supervision of Prof. Volkmar Gieselmann from the Institute of Biochemistry and Molecular Biology, University of Bonn.

4.3.1 Beta Arr1 and sGC beta1 are co-precipitated in HEK293 cells

4.3.1.1 Beta Arr1 IP

Co-IPs were performed by usage of anti-beta Arr1 antibody in lysates of Δbeta Arr1/2 HEK293 cells and GFP-beta Arr1 HEK293 cells transiently overexpressing sGC alpha1 beta1. IBs of supernatant and pellet of the Co-IP were incubated first with anti-sGC beta1 antibody to detect sGC beta1 followed by anti-GFP antibody to detect GFP-beta Arr1. Experiments were repeated with 3 different cell passages (n=3).

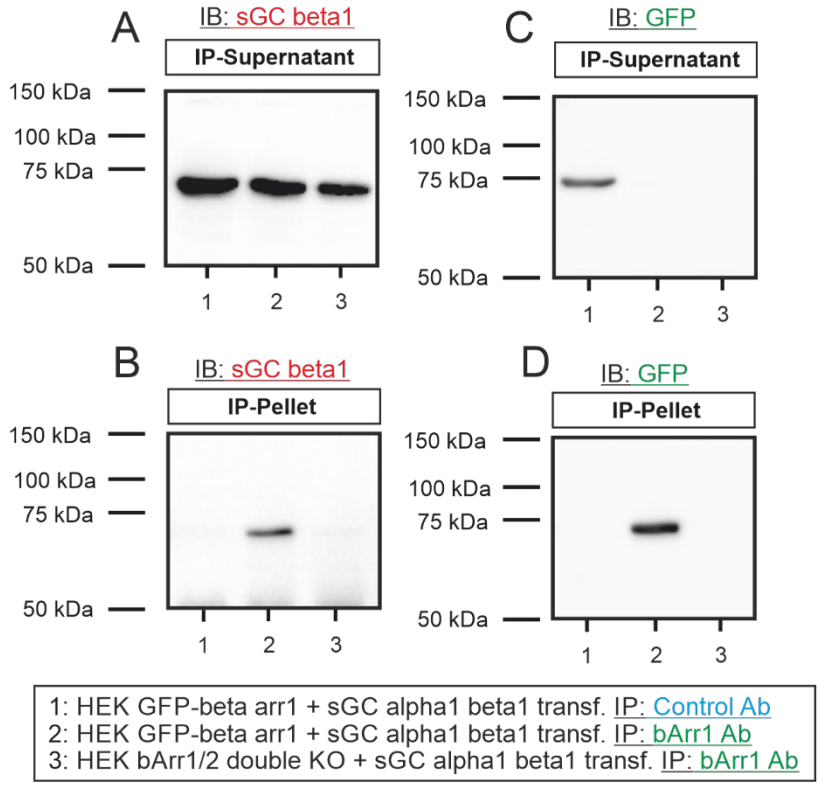

Figure 24: IBs of sGC beta1 and beta Arr1 in HEK293 cells after beta Arr1 IP.
(**A**) IB for sGC beta1 of the supernatant revealed sGC beta1 signals in all 3 lanes. (**B**) IB for sGC beta1 of the pellet revealed a sGC beta1 signal in lane 2. (**C**) IB for GFP of the supernatant revealed a GFP-beta Arr1 signal only in lane 1. (**D**) IB for GFP of the pellet revealed a signal for GFP-beta Arr1 in lane 2, indicating a successful beta Arr1 IP; n=3

IBs incubated with anti-sGC beta1 antibody revealed sGC beta1 signals in the supernatant of all three lanes (Figure 24A). This indicated successful expression of sGC beta1. IBs of the pellet fraction incubated with sGC beta1 antibody revealed only a signal in lane 2, while lane 1 and 3 showed no signal (Figure 24B). This indicated a direct binding of sGC beta1 to the immunoprecipitated GFP-beta Arr1 in lane 2 (Figure 24B). The absence of a sGC beta1 signal in lane 1 and 3 indicated that the detected interaction between sGC beta1 and beta Arr1 is highly specific.

IBs incubated with GFP revealed GFP-beta Arr1 signals in the supernatant of lane 1, while this signal was absent in lane 2 and 3 (Figure 24C). Furthermore, in the pellet no GFP signal was detected in lane 1 and 3 while a signal appeared in lane 2 (Figure 24D). A signal for GFP-beta Arr1 in the supernatant of lane 1 (Figure 24C) but no signal in the pellet of lane 1 (Figure 24D) indicated that the Co-IP was specific, as no pulldown occurred in lane 1 with an IgG control (mock) antibody. The GFP signal in the pellet of lane 2 confirms successful pulldown of GFP-beta Arr1, this pulldown was very effective as the signal completely disappeared in the supernatant (Figure 24C). Lane 3 represented a negative control, as there is no GFP-beta Arr1 protein in the lysate resulting in the absence of a GFP-beta Arr1 signal in supernatant (Figure 24C) and pellet (Figure 24D)

Taken together, results revealed a complete pulldown of GFP-beta Arr1 and binding of of sGC beta1 to beta Arr1. These findings indicated a specific interaction between sGC beta1 and GFP-beta Arr1.

4.3.1.2 sGC beta1 IP

Previous results showed a direct interaction of sGC beta1 and GFP-beta Arr1 in IP experiments using the anti-beta Arr1 antibody for pulldown (chapter 4.3.1). To further strengthen and validate these findings, IP experiments were also performed with the anti-sGC beta1 antibody for pulldown. Identical cell lysates as in chapter 4.3.1 were used and experiments were repeated with 3 different cell passages (n=3).

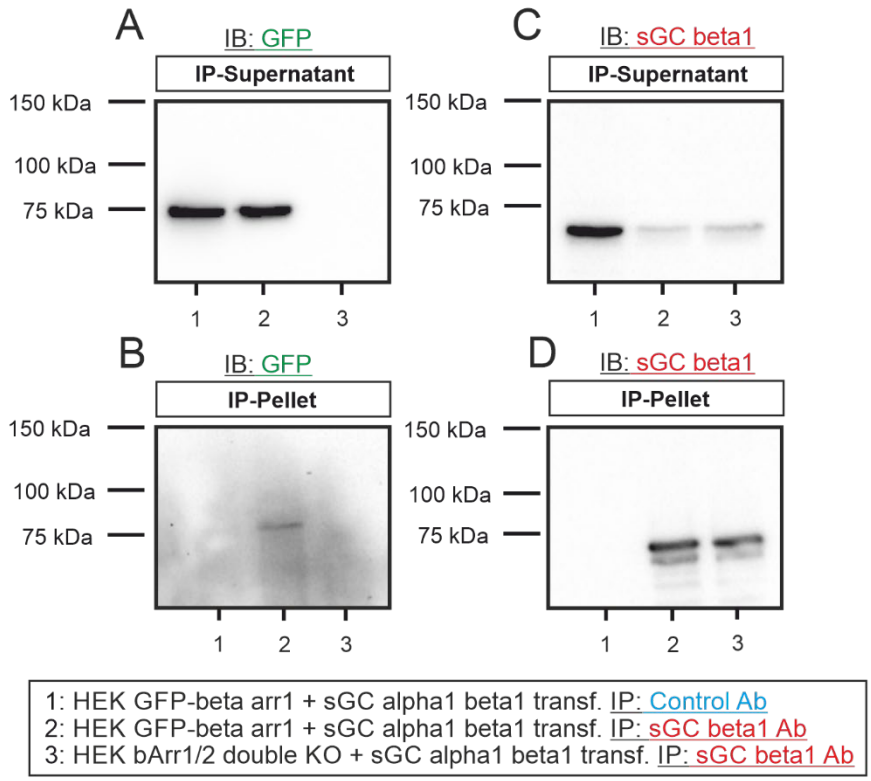

Figure 25: IBs of GFP and sGC beta1 in HEK293 cells after sGC beta1 IP.
(**A**) IB for GFP of the supernatant revealed GFP-beta Arr1 signals in lane 1 and 2. (**B**) IB for GFP of the pellet revealed a GFP-beta Arr1 signal in lane 2, indicating an interaction between sGC beta1 and GFP-beta Arr1. (**C**) IB for sGC beta1 of the supernatant revealed a strong sGC beta1 signal only in lane 1, while lane 2 and 3 revealed weak signals indicating a nearly complete pulldown in lane 2 and 3. (**D**) IB for sGC beta1 of the pellet revealed a signal for sGC beta1 in lane 2 and 3, indicating a successful sGC beta1 IP; n=3

IBs incubated with anti-GFP antibody revealed GFP-beta Arr1 in the supernatant of lane 1 and 2 (Figure 25A). In the pellet, IBs incubated with anti-GFP antibody detected a GFP-beta Arr1 signal solely in lane 2 (Figure 25B). A signal in the supernatant for GFP-beta Arr1 (Figure 25A) in lane 1 and 2 indicated that GFP-beta Arr1 HEK293 cells expressed GFP-beta Arr1. Lane 3 contained protein lysates from Δbeta Arr1/2 HEK293 cells. Here, absence of GFP-beta Arr1 was expected. A signal for GFP-beta Arr1 in the pellet (Figure 25B) only in lane 2 indicated a binding of GFP-beta Arr1 to the immunoprecipitated sGC beta1 protein. In addition, the absence of GFP-beta Arr1 signals in lane 1 and 3 illustrated that the detected interaction between sGC beta1 and beta Arr1 was highly specific.

IBs incubated with anti-sGC beta antibody revealed a strong sGC beta1 signal in the supernatant in lane 1, while faint signals were found in lane 2 and 3 (Figure 25C). Furthermore, no sGC beta1 signal was detected in the pellet of lane 1 (Figure 25D). This indicated that the IP was specific for the sGC beta1 antibody, as no pulldown occured in lane 1 where an IgG control antibody (mock) was used for the pulldown. IBs of the pellet incubated with anti-sGC beta antibody revealed sGC beta1 signals in lane 2 and 3 (Figure 25D). IP with the anti-sGC beta1 antibody resulted in a strong reduction of the sGC beta1 signal in the supernatant (lanes 2, 3) indicating a pulldown of sGC beta1 protein (Figure 25C).

The signals in the pellet (Figure 25D) confirmed the pulldown of sGC beta1 while lane 3 represented a negative control, as there was no eGFP-beta Arr1 protein in the lysate.

Taken together, results in Figure 25 displayed a pulldown of sGC beta1 and binding of GFP-beta Arr1 in HEK293 cells. Reciprocal pulldowns with both targets, sGC beta1 and GFP-beta Arr1, in three independent experiments (n=3) provide strong evidence for a direct interaction of beta Arr1 and sGC beta1.

4.3.2 Beta Arr1 and the control protein Laptm4a do not co-precipitate in HEK293 cells

Previous IP experiments revealed a binding of GFP-beta Arr1 and sGC beta1. Because beta arrestins in general are known to be potential binding partners for different proteins involved in various signaling cascades,[96] next, we tested the specifity of the binding of beta Arr1 and sGC beta1.

To exclude unspecific binding of expressed GFP-beta Arr1 in IP experiments, instead of the sGC alpha1 beta1 heterodimer a control protein was overexpressed in Δbeta Arr1/2 and GFP-beta Arr1 HEK293 cells. The construct for the control protein Laptm4a was kindly provided by Prof. Volkmar Gieselmann from the Institute of Biochemistry and Molecular Biology, University of Bonn. Laptm4a contains a myc-tag sequence to enable efficient detection by commercially available anti-myc-antibodies. Overexpression of sGC alpha1 beta1 or Laptm4a was performed in parallel and according to similar transfection and isolation protocols (chapter 3.2.4) in order to enable comparable results in protein expression. Laptm4a is a four-transmembrane-spanning protein in lysosomes and endosomes and functions as a regulator of endocytic recruitment upon interaction with human organic cation transporter 2.[97] It was chosen as control protein, as it shared similar structural properties with the sGC, both molecules contain a myc-DDK tag at the C-terminus. Further, it also possesses protein binding capacity, and thus represents a suitable binding control.

4.3.2.1 Beta Arr1 IP

Lane 1 and 2 contained lysates of GFP-beta Arr1 HEK293 cells expressing the Laptm4a control protein and lane 3 consisted of lysate of Δbeta Arr1/2 HEK293 cells expressing Laptm4a control protein. Lane 4 was a positive control for Laptm4a detection and consisted of lysate of GFP-beta Arr1 HEK293 cells expressing the Laptm4a control protein that was not immunoprecipitated but directly applied to the SDS-gel.

Unspecific coimmunoprecipitation of coexpressed Laptm4a control protein was tested by beta Arr1 pulldown. We hypothesized an absence of the myc signal in the pellet when Laptm4a is overexpressed instead of sGC beta1. IBs of myc-Laptm4a expressing samples were incubated with anti-myc antibody

(Figure 26A, B). IB incubated with GFP-antibody (Figure 26C, D) were performed to analyze GFP-beta Arr1 pulldown.

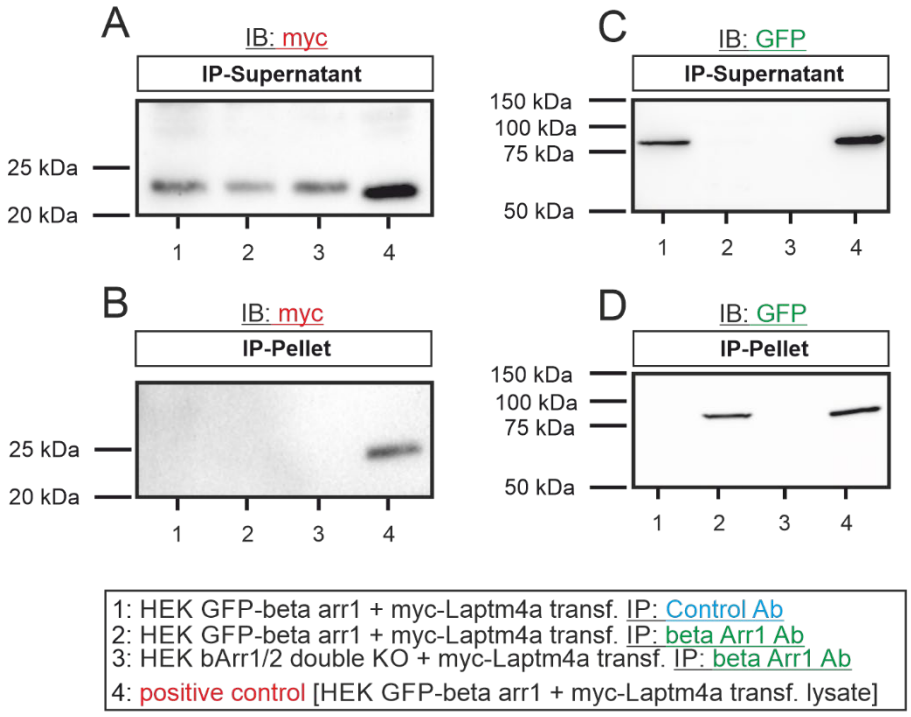

Figure 26: IBs of myc-Laptm4a and beta Arr1 in HEK293 cells after beta Arr1 pull down.
(**A**) IB for myc-Laptm4a of the supernatant revealed myc-Laptm4a signals in lane 1-4. (**B**) IB for myc of the pellet revealed no signal in lane in lane 1-3, only a signal for the positive control in lane 7. This indicated no unspecific beta Arr1 binding to the control peptide myc-Laptm4a in IP experiments. (**C**) IB for GFP of the supernatant revealed a GFP-beta Arr1 signal only in lane 1 and in the positive control (lane 4). (**D**) IB for GFP of the pellet revealed a signal for GFP-beta Arr1 in lane 2 and 4, indicating a successful beta Arr1 IP.

IBs incubated with anti-myc antibody revealed signals for myc-Laptm4a in lanes 1-4 in the supernatant (Figure 26A). IBs incubated with anti-myc antibody revealed signals for myc-Laptm4a only in lane 4 in the pellet (Figure 26B). Lane 4 served as a positive control as myc-Laptm4a protein was not immunoprecipitated but directly applied to the SDS-gel. The presence of myc-Laptm4a protein signals in the supernatant (Figure 26A) of lane 1-4 indicated a successful expression of the myc-Laptm4a control protein. However, the absence of myc-Laptm4a signals in lanes 1, 2 and 3 in the pellet (Figure 26B) confirmed that the expressed GFP-beta Arr1 did not bind to Laptm4a, thus there is no unspecific binding to this structurally similar transiently expressed protein.

IBs incubated with anti-GFP antibody revealed GFP-beta Arr1 signals in the supernatant of lane 1 and 4 while absent in lane 2 and 3 (Figure 26 C). IBs incubated with anti-GFP antibody revealed GFP-beta Arr1 signals in the pellet of lane 2 and 4 while absent in lane 1 and 3 (Figure 26 D). As explained earlier (chapter 4.3.1), lane 1 was immunoprecipitated with an IgG control antibody (mock control) and thus revealed a strong signal for GFP-beta Arr1 in the supernatant (Figure 26C) while no signal was detected in the pellet (Figure 26D). There was no signal in lanes 2 for GFP-beta Arr1 in the supernatant (Figure

26C), however a strong signal appeared in the pellet blot (Figure 26D) because all containing GFP-beta Arr1 protein was immunoprecipitated by the anti-beta Arr1 antibody. Lane 3 showed no GFP-beta Arr1 signal at all since Δbeta Arr1/2 HEK293 cell lysates were used and no GFP-beta Arr1 protein was expressed in these cells.

In summary, results in Figure 26 revealed a complete GFP-beta Arr1 pulldown but no coimmunoprecipitation for the Laptm4a control protein was detected. Absence of unspecific coimmunoprecipitation of coexpressed Laptm4a control protein further underlines the specificity of the demonstrated interaction of beta Arr1 and sGC beta1 shown above (chapter 4.3.1). IPs of Δbeta Arr1/2 HEK293 and GFP-beta1 HEK293 cells overexpressing sGC alpha1 beta1 have been performed in parallel and did not differ from previous results in chapter 4.3.1.1, but they are not shown here for the sake of clarity.

4.4 Analysis of Cyb5r3 and its potential role for sGC function in the absence of beta Arr1

Previous findings revealed an impaired sGC activity in cells and tissues when beta Arr1 is absent, while sGC expression remained unaltered. Furthermore, immunoprecipitation experiments proved a direct interaction of beta Arr1 and sGC beta1. Application of sGC stimulators and activators in *ex vivo* experiments suggested an impairment of the heme domain of the sGC enzyme in absence of beta Arr1 in murine PAs. NO-dependent sGC activation is highly dependent on the intact Fe^{2+} heme structure at the n-terminal HNOX domain of the enzyme. Oxidation of ferrous (Fe^{2+}) to ferric (Fe^{3+}) heme or complete loss of the heme-group (apo-sGC) results in diminished sGC activity.[98] We hypothesized that the impaired sGC activity in beta Arr1-/- systems could be due to oxidized or lost heme.

Little is known about the endogenous repair mechanisms of ferric and apo-sGC, but the Cyb5r3 enzyme was shown to reduce impaired ferric sGC to fully functional ferrous sGC.[99]

Diminished Cyb5r3 expression or impaired function in absence of beta Arr1 could potentially lead to a minimized NO sensitivity of sGC. To address this, I first analyzed the Cyb5r3 protein expression in HEK293 parental, Δbeta Arr1/2, GFP-beta Arr1 and GFP-beta Arr2 cells.

4.4.1 Cyb5r3 is similarly expressed in GFP-beta Arr1 and 2-transfected HEK293 cells

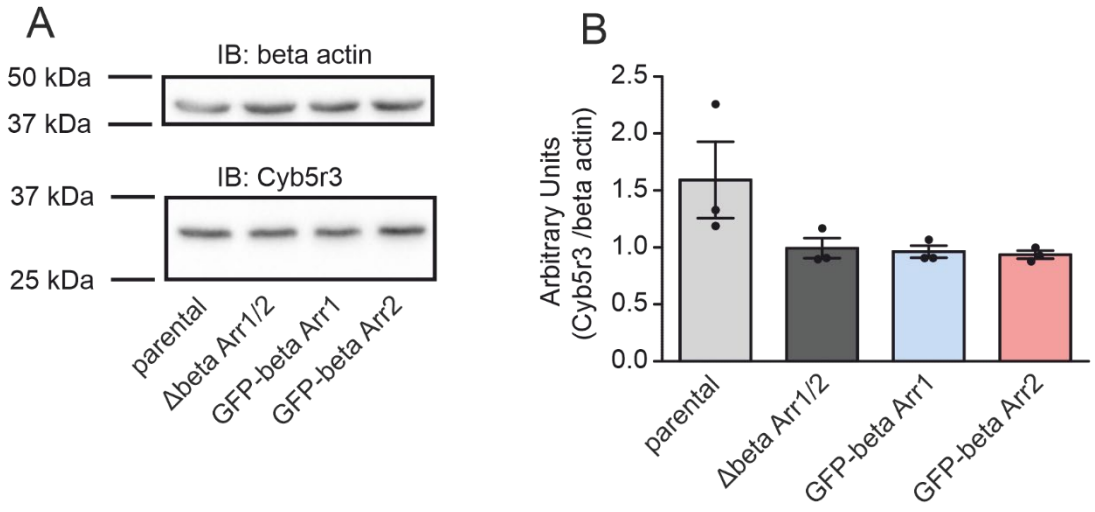

Figure 27: Quantification of Cyb5r3 protein expression in HEK293 cells using IBs.
(**A**) IBs of Cyb5r3 and beta actin suggested similar protein expression in HEK293 parental, Δbeta Arr1/2, GFP-beta Arr1 and GFP-beta Arr2 cells (n=3; representative blot is shown) (**B**) Quantification of Cyb5r3 protein expression normalized to beta actin expression in HEK293 parental, Δbeta Arr1/2, GFP-beta Arr1 and GFP-beta Arr2 cells (n=3), shown in A. Quantification confirmed similar Cyb5r3 expression levels in HEK293 parental, Δbeta Arr1/2, GFP-beta Arr1 and GFP-beta Arr2 cells. One-way ANOVA, post-hoc test: Tukey. n.s. > 0.05. All data are indicated as means ± s.e.m.

IBs for Cyb5r3 and beta actin revealed protein expression in HEK293 parental, Δbeta Arr1/2, GFP-beta Arr1 and GFP-beta Arr2 cells (n=3) (Figure 27A, representative blot). Expression of Cyb5r3 was normalized to the housekeeper beta actin and quantified (Figure 27B). HEK293 parental, Δbeta Arr1/2, GFP-beta Arr1 and GFP-beta Arr2 cells revealed similar Cyb5r3 protein expression levels.

Cyb5r3 protein expression remained unaltered when beta Arr1 or 2 were completely absent or one of the proteins was re-expressed. Thus, impaired sGC activity in beta Arr1-/- cells was not attributable to an altered protein expression of the heme iron reductase Cyb5r3.

4.4.2 Beta Arr1 and Cyb5r3 are co-precipitated in HEK293 cells

To check, if there exists a direct interaction between beta Arr1 and Cyb5r3 pulldown experiments were performed in HEK293 Δbeta Arr1/2 and GFP-beta Arr1 cells. Myc-tagged Cyb5r3 was transiently expressed (chapter 3.2.4). Experiments were designed similarly to previous beta Arr1 and sGC alpa1 beta1 Co-IP experiments (chapter 4.3), but GFP- and myc-trap agarose beads were used for the pulldown.

Lane 1 represents again the control (mock) for the specificity of the immunoprecipitating agarose: lysate of HEK293 cells expressing GFP-beta Arr1 and Cyb5r3 was used but precipitation was performed

with binding control agarose (mock). No precipitation should occur in this sample and no signal should appear in the pellet.

Lane 2 represents our main target of interest: lysate of HEK293 cells, expressing GFP-beta Arr1 and Cyb5r3, is precipitated with GFP- or myc-trap agarose. We hypothesized a signal mainly in the pellet but not in the supernatant, as most protein of interest should be precipitated.

Lane 3 represents a control for our hypothesis that beta Arr1 and Cyb5r3 interact: lysate of HEK293 Δbeta Arr1/2 cells expressing Cyb5r3 was precipitated with GFP- or myc-trap agarose. We expect no GFP-pulldown, as no beta Arr1 was present in the sample, while the myc-pulldown should be comparable to lane 2. When GFP-beta Arr1 and Cyb5r3 are coprecipitated in lane 2 but no signals are detected in lane 3 we concluded a specific interaction of both binding partners.

4.4.2.1 GFP trap agarose pulldown

Experiments were performed by usage of GFP-trap agarose beads for the pulldown in HEK293 GFP-beta Arr1 and Δbeta Arr1/2 cell lysates transiently overexpressing myc-Cyb5r3. IBs of supernatant and pellet of the pulldown were incubated first with anti-Cyb5r3 antibody to detect binding Cyb5r3 protein followed by anti-GFP antibody to confirm successful pulldown. Experiments were repeated with 3 different cell passages (n=3).

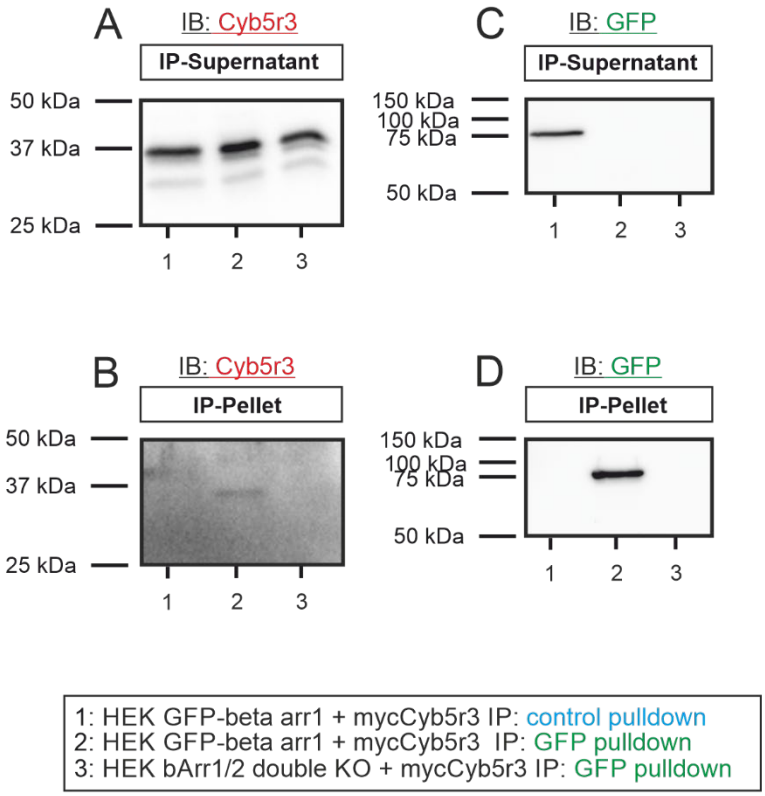

Figure 28: IBs of Cyb5r3 and beta Arr1 in HEK293 cells after GFP-beta Arr1 pulldown.
(**A**) IB for Cyb5r3 of the supernatant revealed Cyb5r3 signals in all 3 lanes. (**B**) IB for Cyb5r3 of the pellet revealed a Cyb5r3 signal in lane 2, indicating a direct interaction between beta Arr1 and Cyb5r3. (**C**) IB for GFP of the supernatant revealed a GFP-beta Arr1 signal only in lane 1. (**D**) IB for GFP of the pellet revealed a signal for GFP-beta Arr1 in lane 2, indicating GFP-beta Arr1 pulldown; n=3

IBs incubated with anti-Cyb5r3 antibody revealed Cyb5r3 signals in the supernatant of all three samples (Figure 28A). This indicated successful expression of Cyb5r3 (Figure 28A). IBs incubated for Cyb5r3 in the pellet revealed only a signal in lane 2, while lane 1 and 3 showed no signal (Figure 28B). This indicated a binding of Cyb5r3 to the precipitated GFP-beta Arr1 in lane 2 (Figure 28B). The absence of a Cyb5r3 signal in lane 1 and 3 indicated that the detected interaction between Cyb5r3 and beta Arr1 is specific.

IBs incubated with anti-GFP antibody of the supernatant revealed GFP-beta Arr1 signals in the supernatant of lane 1, while it was absent in lane 2 and 3 (Figure 28C). No GFP signal was detected in the pellet of lane 1 and 3, while a signal appeared in lane 2 (Figure 28D). A signal for GFP-beta Arr1 in the supernatant of lane 1 (Figure 28C) but no signal in the pellet of lane 1 (Figure 28D) indicated that the IP was specific, as no pulldown occurred in lane 1 by use of binding control agarose (mock). Lane 2 represented our target-of-interest. Here, a complete and successful pulldown of GFP-beta Arr1 occurred, as upon use of GFP-trap agarose for the pulldown the GFP-beta Arr1 signal disappeared in the supernatant (Figure 28C), but appeared in the pellet (Figure 28D). Lane 3 represented a negative control. It contained lysate with Cyb5r3 protein but without GFP-beta Arr1 protein. For lane 3 pulldown

was performed identically to lane 2 with GFP-trap agarose. The absence of a GFP-beta Arr1 signal in the supernatant (Figure 28C) and pellet (Figure 28D) for GFP confirmed a correct genotype -the Δbeta Arr1/2- of the control cells.

Taken together, results revealed a reproducible and stable precipitation of GFP-beta Arr1 (Figure 28C, D) and coprecipitation of Cyb5r3 (Figure 28A, B). These findings indicate a specific interaction between Cyb5r3 and GFP-beta Arr1 when precipitated with GFP-trap agarose.

4.4.2.2 Myc trap agarose pulldown

Previous results revealed an interaction of Cyb5r3 and GFP-beta Arr1 in pulldown experiments with GFP-trap agarose (chapter 4.4.2.1). To further strengthen and validate these findings, pulldown experiments were also performed vice versa with a myc-Cyb5r3 pulldown by use of myc-trap agarose and detection of GFP-beta Arr1 signals. Identical cell lysates as in chapter 4.4.2.1 were used and experiments were repeated with 3 different cell passages (n=3).

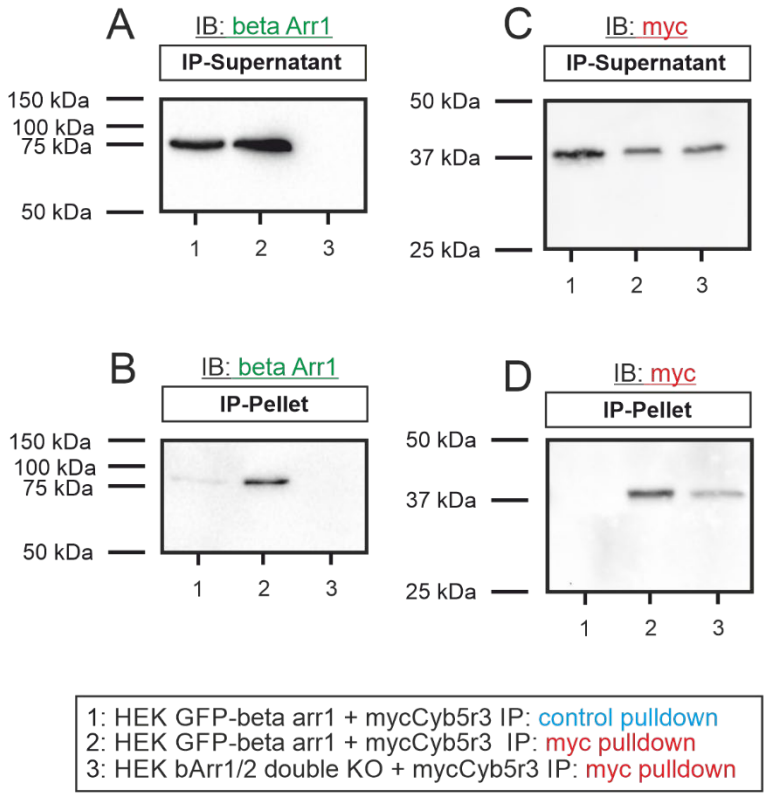

Figure 29: IBs of Cyb5r3 and beta Arr1 in HEK293 cells after myc-Cyb5r3 pulldown.
(**A**) IB for beta Arr1 of the supernatant revealed beta Arr1 signals in lane 1 and 2. (**B**) IB for beta Ar1 of the pellet revealed a beta Arr1 signal in lane 2, indicating an interaction between beta Arr1 and Cyb5r3. (**C**) IB for myc of the supernatant revealed a strong myc-Cyb5r3 signal in lane 1 while lane 2 and 3 revealed weaker signals indicating a pulldown in lane 2 and 3. (**D**) IB for myc of the pellet revealed a signal for myc-Cyb5r3 in lane 2 and 3, indicating a myc-Cyb5r3 pulldown; n=3.

IBs incubated with anti-beta Arr1 antibody revealed GFP-beta Arr1 in the supernatant of lane 1 and 2 (Figure 29A). In the pellet, IBs incubated with anti-beta Arr1 antibody detected a GFP-beta Arr1 signal mainly in lane 2 and a very weak signal in lane 1 (Figure 29B). A signal in the supernatant for GFP-beta Arr1 (Figure 29A) in sample 1 and 2 indicated that HEK293 GFP-beta Arr1 cells expressed GFP-beta Arr1. Lane 3 contained protein lysates from HEK293 Δbeta Arr1/2 cells. Here, absence of GFP-beta Arr1 was expected and confirmed once more the complete beta arrestin knockout. A signal for GFP-beta Arr1 in the pellet (Figure 29B) in lane 2 indicated a binding of GFP-beta Arr1 to the pulled down myc-Cyb5r3. The weak signal in lane 1 in the pellet represented the background by unspecific binding to the binding control beads while the absence of a signal in lane 3 illustrated that the detected interaction between myc-Cyb5r3 and GFP-beta Arr1 was of high specifity (Figure 29B).

IBs incubated with anti-myc antibody revealed a strong myc-Cyb5r3 signal in the supernatant of lane 1, with reduced signals in lane 2 and 3 (Figure 29C). IBs incubated with anti-myc antibody revealed myc-Cyb5r3 signals in the pellet in lane 2 and 3 (Figure 29D). Lane 2 displayed our target-of-interest. Upon use of myc-trap agarose part of the myc-Cyb5r3 signal in lane 2 disappeared in the supernatant (Figure 29C) and appeared in the pellet (Figure 29D) indicating a successful pulldown. Lane 3 represents a negative control. It contained lysate with myc-Cyb5r3 protein but without GFP-beta Arr1 protein. For lane 3 pulldown was performed in a similar manner as in lane 2 with myc-trap agarose. A weak myc-Cyb5r3 signal in the supernatant (Figure 29C) and a strong detection of myc-Cyb5r3 in the pellet (Figure 29D) confirmed successful pulldown. Furthermore, no myc-Cyb5r3 signal was detected in the pellet of lane 1 (Figure 29D). This indicated that the IP was specific for the myc-trap agarose, because in lane 1 binding control agarose (mock) was used for the pulldown.

Summarizing results (Figure 28 and Figure 29), pulldown experiments revealed coprecipitation of beta Arr1 and Cyb5r3 in overexpressing HEK293 cells. Reciprocal pulldowns with both targets, GFP-beta Arr1 and myc-Cyb5r3 in three independent experiments (n=3) provided strong evidence for an interaction between beta Arr1 and Cyb5r3.

4.5 Role of beta Arr1 for murine pulmonary arterial pressure regulation i*n vivo*

Previous findings of this work reveal that a lack of beta Arr1 impairs NO-dependent pulmonary vasorelaxation *ex vivo*. Our myograph experiments together with results in HEK cells suggest that binding of beta Arr1 to sGC and Cyb5r3 is required to provide ferrous (Fe^{2+}) heme in sGC and thereby sensitize the enzyme for NO activation. The sGC is also a target for the therapy of PAH, a severe chronic illness characterized by pulmonary vasoconstriction and increased pulmonary arterial pressure.[57] Therefore, we first analyzed pulmonary blood pressure in beta Arr1-/- mice *in vivo* and then applied a

disease model for hypoxia-induced PH in mice lacking beta Arr1 to analyze the role of beta Arr1 for the development of PH.

Chronic normobaric hypoxia is a well-known trigger for PH and it is the most common physiological stimulus for induction of PH in mice.[100] To evaluate the effect of beta Arr1 absence for tone regulation under normoxia and the development of PH, wildtype and beta Arr1-/- animals were analyzed either after three weeks of normoxia (21% O_2) or chronic hypoxia (10% O_2). Chronic normobaric hypoxia is known to elevate pulmonary arterial pressure, to induce vascular remodeling and to cause right heart hypertrophy in mice.[100] Therefore, three different parameters (right ventricular systolic pressure (RVSP), pulmonary vessel wall thickness and right heart hypertrophy) were measured to characterize the the role of beta Arr1 for pulmonary vascular regulation under normoxia and hypoxia.

4.5.1 Lack of beta Arr1 increases RVSP under normoxic (21% O_2) and hypoxic (10% O_2) conditions

After three weeks of normoxia (21% O_2) or normobaric chronic hypoxia (10% O_2), right heart catheter measurements of wildtype and beta Arr1-/- animals were performed. RVSP was measured with help of a 1F Millar pressure catheter and the mean systolic pressure was recorded over a period of 8 seconds.

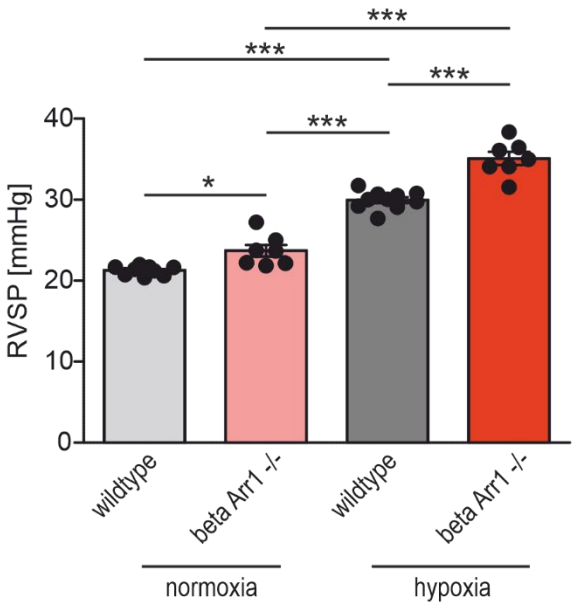

Figure 30: RVSP of wildtype and beta Arr1-/- mice under normoxic (21% O_2) or chronic hypoxic (10% O_2) conditions. RVSP was already increased under normoxic (21% O_2) conditions in beta Arr1-/-. Under hypoxic (3 weeks of 10% O_2) conditions, RVSP of beta Arr1-/- mice was further increased compared to wildtype. One-way ANOVA, post-hoc test: Tukey. ***p < 0.001, **p < 0.01, *p < 0.05 and ns p > 0.05. All data are represented as means ± s.e.m.

Catheter measurements revealed a significantly increased RVSP of beta Arr1-/- animals (n=9; RVSP= 23.7 ± 0.7 mmHg) already under normoxic (21% O_2) conditions compared to wildtype animals (n=9; RVSP= 21.3 ± 0.2 mmHg) (Figure 30). Hypoxic exposure (10% O_2) for 3 weeks demonstrated a further increase of RVSP in wildtype animals (30.0 ± 0.4 mmHg) but also in beta Arr1-/- animals (35.1 ± 0.8 mmHg) (Figure 30).

A significant increase of RVSP as a result of spontaneous PH development in beta Arr1-/- animals already under normoxic conditions and a further aggravation of RVSP under hypoxic conditions indicates that beta Arr1 is required to prevent increased RVSP.

4.5.2 Lack of beta Arr1 increases pulmonary vessel wall thickness under normoxic (21% O_2) and hypoxic (10% O_2) conditions

Because PH is mostly caused by a thickening of pulmonary vessels resulting in elevated vascular resistance, histological analysis of pulmonary vessel wall thickness was assessed next. Lungs were isolated and processed for histological staining. Slices of paraffin-embedded lungs were generated and stained with haematoxylin and eosin to enable analysis of pulmonary vessel wall thickness. Relative vessel wall thickness was assessed by normalization of the vascular wall thickness to the outer arterial diameter. For analysis arteries with a diameter between 30 and 70 µm located adjacent to airways were used.

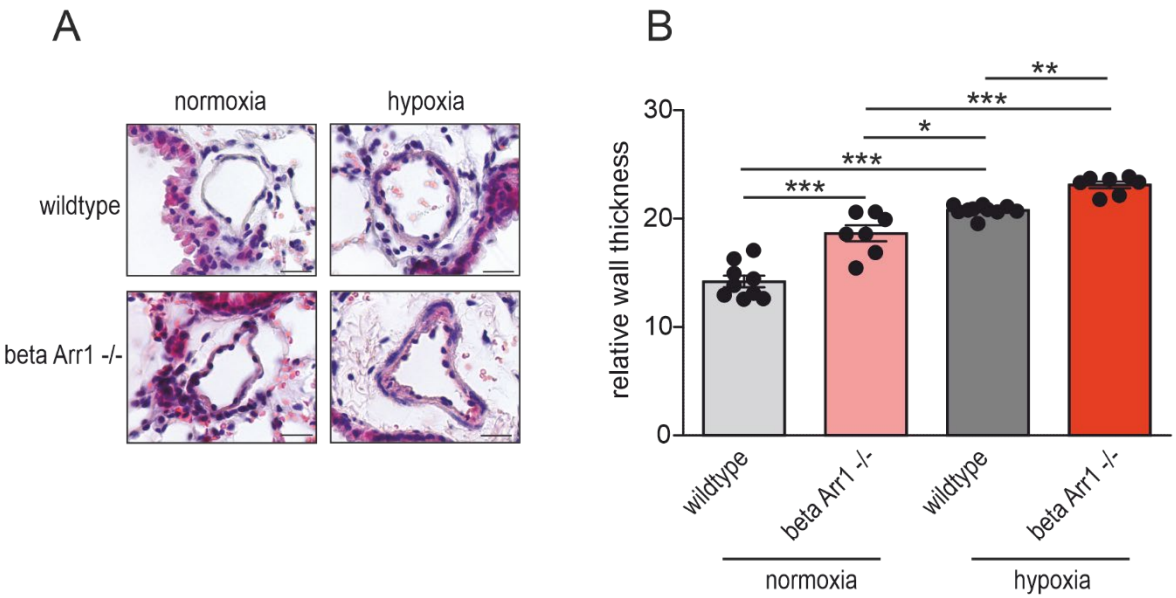

Figure 31: Histological analysis of vessel wall thickness in wildtype and beta Arr1-/- mice under normoxic (21% O_2) and chronic hypoxic (10% O_2) conditions.
(**A**) Representative H&E stainings revealed increased pulmonary vessel wall thickness upon hypoxia (10% O_2) in wildtype and beta Arr1-/- mice; 40x magnification; scale bar = 20 um. (**B**) Relative pulmonary vessel wall thickness of beta Arr1-/- mice was significantly increased compared to wildtype under normoxic (21% O_2) conditions. Under hypoxic (3 weeks of 10% O_2) conditions, relative wall thickness was further elevated in wildtype and beta Arr1-/- mice. One-way ANOVA, post-hoc test: Tukey. ***p < 0.001, **p < 0.01, *p < 0.05 and. All data are indicated as means ± s.e.m.

Representative H&E stainings revealed increased thickness of pulmonary vessel walls in beta Arr1-/ mice compared to wildtype, and a further elevation when hypoxic conditions were applied (Figure 31A). Quantification of the relative pulmonary arterial wall thickness of lung H&E stainings revealed a relative wall thickness in beta Arr1-/- animals of 18.7 ± 0.7 compared to wildtype (14.3 ± 0.5), all housed under normoxic (21% O_2) conditions (Figure 31 B). Three weeks of hypoxia [10% O_2] increased the relative pulmonary vessel wall thickness in wildtype (20.8 ± 0.2). The wall thickness in beta Arr1-/- (23.1 ± 0.3) animals was further enhanced compared to all other experimental groups. The striking elevation of pulmonary vessel wall thickness in beta Arr1-/- animals already under normoxic conditions and a further aggravation of RVSP under hypoxic conditions revealed that beta Arr1 is required to prevent excessive muscularization of distal pulmonary vessels.

4.5.3 Lack of beta Arr1 increases right hearth hypertrophy under normoxic (21% O_2) and hypoxic (10% O_2) conditions

Increased RVSP and increased pulmonary vessel wall thickness are known to introduce right heart hypertrophy in the disease progression of PH.[62] Therefore, right heart hypertrophy was assessed by the Fulton index, comparing the mass of the right ventricle (RV) with the left ventricle (LV) and the septum (S).

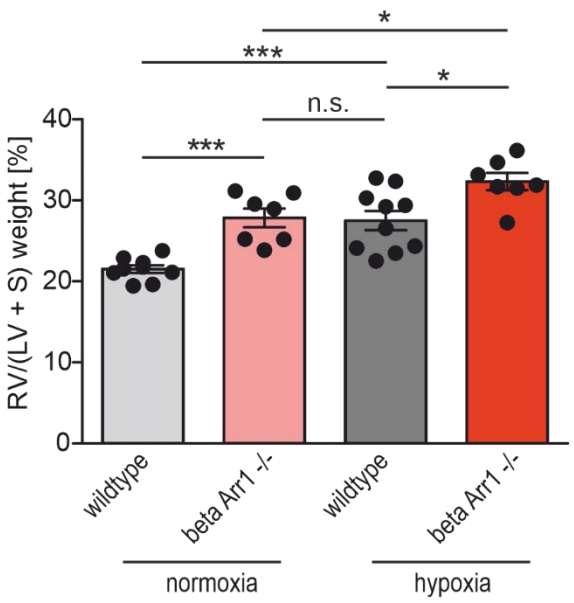

Figure 32: Right heart hypertrophy of wildtype and beta Arr1-/- mice under normoxic (21% O_2) or chronic hypoxic (10% O_2) conditions.
Analysis of right heart hypertrophy (Fulton index) under normoxic (21% O_2) conditions revealed significantly increased Fulton index in beta Arr1-/- compared to wildtype mice. The Fulton index is further increased under hypoxic (3 weeks of 10% O_2) conditions of beta Arr1-/- mice compared to wildtype. One-way ANOVA, post-hoc test: Tukey. ***p < 0.001, *p < 0.05 and ns p > 0.05. All data are represented as means ± s.e.m.

Results of right heart hypertrophy measurements revealed significantly increased Fulton indices in beta Arr1-/- mice (n=9; 27.8 ± 1.1 %) already under normoxic conditions compared to wildtype animals (n=9; 21.52 ± 0.47 %) (Figure 32). After three weeks of hypoxia the Fulton index was increased in wildtype animals (n=10; 27.50 ± 1.20 %) and this was further enhanced in beta Arr1-/- animals (n=7; 32.33 ± 1.07 %) (Figure 32). Previous results revealed increased RVSP and pulmonary vessel wall thickness already under normoxic conditions in beta Arr1-/- mice. These results were completed by increased right heart hypertrophy of beta Arr1-/- mice under normoxic conditions, revealing that three relevant factors of PH disease progression were already increased in beta Arr1-/- mice under normoxic conditions.

In conclusion, my experiments indicated an important role of beta Arr1 for the prevention of PH even under normoxic conditions *in vivo*.

5 Discussion

The motivation of this work was to unravel the role of beta arrestins in vascular tone regulation in the lung. A well-balanced PA tone regulation is central for the functionality of the pulmonary vascular system. PA tone is dysregulated in vascular diseases such as PAH with severe consequences: while PAH remains incurable to date, the 5-year survival rate (from the time of diagnostic right-sided heart catherterization) was 57% in the REVEAL registry.[1,62,101] Beta arrestins are negative regulators of GPCR signaling and responsible for desensitization and internalization of activated GPCRs.[27] Furthermore, beta arrestins were discovered as scaffolding molecules i.e. they are known to mediate activation of MAPKs and recruitment of the tyrosine kinase c-Src.[32,34] While beta arrestins are heavily investigated targests, not much is known about the role of beta arrestins in the pulmonary vascular system: A literature reseach on PubMed.gov revealed that 2496 publications in the last 10 years contained “beta arrestin” in the title, but surprisingly little is found about beta arrestins in the pulmonary vascular system.[102] Merely one recent study analyzed the role of beta Arr1 for the endothelium in the development of PAH.[76] The current work attempted to fill this gap and results from experiments with beta arrestin knockout mice and cells in the context of vascular tone regulation and PH will be discussed next.

5.1 Beta Arr1 affects NO-induced PA relaxation

A well-balanced vascular response to vasoconstrictive and vasorelaxant agents is essential for the precise physiological adaption of blood-flow.[1] We have analyzed beta Arr1 signaling in PA vasorelaxation and discovered a phenotype of impaired NO-dependent activation of sGC in beta Arr1-/- PAs. To unravel the mechanism of impaired PA vasorelaxation of beta Arr1-/- mice, relevant signaling molecules in the NO-sGC signaling pathway were addressed.

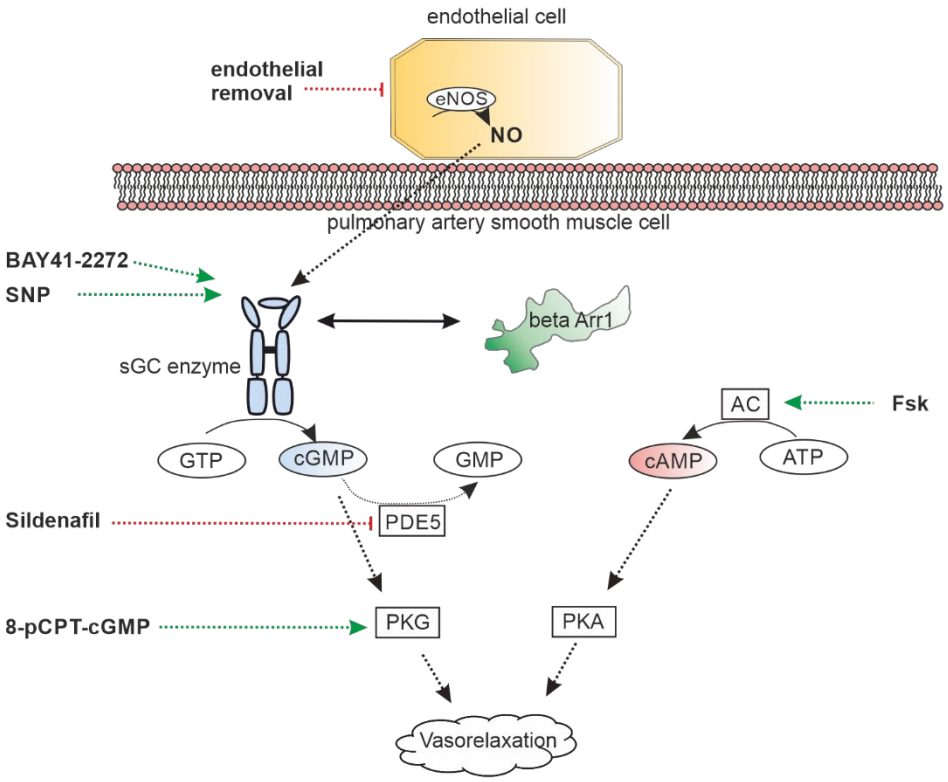

Figure 33: Interaction of bArr1 and NO signaling pathway in PAs.
Molecules of the NO-sGC signaling pathway were targeted in the wire myograph in PAs of wildtype, beta Arr1-/- and beta Arr2-/- PAs. SNP and BAY41-2272 dose-respose curves revealed impaired sGC-dependent vasorelaxation in beta Arr1-/- PAs. Fsk- and 8-pCPT-cGMP dose-response curves as well as sildenafil application revealed no effect of beta Arr1 for AC, PKG or PDE5 activity with relevance for PA vasorelaxation. Removal of the endothelium further excluded endothelial interference for the discovered sGC phenotype.

Various studies have revealed that inhibition of PDE5 resulted in increased SMC relaxation, while inhibition of sGC, PKG and AC resulted in attenuated vasorelaxation.[103–105] In our experiments, PDE5, PKG and AC activity were unaffected in beta Arr1-/-. The use of the sGC stimulator BAY41-2272 and the NO donor SNP pinpointed sGC activity as the prime target of beta Arr1-dependent signaling in PA vasorelaxation, because both sGC agonists revealed impaired vasorelaxation in beta Arr1-/- PAs (overview in Figure 33). This finding was further supported by decreased cGMP production upon SNP stimulation in HEK293 cells lacking beta Arr1 *in vitro*.

Relatively little is known about the role of beta arrestins in vascular tone regulation: Willets et al. revealed an elevated beta Arr1 and 2 expression in rat resistance arteries during development of hypertension, suggesting enhanced desensitization of overactive vasoconstrictor signaling.[106] These findings suggest increased beta arrestin-mediated receptor desensitization of contraction-mediating receptors (i.e. ET_A, $P2Y_2$, and AT_1) as a physiological response to dysregulated vasoconstriction upon hypertension. While our findings also reveal a benefical role of beta Arr1 in vascular tone regulation, we discovered sGC modulation by beta Arr1. Furthermore, our isometric force measurements were

perfomed in PAs of healthy wildtype and beta Arr1-- mice, while Willets et al. highlighted a role of beta arrestins upon pathophysiological emergence of hypertension. Thus, our results extend the role of beta Arr1 beyond Willets et al.´s proposed compensation mechanism of pathophysiologically dysregulated vasoconstriction. We present a benefical role of beta Arr1 for PA tone regulation and prevention of PH already under healthy and physiological conditions.

Willet et al.´s study focused on the classical desensitization and internalization mechanism of beta arrestins in the modulation of vascular tone. Scaffolding functions of beta arrestins in the vascular setting have also been reported, but focused on the endothelium: Liu et al. revealed that beta Arr2 is a critical component of the eNOS/NO signaling pathway in sinusoidal endothelial cells. During sinusoidal portal hypertension beta Arr2 expression and formation of the eNOS-beta Arr2 signalosome was decreased.[107] Furthermore, siRNA-mediated downregulation of both beta arrestins in human saphenous vein endothelial cells resulted in abrogated eNOS-dependent NO production, as shown by Carneiro et al.[108] Our results share with both findings that beta arrestins signal by interaction with crucial targets of vascular signaling pathways. While Liu and Carneiro focused on endothelium-mediated beta arrestin effects, we found a phenotype of impaired NO-mediated PA vasorelaxation also in absence of endothelial cell layers, therefore we proposed a key role of beta Arr1 in smooth muscle physiology. While Carneiro et al. did not differ between the beta arrestin subtypes, Liu et al. precisely described beta Arr2 as a critical component of the endothelial eNOS signalosome. We found no effect of beta Arr2 but of beta Arr1 in PA tone regulation. This suggests that each beta arrestin subtype regulates distinct vascular mechanisms in a tissue- and cell-specific manner: beta Arr2 appears to play a relevant role in endothelial NO production, while our results highlight a beta Arr1 effect in sGC mediated VSMC relaxation. Interestingly, studies in endothelial cells and our results from VSMCs both share a similar signaling axis as a target of beta arrestin signaling: eNOS-dependent NO production and sGC activity are both parts of the NO-mediated vasorelaxation pathway and therefore underline the importance of beta arrestins for this relevant physiological signaling pathways for tone regulation in all types of vessels.

Our findings expand current literature by highlighting a beta Arr1 function in tone regulation of the VSMC. Beta arrestin function in vascular cells was previously often associated with GPCR modulation. Therefore, GPCR and beta Arr1 signaling in context of tone regulation is reviewed next.

5.2 Beta Arr1 and GPCR signaling in PA tone regulation

Generally, a close association of beta arrestins with GPCRs is assumed and the GPCR field is inevitably interweaved with beta arrestin functions.[19] GPCRs and their modulation play an important role in tone

regulation of SMCs. In this context, Pera et al. have examined the role of beta Arrs in GPCR-mediated relaxation of tracheal rings. They revealed an increased isoprenaline (ISO)-induced tracheal relaxation of beta Arr2-/- mice but found no effect in beta Arr1-/- mice.[73] ISO is an agonist for beta-adrenergic receptors and is used for strong direct pulmonary and vascular relaxation.[109] Pera et al. explained their discovery of augmented ISO-mediated relaxation of beta Arr2-/- murine trachea rings by the loss of beta Arr2-mediated GPCR desensitization.[73] We analyzed GPCR downstream signaling by activation of the AC and revealed no effect of beta Arr1 for the AC-mediated cAMP signaling pathway because vasorelaxation by Fsk was unaltered in beta Arr1-/- PAs. Furthermore, our results with SNP revealed an impaired vasorelaxation of beta Arr1-/- PAs and suggested a beneficial effect of beta Arr1 rather than a negative effect of beta arrestins for tracheal relaxation. Therefore, I suggest a relevant scaffolding mechanism of beta Arr1 for sGC activity in PAs.

To integrate our findings in current beta arrestin literature, one has to consider the the paradigm of G protein independent but beta arrestin-dependet signaling. Recently, Grundmann et al. were able to proof that beta arrestins, in absence of any functional G protein ("zero functional G"), were recruited to receptors, but lack typical phosphorylation of ERK1/2 MAPKs.[95] Therefore, a biased arrestin signaling with no canonical GPCR signaling appears rather unlikely, but a pivotal role of beta arrestins in the fine-tuning of GPCR-mediated signaling as well as scaffolding appears to be reasonable.[95] Similarly, our findings of beta Arr1-mediated modulation of sGC also represent a beta Arr scaffolding function apart from direct GPCR modulation. To unravel the mechanism of impaired NO-vasorelaxation in absence of beta Arr1, relevant changes in sGC expression and functionality were considered next.

5.3 Beta Arr1 affects the sGC enzyme

Beta Arr1 was shown to have great impact on NO-mediated vasorelaxation of murine PAs. We hypothesized that beta Arr1 affects sGC expression or activity. To understand the molecular mechanism of the impaired vasorelaxation in beta Arr1 absence, sGC mRNA and protein levels and cGMP production were evaluated.

Our measurements of sGC mRNA and protein expression revealed similar sGC expression in wildtype and beta Arr1-/- PAs. In context of beta arrestin-mediated transcription, Ma and Pei revealed a potential role of beta arrestins in the regulation of transcription. Beta arrestins were shown to translocate from the cytoplasm to the nucleus, associated with transcription factors (i.e. p300 or CREB) and promoted transcription.[110] While we saw an impaired sGC-mediated PA vasorelaxation but no change in sGC expression, we assumed that beta Arr1 does not directly affect sGC transcription and

does not downregulate sGC protein levels. Therefore, a role of beta Arr1 in cGMP production was considered.

CGMP production was measured in HEK293 cells and revealed a strong increase in cGMP levels upon SNP stimulation when beta Arr1 was present and a significantly impaired cGMP production upon stimulation when beta Arr1 was absent. The sGC impairment by beta Arr1 KO consistently appeared in murine PA tissue and a human cell line (HEK293). This suggested sGC modulation as a rather general mechanism of beta Arr1. Since the sGC has outstanding importance as a signaling effector in VSMC, a pivotal role of this interaction in PAs appeared likely.[98] Literature suggests that basal sGC activity is quite robust, while stimulability of the enzyme is highly susceptible to disturbances due to the sensitive heme-group as the NO-binding site.[98] In our experiments, no significant difference in basal cGMP production suggested an impairment of the sGC catalytic activity upon stimulation while basal cGMP production remained unchanged. Therefore, we hypothesized a defect of the sGC protein in absence of beta Arr1 affecting the stimulability of the enzyme. The sGC enzyme is a heterodimeric protein and the β- subunit contains a heme-binding domain, located at its N-terminal site that enables NO binding. The prosthetic heme group in the β- subunit contains a five-coordinated ferrous (Fe^{2+}) heme with a histidine (His-105) as its axial ligand. NO binding causes an interruption of the histidine-bond, resulting in a conformational change of the enzyme and increased catalytic cGMP production at the C-terminus of the enzyme.[49,51] The prosthetic heme group is mandatory for sGC activation via endogenous NO. Removal of the heme group or oxidation of the ferrous ion (Fe^{2+}) abolishes any NO-mediated activity.[49,50] Our data from cGMP ELISA experiments revealed an impaired cGMP production in beta Arr1-/- upon NO stimulation. We assumed a defect of the sGC enzyme in absence of beta Arr1 in the NO-binding domain but with remaining basal activity. Therefore, sGC heme-dependent and heme-independent sGC activation was addressed.

5.4 Beta Arr1 affects the heme-dependent sGC activation in murine PAs

Distinct characterization of sGC heme states can be archieved by usage of sGC stimulating and modulating substances with different sGC activation mechanisms. We hypothesized that beta Arr1 affects the sensitive prosthetic heme group and thus modulates the catalytic enzyme activity. Therefore, we compared PA vasorelaxation of wildtype and beta Arr1-/- mice upon application of heme-dependent and heme-independent sGC modulators in wire myograph experiments.

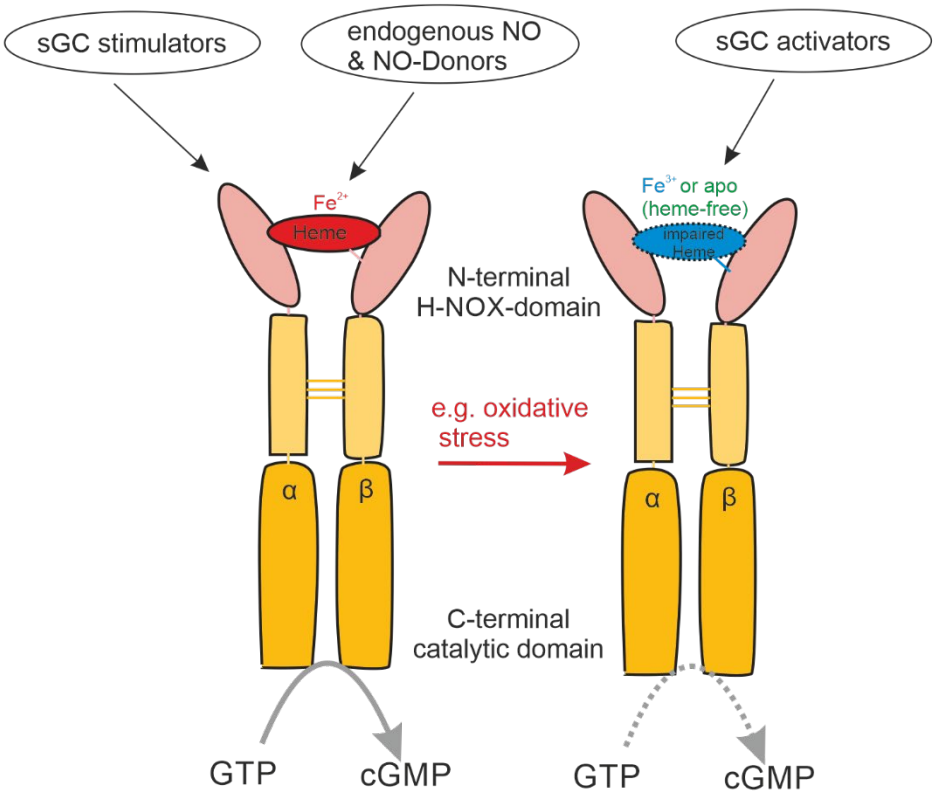

Figure 34: Different activation mechanisms of sGC modulators.
Endogenous NO or NO generated by NO-donors binds to the ferrous (Fe^{2+}) heme and activates the sGC enzyme to generate cGMP. Stimulators of sGC allosterically bind to the enzyme in its ferrous (Fe^{2+}) form. Oxidation or depletion of the heme group renders the sGC enzyme insensitive for NO or sGC stimulators. Activators of sGC bind to oxidized (Fe^{3+}) or heme-free sGC (apo-sGC), and activate the sGC when the heme moiety is NO-insensitive (Fe^{3+}) or absent.[111]

Our experiments revealed an impaired vasorelaxation of beta Arr1-/- PAs in absence of endothelial cells upon application of the sGC stimulator BAY41-2722 or SNP. Pharmacological activation of the sGC enzyme is achieved by different classes of compounds (Figure 34): NO releasing compounds, such as the NO donor SNP, release NO via spontaneous degradation.[92] Released NO functions as the prime agonist for the sGC, resulting in enzme activation and cGMP production. Allosteric activation of the sGC is achieved via sGC stimulators. Although not binding directly to the heme group, a crucial prerequisite for sGC activation via sGC stimulators is the presence of a reduced and ferrous (Fe^{2+}) heme moiety, similar to endogenous NO.[98] Our results with the sGC stimulator BAY41-2272 are consistent with our finding of impaired SNP vasorelaxation in beta Arr1-/- PAs. As literature suggests, both substance classes, NO donors and sGC stimulators, require a reduced and ferrous (Fe^{2+}) heme moiety for sGC activation.[93] Therefore, we found impaired sGC-mediated PA vasorelaxation in absence of beta Arr1 in two independent experiments and hypothesize decreased levels of ferrous (Fe^{2+}) heme sGC as an explanation.

When the sGC activator BAY58-2667 was applied in our experiments, similar vasorelaxation of wildtype and beta Arr1-/- PAs was observed. SGC activators are a rather new substance class and described

effective when the iron ion in the heme moiety is oxidized [thus in a ferric state (Fe^{3+})] or when the heme group is completely absent (overview in Figure 34). While the complete activation mechanism is still under debate, Stasch et al. revealed in radioligand binding assays an interaction of BAY58-2667 with amino acids 371 in the alpha-subunit and 231-310 in the beta-subunit. Therefore, they hypothesized that BAY58-2667 binds to the heme pocket in apo-sGC and mimicks the NO-bound heme group.[98,112] Further, sGG activator BAY58-2667 presented strong sGC activation primarily in ferric (Fe^{3+}) or apo-sGC, supporting an NO- and heme-independet activation mechanism.[112] Our discovery of impaired vasorelaxation by heme-dependent sGC activation (BAY41-2722) in beta Arr1-/- PAs and an unaltered vasorelaxation in response to heme-independent sGC activation (BAY58-2667) indicated reduced levels of the ferrous (Fe^{2+}) heme sGC, while unaltered responses to BAY58-2667 suggested comparable ferric (Fe^{3+}) and apo-sGC levels. The balance between NO-sensitive ferrous (Fe^{2+}) heme-sGC and NO-insensitive ferric (Fe^{3+}) or apo-heme sGC appears to be of high relevance for physiological responses to NO and thus an intact vascular function, but imbalances are difficult to evaluate. Our applied sGC activators and sGC stimulators resemble the most suited tools for analysis of heme-sGC imbalances in tissues.[48,113,114] To integrate our findings in current sGC literature, different sGC heme states have to be adressed.

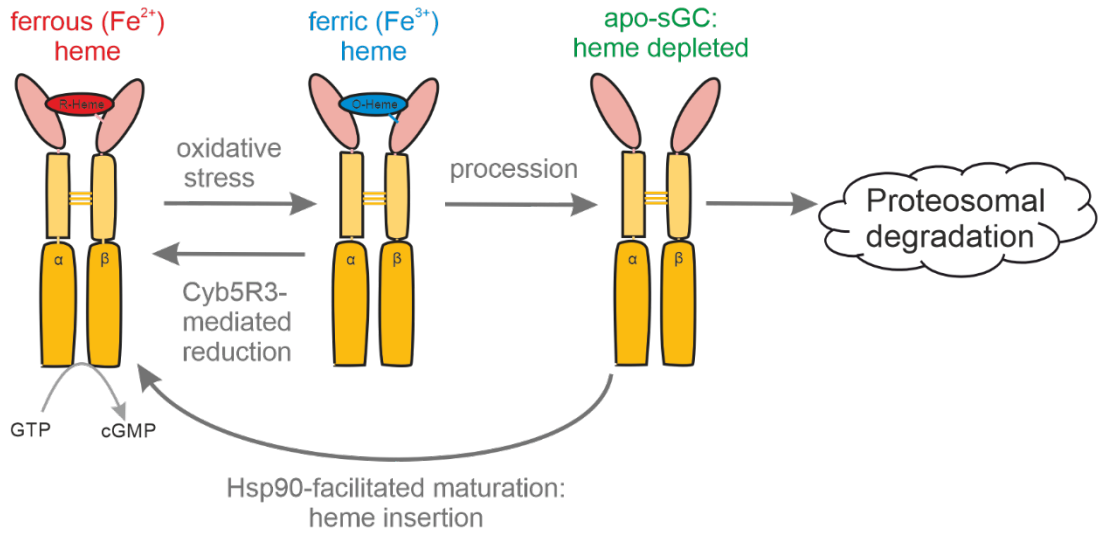

Figure 35: Potential heme states of sGC.
Ferrous (Fe^{2+}) heme sGC is sensitive for NO stimulation. Oxidation by oxidative stress can result in ferric (Fe^{3+}) heme sGC that is further processed to heme-depleted apo-sGC. Apo-sGC is prone to undergo proteosomal degradation. Hsp90-facilitiated maturation was shown to insert heme to apo-sGC, generating ferrous (Fe^{2+}) and NO-sensitive sGC. Ferric (Fe^{3+}) heme sGC can be reduced to ferrous (Fe^{2+}) heme sGC by Cyb5r3.

Oxidation of the ferrous (Fe^{2+}) heme-sGC to ferric (Fe^{3+}) heme, due to oxidative stress, is shown to cause a conformational change of the sGC enzyme which subsequently leads to the complete loss of the heme group. Apo-sGC remains NO-insensitive and only shows basal catalytic activitiy (overview in Figure 35).[98] Oxidation of the heme group is reported as a potential pathophysiological mechanism for

numerous cardiovascular diseases.[98] Indeed, Thoonen et al. described an elevated blood pressure, growth retardation and a reduced life span in genetically modified heme-deficient sGC (apo-sGC) mice.[114] We discovered a phenotype of increased RVSP under normoxic conditions in beta Arr1-/- mice. Furthermore, we also found similar basal cGMP production but impaired production upon NO-stimulation. Our results applying sGC modulators suggested decreased levels of ferrous sGC, but similar levels of ferric- or apo-sGC. Therefore, our results are evaluated in light of heme-dependent sGC degradation.

The exact mechanism underlying degradation of oxidized heme-sGC is not fully clarified, but Meurer et al. and others revealed that apo-sGC is prone to strong polyubiquitination and proteosomal degradation. In this process, sGC ubiquitination is regarded as key and rate-limiting step of sGC degradation. [93,115,116] Ubiquitin-mediated proteosomal degradation in general is regarded as a pathway for internal protein quality control.[116,117] These findings are in contrast with our protein expression data, as we see no decrease of sGC protein despite loss of cGMP production in absence of beta Arr1. Therefore, I concluded an impaired sGC function, but no complete loss or degradation of the sGC enzyme, and hypothesized NO-insensitive sGC in beta Arr1-/-. Oxidized heme-sGC was shown to be NO-insensitive: ODQ was shown to oxidize the ferrous (Fe^{2+}) form of the sGC to the ferric form (Fe^{3+}), resulting in diminished NO sensitivity.[53] Stasch et al. revealed only basal cGMP production upon NO stimulation in different cell systems treated with ODQ while a strong response to the applied sGC activator (BAY58-2667) was detected. These results are in congruence with our experiments, where we revealed similar baseline cGMP production but impaired cGMP production upon stimulation in beta Arr1-/- cells, while beta Arr1-/- PAs revealed similar responses to BAY58-2667. Evaluating the physiological consequences of ferric sGC, a recent study by Ghosh et al. revealed a role of NO-insensitive heme sGC in the bronchodilator therapy of asthma. They suggested that allergic inflammation in asthma affected NO-mediated bronchodilatation and revealed sGC activators as sufficient bronchodilators despite NO-insensitivity.[118] Our results revealed that impaired NO-dependent sGC vasorelaxation is rescued by usage of the sGC activator BAY58-2667 in beta Arr1-/- PAs. Therefore, an impaired heme sGC in beta Arr1-/- is in congruence with Gosh et al.´s findings of NO-insensitive heme sGC and response to sGC activators in human airway SMCs. Furthermore, this gives the perspective that beta Arr1 could also play a role in NO-mediated bronchodilatation in asthma.

In conclusion, the transition between ferrous, ferric and apo-sGC appears to be a complex process and multiple enzymes and binding partners participate in this transition mechanism that is uncompletely understood. Experiments with sGC modulators suggest an influence of beta Arr1 on the balance between NO-sensitive (Fe^{2+}) and NO-insensitive (Fe^{3+}) heme sGC states, while protein expression of

total sGC remained unchanged in beta Arr1 absence. To investigate the relation between beta Arr1 and sGC as a potential explanantion, direct protein interaction was addressed.

5.5 Direct binding partners of beta Arr1

Beta arrestins are multifaceted adaptor proteins and apart from GPCR interaction, binding to various endocytic proteins (i.e. clathrin or AP2) has been described.[119] We hypothesized a direct interaction between beta Arr1 and sGC as an explanation for the impaired sGC activity in absence of beta Arr1. I performed Co-IP experiments to test this hypothesis.

My Co-IP experiments revealed a direct binding of beta Arr1 to sGC. Barella et al. have revealed that beta Arr1 enhances sulfonylurea-induced insulin secretion in pancreatic beta cells by direct interaction with the Epac2 protein.[120] Furthermore, Ma et al. have revealed a direct beta Arr1 interaction with VEGFR3 when overexpressed in HEK293 cells.[76] Both studies performed Co-IP experiments to reveal a direct protein interaction between beta Arr1 and VEGFR3 or Epac2. Our data are consistent with the concept of direct protein binding by the adaptor protein beta Arr1. Ma et al. as well as Barella et al. have overexpressed their target molecules *in vitro* for IP, most likely because native protein expression often appears to be below the detection limit of IP experiments.[76,120] While overexpression is widely accepted, one has to ensure that the claimed interaction between two co-precipitated targets is specific. Our experiments addressed potential unspecific binding, as we used control antibodies and beads for pulldowns, we performed reciprocal pulldowns and further tested unspecific binding by pulldown of the control protein Laptm4a that shares similar structural properties with the sGC. Therefore, our data are in line with literature and present the nature of the interaction between sGC and beta Arr1 as highly specific.

Crépieux et al. reviewed the complex beta arrestin interactome and mapped various binding partners of beta arrestins. In total, they concluded a crucial role of beta arrestins especially for the assembly of multiprotein complexes.[121] Ghosh et al. have further shown a direct protein interaction between sGC beta1 and the heat shock protein 90 (Hsp90). They suggest that Hsp90 is necessary for the sGC maturation process: Hsp90 enables insertion of the heme into apo-sGC.[122] These publications suggest that both of our interacting targests, beta Arr1 and sGC, are part of multiprotein complexes. Therefore, we analyzed a further potential beta Arr1 binding partner that could potentially affect sGC activity.

We performed pulldown experiments with beta Arr1 and Cyb5r3 in HEK293 cells and revealed a protein interaction between beta Arr1 and Cyb5r3. The balance of different heme states appears to be of great importance for physiological sGC function, yet knowledge of specific mechanisms is rather rare. Rahaman et al. have shown that VSMCs apparently have an intrinsic mechanism to reduce oxidized

heme iron (Fe^{3+}) to the ferrous (Fe^{2+}) form: Cyb5r3 was shown to directly bind to the oxidized (Fe^{3+}) sGC enzyme and was able to reduce ferric (Fe^{3+}) heme iron to ferrous heme iron (Fe^{2+}).[99] This process is considered critical for NO-mediated cGMP activity. The Cyb5r3 enzyme is a flavoprotein that transfers electrons from its NADH domain to an electron acceptor, i. e. the ferric (Fe^{3+}) heme iron of the sGC.[99] Our findings extend published knowledge about the Cyb5r3 enzyme and present beta Arr1 as a binding partner. Rahaman et al. revealed a direct binding of ferric heme sGC to Cyb5r3 in IP experiments.[99] This was required for the reduction of ferric heme sGC. Our finding of a direct interaction between beta Arr1 and Cyb5r3 complement this and present Cyb5r3 as another binding partner of beta Arr1 with previously described relevance for sGC heme balance.[123]

Thus, our data suggest that bArr1 binds sGC and Cyb5r3 and thereby contributes to the interaction of these proteins that is required to reduce oxidized, NO-insensitive sGC. To evaluate the *in vivo* relevance of our findings about impaired sGC-mediated vasorelaxation in beta Arr1-/- PAs, we analyzed beta Arr1-/- mice in context of PH development next.

5.6 Beta Arr1 is relevant for the prevention of PH

PAH is a severe disease and current pharmacological therapy often focusses on the compensation of excessive vasoconstriction.[57] We revealed a relevant role of beta Arr1 for sGC-mediated tone regulation of murine PAs. Thus, we hypothesized that chronic hypoxia-induced PH could be routed in impaired sGC signaling in the PAs in beta Arr1-/- mice.

My experiments revealed that beta Arr1-/- mice manifested a significant increase of RVSP, vascular remodeling and right heart hypertrophy already under normoxic conditions. Upon 3 weeks of chronic hypoxia, RVSP, vascular remodeling and right heart hypertrophy were significantly increased in wildtype animals and further elevated in beta Arr1-/- mice, suggesting that the lack of beta Arr1 appears to increase the development of PH. A recent study by Ma et al. supports our findings and revealed independently a severe phenotype of PH induced by hypobaric hypoxia in beta Arr1-/- mice compared to wildtype and beta Arr2-/- animals. Also in this study, beta Arr1-/- mice developed a significant increase of RVSP, increased vascular medial thickness and right heart hypertrophy.[76] Strikingly, Ma et al. revealed no phenotype under normoxic conditions, while we saw a significant increase of RVSP, vascular remodeling and right heart hypertrophy already under normoxic conditions.[76] To shed light on this discrepancy, supportive *ex vivo* data and differences in the study design have to be taken into consideration. To explain our findings under normoxic conditions, I correlated our results from signaling experiments with current literature about PH: Persisting vasoconstriction remains a signature symptom of PAH and is target of various pharmacological

therapeutic approaches.[57] My signaling experiments revealed an impaired sGC function in absence of beta Arr1 *ex vivo* and *in vitro* under normoxic conditions. Therefore, an impaired PA vasorelaxation *in vivo* due to impaired NO-sGC signaling explains a high susceptibility of beta Arr1-/- animals to increased RVSP, hypertrophy and pulmonary vascular remodeling already under normoxic conditions. Various other studies have addressed a central role for dysregulated sGC in PH.[98,124,125] Elevated blood pressure was detected in mice with impaired sGC heme function.[114] Additionally, Dumitrascu et al. even revealed that the application of different sGC modulators reversed the PH symptoms of chronic hypoxia in wildtype mice.[124] These results are in line with our findings of impaired sGC mediated PA vasorelaxation and cGMP production in beta Arr1-/- and explain the discovered strong PH phenotype of beta Arr1-/- mice with impaired sGC activity in absence of beta Arr1. Further differences in the study design of ours and Ma et al.´s study was considered:

Our results were consistent in both genders for all murine experiments, whereas Ma et al. have reported a lower susceptibility of female beta Arr1-/- mice to hypoxia induced PH and used only male mice for PH induction in their following studies.[76] Neupane et al. recently (2020) revealed no difference between male and female mice upon hypoxia-induced PH in their study.[126,127] Our studies are in congruence with Neupane et al., we also detected no significant difference in RVSP, right heart hypertrophy and increased vascular medial thickness when comparing male and female mice (data not shown). Thus, beta Arr1-/- mice revealed significant development of PH upon chronic hypoxia independent of gender and researching both genders is considered an additional strength of our study. Ma et al. revealed that beta Arr1 was required for VEGFR3 activation. Downregulation of beta Arr1 resulted in decreased cell proliferation, migration and angiogenesis in human microvascular endothelial cells from lung.[76] While VEGFR3 belongs to the family of receptor tyrosine-kinases, they suggested a cross-talk between GPCRs and VEGFRs with importance for PH treatment.[76] Both studies share a significant effect of beta Arr1 for PH development, both differ in the proposed cell target: Ma et al. highlighted a role of beta Arr1 for pulmonary endothelial cells, while we excluded an effect of beta Arr1 in the endothelium in our *ex vivo* experiments by removal of endothelial cell layers, and still a significant impairment of beta Arr1-/- PA vasorelaxation by SNP was observed. Therefore, we proposed impaired sGC signaling in beta Arr1-/- PASMCs as an explanation for increased development of PH.

Both studies share that beta Arr1 apprears relevant for PA tone regulation and development of PH. Ma et al.´s study highlighted a beta Arr1-interaction with a non-GPCR target as relevant for PH progression.[76] We also discovered a beta Arr1 interaction aside from direct GPCR modulation, because application of SNP in myograph experiments did not activate GPCRs but the intracellular sGC enzyme. Thus, both studies extend the concept of non-GPCR modulation of beta Arr1 with respect to PH.

5.7 Outlook

This work has extended current knowledge about the role of beta Arr1 in PA tone regulation and PH development. It reveals a specific interaction of beta Arr1 and the sGC enzyme with physiological and pathophysiological relevance. A central finding is the decreased sGC activity caused by beta Arr1 absence, resulting in decreased cGMP production upon NO-dependent stimulation while sGC expression was unaltered. For the first time, we present sGC as a new and physiologically relevant interaction partner of beta Arr1. First evidence of beta Arr1 relevance for the development of PAH was recently (2019) revealed by Ma et al. in PAH human lung samples.[76] Our *in vivo* findings confirm and expand this by uncovering significant defects in beta Arr1-/- mice already under normoxic conditions. Therefore, we present beta Arr1 as a new modulator of the well-known and common therapeutic target of PAH, the NO-sGC signaling pathway. While the relevance of the beta Arr1 and sGC interaction has been clearly elucidated in this work, also a mechanism of the beta Arr1 mediated sGC defect was proposed.

Literature research offered data about the physiological and pathophysiological role of impaired heme-sGC, but precise information about the molecular analysis of different heme sGC states were scarce.[98] Usage of sGC stimulators and activators represented the best-described method for the characterization of sGC heme states *ex vivo* and *in vivo* and was performed in this work.[48,113,114] Further molecular analysis of the sGC heme states appears complicated yet desirable. Russwurm et al. presented an ultraviolet-spectroscopic study of sGC heme states and used different absorbance wave length for ferrous (Fe^{2+}) and ferric (Fe^{3+}) heme sGC .[51] Together with Dr. Russwurm, we established a protocol of sGC purification and ultraviolet-spectroscopic analysis of sGC with different heme states in bArr1 KO and bArr1 re-expressing HEK293 cells. The sGC purification turned out to be critical for comparability of the results and technical limitations prevented clear results for this work. Nevertheless, a precise molecular analysis of the sGC heme state *in vitro* in the presence or absence of beta Arr1 is desirable in future to better understand the role of bArr1 for sGC function.

In conclusion, the modulation of sGC by beta Arr1 appears to be a general mechanism with high relevance for PA tone regulation and PH development. Direct interaction between beta Arr1 and sGC reveals a new mechanism of beta Arr1 signaling aside from GPCR modulation. Our suggested signaling mechanism of impaired heme-dependent sGC activity further supports current discoveries about the balance of different sGC heme states and their role in vascular tone regulation.[99]

6 Summary

Vascular tone regulation is facilitated by a complex interplay of various constricting and relaxing mechanisms. Excessive vasoconstriction is a prominent symptom of multiple vascular diseases and target of numerous pharmacotherapeutic treatments. Pulmonary arterial hypertension (PAH) is a severe pulmonary vascular disease characterized by excessive vasoconstriction of pulmonary arteries (PAs) and adverse vascular remodeling.[57,58] The NO-sGC signaling axis is an important vasorelaxant signaling pathway in tone regulation of PAs. Beta arrestins are well-known for their regulation of GPCR signaling as well as their function as scaffolds in numerous signaling pathways.[27]. The motivation of this work is to unravel the role of beta arrestins in vascular tone regulation in the lung. Two studies revealed that beta Arr2 modulates murine bronchorelaxation by desensitization of beta-adrenergic receptors in airway smooth muscle cells.[72,73] So far, little is known about the role of beta Arr1 in vascular tone regulation, especially in PAH. This work tries to fill this gap and characterizes the role of beta Arr1 in PA tone regulation and in PAH.

Force measurement experiments in murine PA rings revealed an impaired vasorelaxation upon application of the NO donor SNP in the absence of beta Arr1. To unravel the mechanism of impaired NO-mediated vasorelaxation in beta Arr1-/- mice, relevant signaling molecules in the NO-sGC signaling pathway were tested. Inhibition of phosphodiesterase 5 (PDE5) by Sildenafil, as well as direct activation of the protein kinase G by 8-pCPT-cGMP and adenylyl cyclase by Forskolin revealed no difference in beta Arr1-/- PA vasorelaxation. A contribution of endothelial cells was excluded by removal of the PA endothelium. Conclusively, modulation of other relevant molecules of the NO-sGC signaling pathway remained unaffected suggesting a direct impact of the sGC enzyme on impaired vasorelaxation in absence of beta Arr1.

Analysis of mRNA and protein expression revealed unaltered sGC levels despite absence of beta Arr1 in PAs indicating a functional defect rather than a downregulation of sGC. Measurements of cGMP production confirmed an impaired NO-dependent sGC activation in HEK293 cells lacking beta Arr1. The sGC enzyme contains a NO-binding heme group and removal of the heme group or oxidation of the ferrous ion (Fe^{2+}) abolishes any NO-mediated activity.[49,50] Characterization of sGC heme states was performed in force measurement experiments by application of sGC modulators with different sGC activation mechanisms: application of the sGC stimulator BAY41-2271 indicates an impaired function of NO-sensitive ferrous (Fe^{2+}) sGC in absence of beta Arr1. Administration of the sGC activator BAY58-2667 in the same setting suggested that heme-independent sGC remains unaffected. Therefore, this work reveals an impaired heme-dependent sGC activation in absence of beta Arr1.

Immunoprecipitation experiments in HEK293 cells highlights a direct interaction between beta Arr1 and the sGC, as well as between beta Arr1 and the heme iron reductase Cyb5r3. Finally, beta Arr1-/- mice had increased right ventricular systolic pressure, pulmonary vascular remodeling and right heart hypertrophy already under normoxic conditions, which were further increased upon chronic hypoxia. These experiments indicated an important role of beta Arr1 for the prevention of pulmonary hypertension even under normoxic conditions *in vivo.*

In summary, this work uncovered an important role of beta Arr1 in NO-dependent vasorelaxation of murine PAs. We provided evidence that beta Arr1 is relevant for heme-dependent sGC activation in PAs with physiological and pathophysiological relevance. In addition, significantly impaired sGC stimulability and beta Arr1-sGC interaction in HEK293 cells suggest a global beta Arr1 effect beyond PAs and thus expand current knowledge about the beta Arr1 functions.

7 References

1. Pugsley, M. K. & Tabrizchi, R. The vascular system. *Journal of pharmacological and toxicological methods* **44,** 333–340; 10.1016/S1056-8719(00)00125-8 (2000).
2. Silbernagl, S., Despopoulos, A., Gay, R. & Rothenburger, A. *Taschenatlas Physiologie.* 7th ed. (Thieme, Stuttgart, 2007).
3. Circulatory Pathways | SEER Training. Available at https://training.seer.cancer.gov/anatomy/cardiovascular/blood/pathways.html (2019).
4. Amboss Aufbau und Funktion der Blutgefäße. AMBOSS - Fachwissen für Mediziner (2019). Printausgabe Fokus Physikum 2018/2019 -Band 2, Seite 205. aufgerufen am 10.07.2020. Available at https://www.amboss.com/de/wissen/Aufbau_und_Funktion_der_Blutgef%25C3%25A4%25C3%259Fe (2018/2019).
5. Townsley, M. I. Structure and composition of pulmonary arteries, capillaries, and veins. *Comprehensive Physiology* **2,** 675–709; 10.1002/cphy.c100081 (2012).
6. Huppelsberg, J. & Walter, K. *Kurzlehrbuch Physiologie. Nach dem neuen GK1] ; 42 Tabellen* (Thieme, Stuttgart, 2003).
7. Emori, T. *et al.* Cellular mechanism of endothelin-1 release by angiotensin and vasopressin. *Hypertension (Dallas, Tex. : 1979)* **18,** 165–170; 10.1161/01.hyp.18.2.165 (1991).
8. Wood, A. W. *Physiology, Biophysics, and Biomedical Engineering* (CRC Press, Hoboken, 2012).
9. Huxley, A. F. Muscular contraction. *The Journal of Physiology* **243,** 1–43; 10.1113/jphysiol.1974.sp010740 (1974).
10. Webb, R. C. Smooth muscle contraction and relaxation. *Advances in physiology education* **27,** 201–206; 10.1152/advan.00025.2003 (2003).
11. Frishman, D. (ed.). *Structural Bioinformatics of Membrane Proteins* (Springer-Verlag Vienna, Vienna, 2010).
12. Neves, S. R., Ram, P. T. & Iyengar, R. G protein pathways. *Science* **296,** 1636–1639; 10.1126/science.1071550 (2002).
13. Duc, N. M., Kim, H. R. & Chung, K. Y. Structural mechanism of G protein activation by G protein-coupled receptor. *European journal of pharmacology* **763,** 214–222; 10.1016/j.ejphar.2015.05.016 (2015).
14. Mutschler, E., Geisslinger, G., Kroemer, H. K., Menzel, S. & Ruth, P. *Mutschler Arzneimittelwirkungen. Lehrbuch der Pharmakologie, der klinischen Pharmakologie und Toxikologie : mit einführenden Kapiteln in die Anatomie, Physiologie und Pathophysiologie.* 10th ed. (WVG Wissenschaftliche Verlagsgesellschaft, Stuttgart, 2013).
15. Hepler, J. R. & Gilman, A. G. G proteins. *Trends in Biochemical Sciences* **17,** 383–387; 10.1016/0968-0004(92)90005-T (1992).
16. Hilger, D., Masureel, M. & Kobilka, B. K. Structure and dynamics of GPCR signaling complexes. *Nat Struct Mol Biol* **25,** 4–12; 10.1038/s41594-017-0011-7 (2018).
17. Weis, W. I. & Kobilka, B. K. The Molecular Basis of G Protein-Coupled Receptor Activation. *Annual review of biochemistry* **87,** 897–919; 10.1146/annurev-biochem-060614-033910 (2018).
18. Hanlon, C. D. & Andrew, D. J. Outside-in signaling--a brief review of GPCR signaling with a focus on the Drosophila GPCR family. *Journal of Cell Science* **128,** 3533–3542; 10.1242/jcs.175158 (2015).
19. Gurevich, V. V. & Gurevich, E. V. GPCR Signaling Regulation: The Role of GRKs and Arrestins. *Front. Pharmacol.* **10,** 125; 10.3389/fphar.2019.00125 (2019).
20. Shenoy, S. K. & Lefkowitz, R. J. β-Arrestin-mediated receptor trafficking and signal transduction. *Trends in pharmacological sciences* **32,** 521–533; 10.1016/j.tips.2011.05.002 (2011).
21. Pfister, C. *et al.* Retinal S antigen identified as the 48K protein regulating light-dependent phosphodiesterase in rods. *Science (New York, N.Y.)* **228,** 891–893; 10.1126/science.2988124 (1985).
22. Lohse, M. J., Benovic, J. L., Codina, J., Caron, M. G. & Lefkowitz, R. J. beta-Arrestin: a protein that regulates beta-adrenergic receptor function. *Science (New York, N.Y.)* **248,** 1547–1550; 10.1126/science.2163110 (1990).
23. Zastrow, M. von & Kobilka, B. K. Ligand-regulated internalization and recycling of human beta 2-adrenergic receptors between the plasma membrane and endosomes containing transferrin receptors. *J. biol. chem.* **267,** 3530–3538 (1992).

24. Benovic, J. L., Strasser, R. H., Caron, M. G. & Lefkowitz, R. J. Beta-adrenergic receptor kinase: identification of a novel protein kinase that phosphorylates the agonist-occupied form of the receptor. *Proceedings of the National Academy of Sciences of the United States of America* **83,** 2797–2801; 10.1073/pnas.83.9.2797 (1986).

25. Benovic, J. L. *et al.* Functional desensitization of the isolated beta-adrenergic receptor by the beta-adrenergic receptor kinase: potential role of an analog of the retinal protein arrestin (48-kDa protein). *Proceedings of the National Academy of Sciences of the United States of America* **84,** 8879–8882; 10.1073/pnas.84.24.8879 (1987).

26. Caron, M. G. & Barak, L. S. A Brief History of the β-Arrestins. *Methods in molecular biology (Clifton, N.J.)* **1957,** 3–8; 10.1007/978-1-4939-9158-7_1 (2019).

27. DeWire, S. M., Ahn, S., Lefkowitz, R. J. & Shenoy, S. K. Beta-arrestins and cell signaling. *Annual review of physiology* **69,** 483–510; 10.1146/annurev.physiol.69.022405.154749 (2007).

28. Mayer, D. *et al.* Distinct G protein-coupled receptor phosphorylation motifs modulate arrestin affinity and activation and global conformation. *Nat Commun* **10,** 1261; 10.1038/s41467-019-09204-y (2019).

29. Santini, F., Penn, R. B., Gagnon, A. W., Benovic, J. L. & Keen, J. H. Selective recruitment of arrestin-3 to clathrin coated pits upon stimulation of G protein-coupled receptors. *Journal of Cell Science* **113 (Pt 13),** 2463–2470 (2000).

30. Spillmann, M. *et al.* New Insights into Arrestin Recruitment to GPCRs. *International journal of molecular sciences* **21,** 4949; 10.3390/ijms21144949 (2020).

31. Kohout, T. A., Lin, F. S., Perry, S. J., Conner, D. A. & Lefkowitz, R. J. beta-Arrestin 1 and 2 differentially regulate heptahelical receptor signaling and trafficking. *Proceedings of the National Academy of Sciences of the United States of America* **98,** 1601–1606; 10.1073/pnas.041608198 (2001).

32. Daaka, Y. *et al.* Essential role for G protein-coupled receptor endocytosis in the activation of mitogen-activated protein kinase. *J. biol. chem.* **273,** 685–688; 10.1074/jbc.273.2.685 (1998).

33. Luttrell, L. M. *et al.* Beta-arrestin-dependent formation of beta2 adrenergic receptor-Src protein kinase complexes. *Science (New York, N.Y.)* **283,** 655–661; 10.1126/science.283.5402.655 (1999).

34. DeFea, K. A. *et al.* The proliferative and antiapoptotic effects of substance P are facilitated by formation of a beta -arrestin-dependent scaffolding complex. *Proceedings of the National Academy of Sciences of the United States of America* **97,** 11086–11091; 10.1073/pnas.190276697 (2000).

35. Luttrell, L. M. *et al.* Activation and targeting of extracellular signal-regulated kinases by beta-arrestin scaffolds. *Proceedings of the National Academy of Sciences of the United States of America* **98,** 2449–2454; 10.1073/pnas.041604898 (2001).

36. Pitcher, J. A. *et al.* Role of beta gamma subunits of G proteins in targeting the beta-adrenergic receptor kinase to membrane-bound receptors. *Science (New York, N.Y.)* **257,** 1264–1267; 10.1126/science.1325672 (1992).

37. Michel, M. C. & Charlton, S. J. Biased Agonism in Drug Discovery-Is It Too Soon to Choose a Path? *Mol Pharmacol* **93,** 259–265; 10.1124/mol.117.110890 (2018).

38. Althoff, T. F. & Offermanns, S. G-protein-mediated signaling in vascular smooth muscle cells - implications for vascular disease. *J Mol Med* **93,** 973–981; 10.1007/s00109-015-1305-z (2015).

39. Gohla, A., Schultz, G. & Offermanns, S. Role for G(12)/G(13) in agonist-induced vascular smooth muscle cell contraction. *Circulation research* **87,** 221–227; 10.1161/01.res.87.3.221 (2000).

40. Murthy, K. S. Signaling for contraction and relaxation in smooth muscle of the gut. *Annual review of physiology* **68,** 345–374; 10.1146/annurev.physiol.68.040504.094707 (2006).

41. Paul, R. J. The role of phospholamban and SERCA3 in regulation of smooth muscle-endothelial cell signalling mechanisms: evidence from gene-ablated mice. *Acta physiologica Scandinavica* **164,** 589–597; 10.1111/j.1365-201x.1998.tb10704.x (1998).

42. Hill-Eubanks, D. C., Werner, M. E., Heppner, T. J. & Nelson, M. T. Calcium Signaling in Smooth Muscle. *Cold Spring Harbor Perspectives in Biology* **3**; 10.1101/cshperspect.a004549 (2011).

43. Keravis, T. & Lugnier, C. Cyclic nucleotide phosphodiesterase (PDE) isozymes as targets of the intracellular signalling network: benefits of PDE inhibitors in various diseases and perspectives for future therapeutic developments. *British journal of pharmacology* **165,** 1288–1305; 10.1111/j.1476-5381.2011.01729.x (2012).

44. Bender, A. T. & Beavo, J. A. Cyclic nucleotide phosphodiesterases: molecular regulation to clinical use. *Pharmacological reviews* **58,** 488–520; 10.1124/pr.58.3.5 (2006).

45. Lehners, M., Dobrowinski, H., Feil, S. & Feil, R. cGMP Signaling and Vascular Smooth Muscle Cell Plasticity. *Journal of cardiovascular development and disease* **5**; 10.3390/jcdd5020020 (2018).

46. Fleming, I. Signal transduction of eNOS activation. *Cardiovascular Research* **43,** 532–541; 10.1016/S0008-6363(99)00094-2 (1999).

47. Kobiałka, M. & Gorczyca, W. A. Particulate guanylyl cyclases: multiple mechanisms of activation. *Acta biochimica Polonica* **47,** 517–528 (2000).

48. Costell, M. H. *et al.* Comparison of soluble guanylate cyclase stimulators and activators in models of cardiovascular disease associated with oxidative stress. *Frontiers in pharmacology* **3,** 128; 10.3389/fphar.2012.00128 (2012).

49. Friebe, A. & Koesling, D. Regulation of nitric oxide-sensitive guanylyl cyclase. *Circulation research* **93,** 96–105; 10.1161/01.RES.0000082524.34487.31 (2003).

50. Ignarro, L. J., Adams, J. B., Horwitz, P. M. & Wood, K. S. Activation of soluble guanylate cyclase by NO-hemoproteins involves NO-heme exchange. Comparison of heme-containing and heme-deficient enzyme forms. *J. biol. chem.* **261,** 4997–5002 (1986).

51. Russwurm, M. & Koesling, D. NO activation of guanylyl cyclase. *The EMBO journal* **23,** 4443–4450; 10.1038/sj.emboj.7600422 (2004).

52. Zhao, Y., Schelvis, J. P., Babcock, G. T. & Marletta, M. A. Identification of histidine 105 in the beta1 subunit of soluble guanylate cyclase as the heme proximal ligand. *Biochemistry* **37,** 4502–4509; 10.1021/bi972686m (1998).

53. Schrammel, A., Behrends, S., Schmidt, K., Koesling, D. & Mayer, B. Characterization of 1H-1,2,4oxadiazolo4,3-aquinoxalin-1-one as a heme-site inhibitor of nitric oxide-sensitive guanylyl cyclase. *Molecular pharmacology* **50,** 1–5 (1996).

54. Denninger, J. W. & Marletta, M. A. Guanylate cyclase and the ·NO/cGMP signaling pathway. *Biochimica et Biophysica Acta (BBA) - Bioenergetics* **1411,** 334–350; 10.1016/S0005-2728(99)00024-9 (1999).

55. Francis, S. H., Busch, J. L., Corbin, J. D. & Sibley, D. cGMP-dependent protein kinases and cGMP phosphodiesterases in nitric oxide and cGMP action. *Pharmacological reviews* **62,** 525–563; 10.1124/pr.110.002907 (2010).

56. Alioua, A. *et al.* The large conductance, voltage-dependent, and calcium-sensitive K+ channel, Hslo, is a target of cGMP-dependent protein kinase phosphorylation in vivo. *J. biol. chem.* **273,** 32950–32956; 10.1074/jbc.273.49.32950 (1998).

57. Thenappan, T., Ormiston, M. L., Ryan, J. J. & Archer, S. L. Pulmonary arterial hypertension: pathogenesis and clinical management. *BMJ (Clinical research ed.)* **360,** j5492; 10.1136/bmj.j5492 (2018).

58. Prins, K. W. & Thenappan, T. World Health Organization Group I Pulmonary Hypertension: Epidemiology and Pathophysiology. *Cardiology clinics* **34,** 363–374; 10.1016/j.ccl.2016.04.001 (2016).

59. Hoeper, M. M. *et al.* Pulmonary Hypertension. *Deutsches Arzteblatt international* **114,** 73–84; 10.3238/arztebl.2017.0073 (2017).

60. Ryan, J. J. *et al.* The WHO classification of pulmonary hypertension: A case-based imaging compendium. *Pulmonary circulation* **2,** 107–121; 10.4103/2045-8932.94843 (2012).

61. Rose-Jones, L. J. & Mclaughlin, V. V. Pulmonary hypertension: types and treatments. *Current cardiology reviews* **11,** 73–79; 10.2174/1573403x09666131117164122 (2015).

62. Rabinovitch, M. Molecular pathogenesis of pulmonary arterial hypertension. *The Journal of Clinical Investigation* **122,** 4306–4313; 10.1172/JCI60658 (2012).

63. Galiè, N. *et al.* 2015 ESC/ERS Guidelines for the diagnosis and treatment of pulmonary hypertension: The Joint Task Force for the Diagnosis and Treatment of Pulmonary Hypertension of the European Society of Cardiology (ESC) and the European Respiratory Society (ERS): Endorsed by: Association for European Paediatric and Congenital Cardiology (AEPC), International Society for Heart and Lung Transplantation (ISHLT). *European heart journal* **37,** 67–119; 10.1093/eurheartj/ehv317 (2016).

64. Medarov, B. I. & Judson, M. A. The role of calcium channel blockers for the treatment of pulmonary arterial hypertension: How much do we actually know and how could they be positioned today? *Respiratory medicine* **109,** 557–564; 10.1016/j.rmed.2015.01.004 (2015).

65. La, M. & Reid, J. J. Endothelin-1 and the regulation of vascular tone. *Clinical and experimental pharmacology & physiology* **22,** 315–323; 10.1111/j.1440-1681.1995.tb02008.x (1995).

66. Wynne, B. M., Chiao, C.-W. & Webb, R. C. Vascular Smooth Muscle Cell Signaling Mechanisms for Contraction to Angiotensin II and Endothelin-1. *Journal of the American Society of Hypertension : JASH* **3,** 84–95; 10.1016/j.jash.2008.09.002 (2009).

67. Kass, D. A., Champion, H. C. & Beavo, J. A. Phosphodiesterase type 5: expanding roles in cardiovascular regulation. *Circulation research* **101,** 1084–1095; 10.1161/CIRCRESAHA.107.162511 (2007).

68. Ruan, C.-H., Dixon, R. A., Willerson, J. T. & Ruan, K.-H. Prostacyclin Therapy for Pulmonary Arterial Hypertension. *Texas Heart Institute Journal* **37,** 391–399 (2010).

69. Iyinikkel, J. & Murray, F. GPCRs in pulmonary arterial hypertension: tipping the balance. *British journal of pharmacology* **175,** 3063–3079; 10.1111/bph.14172 (2018).

70. Thenappan, T., Shah, S. J., Rich, S. & Gomberg-Maitland, M. A USA-based registry for pulmonary arterial hypertension: 1982-2006. *The European respiratory journal* **30,** 1103–1110; 10.1183/09031936.00042107 (2007).

71. Bond, R. A., Lucero Garcia-Rojas, E. Y., Hegde, A. & Walker, J. K. L. Therapeutic Potential of Targeting ß-Arrestin. *Frontiers in pharmacology* **10,** 124; 10.3389/fphar.2019.00124 (2019).

72. Deshpande, D. A., Theriot, B. S., Penn, R. B. & Walker, J. K. L. Beta-arrestins specifically constrain beta2-adrenergic receptor signaling and function in airway smooth muscle. *FASEB journal : official publication of the Federation of American Societies for Experimental Biology* **22,** 2134–2141; 10.1096/fj.07-102459 (2008).

73. Pera, T. *et al.* Specificity of arrestin subtypes in regulating airway smooth muscle G protein-coupled receptor signaling and function. *FASEB journal : official publication of the Federation of American Societies for Experimental Biology* **29,** 4227–4235; 10.1096/fj.15-273094 (2015).

74. Walker, J. K. L. *et al.* Beta-arrestin-2 regulates the development of allergic asthma. *The Journal of Clinical Investigation* **112,** 566–574; 10.1172/JCI17265 (2003).

75. Hwangbo, C. *et al.* Modulation of Endothelial Bone Morphogenetic Protein Receptor Type 2 Activity by Vascular Endothelial Growth Factor Receptor 3 in Pulmonary Arterial Hypertension. *Circulation* **135,** 2288–2298; 10.1161/CIRCULATIONAHA.116.025390 (2017).

76. Ma, Z. *et al.* Vascular Endothelial Growth Factor Receptor 3 Regulates Endothelial Function Through β-Arrestin 1. *Circulation* **139,** 1629–1642; 10.1161/CIRCULATIONAHA.118.034961 (2019).

77. Conner, D. A. *et al.* beta-Arrestin1 knockout mice appear normal but demonstrate altered cardiac responses to beta-adrenergic stimulation. *Circulation research* **81,** 1021–1026; 10.1161/01.res.81.6.1021 (1997).

78. Bohn, L. M. *et al.* Enhanced morphine analgesia in mice lacking beta-arrestin 2. *Science (New York, N.Y.)* **286,** 2495–2498; 10.1126/science.286.5449.2495 (1999).

79. O'Hayre, M. *et al.* Genetic evidence that β-arrestins are dispensable for the initiation of β2-adrenergic receptor signaling to ERK. *Science signaling* **10**; 10.1126/scisignal.aal3395 (2017).

80. Yallop, C. A. & Svendsen, I. The effects of G418 on the growth and metabolism of recombinant mammalian cell lines. *Cytotechnology* **35,** 101–114; 10.1023/A:1017550902771 (2001).

81. Knapp, J. *et al.* Comparison of contractile responses in isolated mouse aorta and pulmonary artery: Influence of strain and sex. *Journal of cardiovascular pharmacology* **48,** 820–826; 10.1097/01.fjc.0000232062.80084.4f (2006).

82. Vermeersch, P. *et al.* Soluble guanylate cyclase-alpha1 deficiency selectively inhibits the pulmonary vasodilator response to nitric oxide and increases the pulmonary vascular remodeling response to chronic hypoxia. *Circulation* **116,** 936–943; 10.1161/CIRCULATIONAHA.106.677245 (2007).

83. Evora, P. R. B., Evora, P. M., Celotto, A. C., Rodrigues, A. J. & Joviliano, E. E. Cardiovascular therapeutics targets on the NO-sGC-cGMP signaling pathway: a critical overview. *Current drug targets* **13,** 1207–1214; 10.2174/138945012802002348 (2012).

84. Bradley, S. A. & Steinert, J. R. Characterisation and comparison of temporal release profiles of nitric oxide generating donors. *Journal of neuroscience methods* **245,** 116–124; 10.1016/j.jneumeth.2015.02.024 (2015).

85. Lundberg, J. O. & Weitzberg, E. NO generation from nitrite and its role in vascular control. *Arteriosclerosis, thrombosis, and vascular biology* **25,** 915–922; 10.1161/01.ATV.0000161048.72004.c2 (2005).

86. Friederich, J. A. & Butterworth, J. F. Sodium nitroprusside: twenty years and counting. *Anesthesia and analgesia* **81,** 152–162; 10.1097/00000539-199507000-00031 (1995).

87. Furchgott, R. F. & Zawadzki, J. V. The obligatory role of endothelial cells in the relaxation of arterial smooth muscle by acetylcholine. *Nature* **288,** 373–376; 10.1038/288373a0 (1980).

88. Rabe, K. F. *et al.* Identification of PDE isozymes in human pulmonary artery and effect of selective PDE inhibitors. *The American journal of physiology* **266,** L536-43; 10.1152/ajplung.1994.266.5.L536 (1994).

89. Galiè, N. *et al.* Sildenafil citrate therapy for pulmonary arterial hypertension. *The New England journal of medicine* **353,** 2148–2157; 10.1056/NEJMoa050010 (2005).

90. Ishikawa, Y. & Homcy, C. J. The adenylyl cyclases as integrators of transmembrane signal transduction. *Circulation research* **80,** 297–304; 10.1161/01.RES.80.3.297 (1997).

91. Zaccolo, M. & Movsesian, M. A. cAMP and cGMP signaling cross-talk: role of phosphodiesterases and implications for cardiac pathophysiology. *Circulation research* **100,** 1569–1578; 10.1161/CIRCRESAHA.106.144501 (2007).

92. Pinto, C. *et al.* Activation and inhibition of adenylyl cyclase isoforms by forskolin analogs. *The Journal of pharmacology and experimental therapeutics* **325,** 27–36; 10.1124/jpet.107.131904 (2008).

93. Sandner, P. *et al.* Soluble Guanylate Cyclase Stimulators and Activators. *Handbook of experimental pharmacology*; 10.1007/164_2018_197 (2019).

94. Nossaman, B., Pankey, E. & Kadowitz, P. Stimulators and activators of soluble guanylate cyclase: review and potential therapeutic indications. *Critical care research and practice* **2012,** 290805; 10.1155/2012/290805 (2012).

95. Grundmann, M. *et al.* Lack of beta-arrestin signaling in the absence of active G proteins. *Nat Commun* **9,** 341; 10.1038/s41467-017-02661-3 (2018).

96. Schmoldt, A., Benthe, H. F. & Haberland, G. Digitoxin metabolism by rat liver microsomes. *Biochemical pharmacology* **24,** 1639–1641 (1975).

97. Grabner, A. *et al.* LAPTM4A interacts with hOCT2 and regulates its endocytotic recruitment. *Cellular and molecular life sciences : CMLS* **68,** 4079–4090; 10.1007/s00018-011-0694-6 (2011).

98. Stasch, J.-P., Pacher, P. & Evgenov, O. V. Soluble guanylate cyclase as an emerging therapeutic target in cardiopulmonary disease. *Circulation* **123,** 2263–2273; 10.1161/CIRCULATIONAHA.110.981738 (2011).

99. Rahaman, M. M. *et al.* Cytochrome b5 Reductase 3 Modulates Soluble Guanylate Cyclase Redox State and cGMP Signaling. *Circulation research* **121,** 137–148; 10.1161/CIRCRESAHA.117.310705 (2017).

100. Pak, O. *et al.* Animal models of pulmonary hypertension: role in translational research. *Drug Discovery Today: Disease Models* **7,** 89–97; 10.1016/j.ddmod.2011.02.002 (2010).

101. Benza, R. L. *et al.* An evaluation of long-term survival from time of diagnosis in pulmonary arterial hypertension from the REVEAL Registry. *CHEST* **142,** 448–456; 10.1378/chest.11-1460 (2012).

102. Pubmed Suchergebis "beta arrestin". Available at https://pubmed.ncbi.nlm.nih.gov/?term=beta+arrestin&filter=datesearch.y_10.

103. Hofmann, F., Ammendola, A. & Schlossmann, J. Rising behind NO: cGMP-dependent protein kinases. *Journal of Cell Science* **113 (Pt 10),** 1671–1676 (2000).

104. Rybalkin, S. D., Yan, C., Bornfeldt, K. E. & Beavo, J. A. Cyclic GMP phosphodiesterases and regulation of smooth muscle function. *Circulation research* **93,** 280–291; 10.1161/01.RES.0000087541.15600.2B (2003).

105. O. A. López-Canales *et al.* Role of adenylyl cyclase in reduced β-adrenoceptor-mediated vasorelaxation during maturation. *undefined* (2016).

106. Willets, J. M., Nash, C. A., Rainbow, R. D., Nelson, C. P. & Challiss, R. A. J. Defining the roles of arrestin2 and arrestin3 in vasoconstrictor receptor desensitization in hypertension. *American journal of physiology. Cell physiology* **309,** C179-89; 10.1152/ajpcell.00079.2015 (2015).

107. Liu, S., Luttrell, L. M., Premont, R. T. & Rockey, D. C. β-Arrestin2 is a critical component of the GPCR-eNOS signalosome. *Proceedings of the National Academy of Sciences of the United States of America* **117,** 11483–11492; 10.1073/pnas.1922608117 (2020).

108. Carneiro, A. P., Fonseca-Alaniz, M. H., Dallan, L. A. O., Miyakawa, A. A. & Krieger, J. E. β-arrestin is critical for early shear stress-induced Akt/eNOS activation in human vascular endothelial cells. *Biochemical and biophysical research communications* **483,** 75–81; 10.1016/j.bbrc.2017.01.003 (2017).

109. Hauck, R. W. *et al.* Effects of beta 2-agonist- and dexamethasone-treatment on relaxation and regulation of beta-adrenoceptors in human bronchi and lung tissue. *British journal of pharmacology* **121,** 1523–1530; 10.1038/sj.bjp.0701289 (1997).

110. Ma, L. & Pei, G. Beta-arrestin signaling and regulation of transcription. *Journal of Cell Science* **120,** 213–218; 10.1242/jcs.03338 (2007).

111. Hoffmann, L. S. *et al.* Distinct molecular requirements for activation or stabilization of soluble guanylyl cyclase upon haem oxidation-induced degradation. *British journal of pharmacology* **157,** 781–795; 10.1111/j.1476-5381.2009.00263.x (2009).

112. Stasch, J.-P. *et al.* NO- and haem-independent activation of soluble guanylyl cyclase: molecular basis and cardiovascular implications of a new pharmacological principle. *British journal of pharmacology* **136,** 773–783; 10.1038/sj.bjp.0704778 (2002).

113. Stasch, J.-P. *et al.* Targeting the heme-oxidized nitric oxide receptor for selective vasodilatation of diseased blood vessels. *The Journal of Clinical Investigation* **116,** 2552–2561; 10.1172/JCI28371 (2006).

114. Thoonen, R. *et al.* Cardiovascular and pharmacological implications of haem-deficient NO-unresponsive soluble guanylate cyclase knock-in mice. *Nature communications* **6,** 8482; 10.1038/ncomms9482 (2015).

115. Pan, J. *et al.* The molecular mechanism of heme loss from oxidized soluble guanylate cyclase induced by conformational change. *Biochimica et biophysica acta* **1864,** 488–500; 10.1016/j.bbapap.2016.02.012 (2016).

116. Meurer, S. *et al.* Nitric oxide-independent vasodilator rescues heme-oxidized soluble guanylate cyclase from proteasomal degradation. *Circulation research* **105,** 33–41; 10.1161/CIRCRESAHA.109.198234 (2009).

117. Ciechanover, A. Proteolysis: from the lysosome to ubiquitin and the proteasome. *Nat Rev Mol Cell Biol* **6,** 79–87; 10.1038/nrm1552 (2005).

118. Ghosh, A. *et al.* Soluble guanylate cyclase as an alternative target for bronchodilator therapy in asthma. *Proceedings of the National Academy of Sciences of the United States of America* **113,** E2355-62; 10.1073/pnas.1524398113 (2016).

119. Shenoy, S. K. & Lefkowitz, R. J. Multifaceted roles of beta-arrestins in the regulation of seven-membrane-spanning receptor trafficking and signalling. *The Biochemical journal* **375,** 503–515; 10.1042/BJ20031076 (2003).

120. Barella, L. F. *et al.* β-Cell-intrinsic β-arrestin 1 signaling enhances sulfonylurea-induced insulin secretion. *The Journal of Clinical Investigation* **129,** 3732–3737; 10.1172/JCI126309 (2019).

121. Crépieux, P. *et al.* A Comprehensive View of the β-Arrestinome. *Frontiers in Endocrinology* **8,** 32; 10.3389/fendo.2017.00032 (2017).

122. Ghosh, A. & Stuehr, D. J. Soluble guanylyl cyclase requires heat shock protein 90 for heme insertion during maturation of the NO-active enzyme. *Proceedings of the National Academy of Sciences of the United States of America* **109,** 12998–13003; 10.1073/pnas.1205854109 (2012).

123. Ghosh, A. & Stuehr, D. J. Regulation of sGC via hsp90, Cellular Heme, sGC Agonists, and NO: New Pathways and Clinical Perspectives. *Antioxidants & Redox Signaling* **26,** 182–190; 10.1089/ars.2016.6690 (2017).

124. Dumitrascu, R. *et al.* Activation of soluble guanylate cyclase reverses experimental pulmonary hypertension and vascular remodeling. *Circulation* **113,** 286–295; 10.1161/CIRCULATIONAHA.105.581405 (2006).

125. Toxvig, A. K., Wehland, M., Grimm, D., Infanger, M. & Krüger, M. A focus on riociguat in the treatment of pulmonary arterial hypertension. *Basic & clinical pharmacology & toxicology* **125,** 202–214; 10.1111/bcpt.13272 (2019).

126. Dempsie, Y. & MacLean, M. R. The influence of gender on the development of pulmonary arterial hypertension. *Experimental physiology* **98,** 1257–1261; 10.1113/expphysiol.2012.069120 (2013).

127. Neupane, B. *et al.* Influence of gender in monocrotaline and chronic hypoxia induced pulmonary hypertension in obese rats and mice. *Respir Res* **21,** 136; 10.1186/s12931-020-01394-0 (2020).

List of publications

ORAL PRESENTATIONS

L. F. Lebender, B. K. Fleischmann, D. Wenzel. *The role of beta arrestin 1 in smooth muscle tone regulation of pulmonary arteries (PAs) (talk).* International Symposium of the Research Training Group 1873, Pharmacology of the 7-TM receptors and downstream signaling pathways, Bonn, Germany, 2019

POSTER PRESENTATIONS

L. F. Lebender, A. Seidinger, S. Rieck, B. K. Fleischmann, D. Wenzel. *The role of beta arrestin 1 in smooth muscle tone regulation of pulmonary arteries (PAs) (poster).* International Symposium of the Research Training Group 1873, Pharmacology of the 7-TM receptors and downstream signaling pathways, Bonn, Germany, 2019

L. F. Lebender, A. Seidinger, S. Rieck, B. K. Fleischmann, D. Wenzel. *The role of beta arrestin 1 in smooth muscle tone regulation of pulmonary arteries.* 98th meeting of the Deutsche Physiologische Gesellschaft (DPG), 2019, Ulm, Germany, 2019

L. F. Lebender, B. K. Fleischmann, D. Wenzel. *The role of beta arrestins and PDEs in smooth muscle tone regulation of vessels and airways.* Europhysiology 2018, The Physiological Society, London, UK, 2018